Thermal Processing for Gear Solutions
Spring/Summer 2015

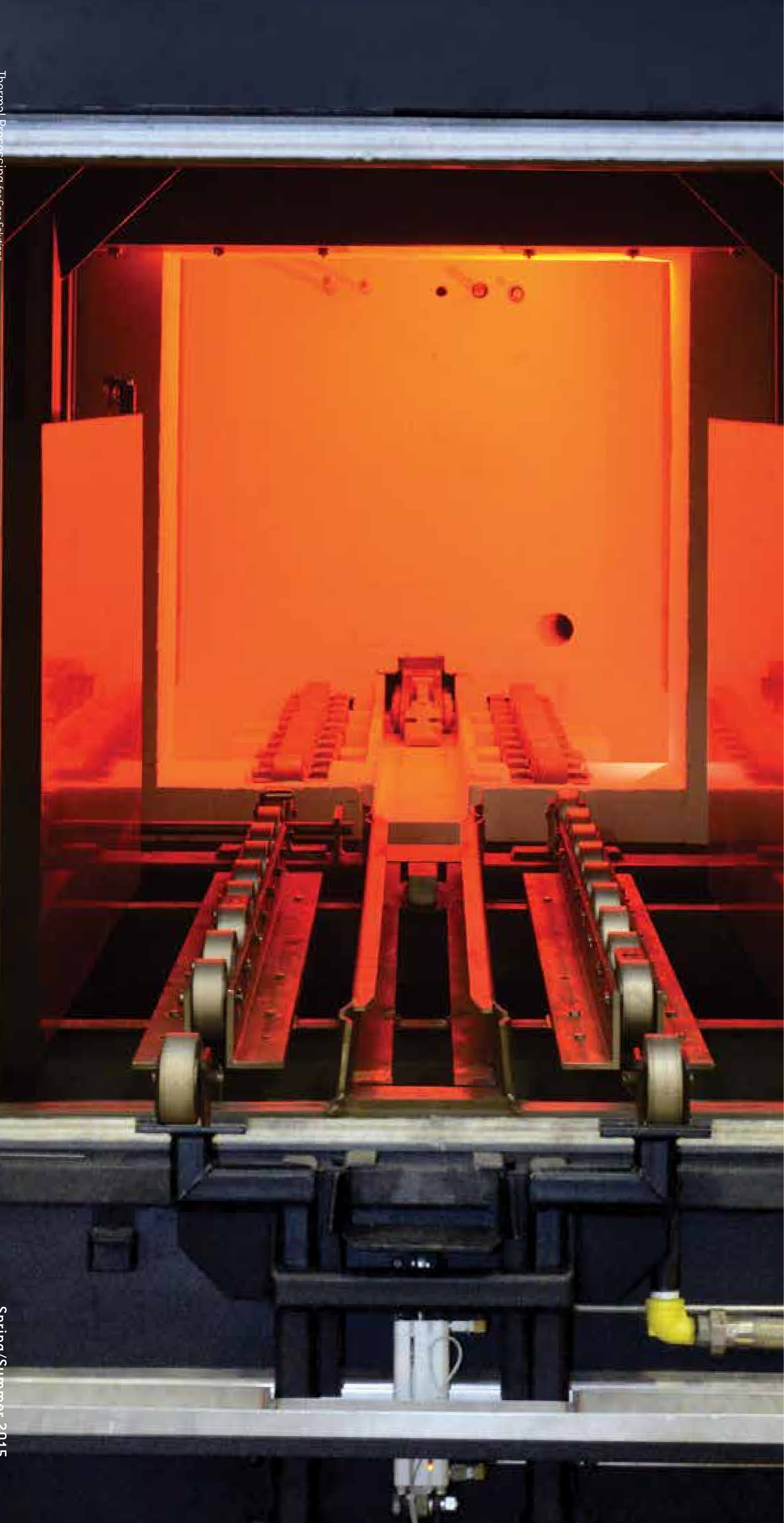

Thermal processing for Gear Solutions

Spring/Summer 2015
thermalprocessing.com

Stronger Longer Lasting Gears

Reliable • Precise • Efficient • Innovative

Just like gears, induction heating is all about **Precision**. Inductoheat's precision controlled, induction gear hardening systems provide ideal metallurgical patterns, minimum shape distortion, increased wear resistance and exceptional contact fatigue strength.

- FEA computer modeling
- Single part process monitoring
- Single-shot, scanning, tooth by tooth
- Single-coil dual-frequency technology
- Wide range of gear & bearing diameters
- Hypoid ring, spiral bevel, worm and pinion gears

Visit our website to learn more about our induction heat treating equipment!

Inductoheat, Inc. • Madison Heights, MI • (248) 585-9393
www.inductoheat.com

INDUCTOTHERM GROUP

Leading Manufacturers of Melting, Thermal Processing and Production Systems for the Metals and Materials Industry Worldwide.

HEAT TREAT 2015
Booth #303

FEATURES

Spring/Summer 2015

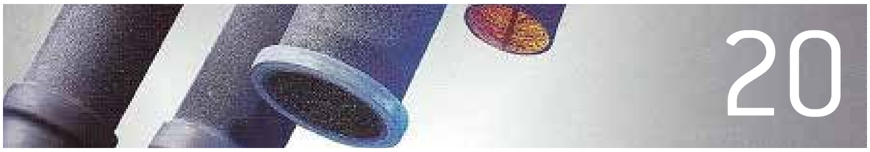

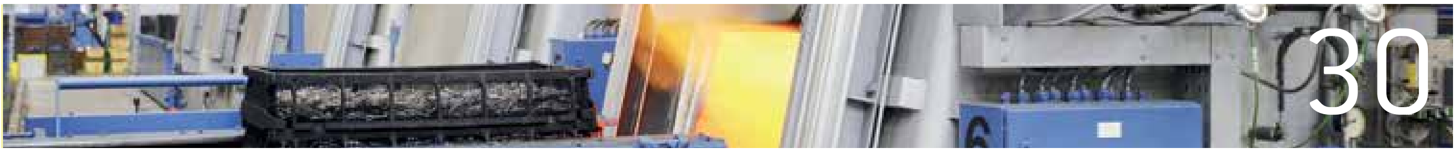

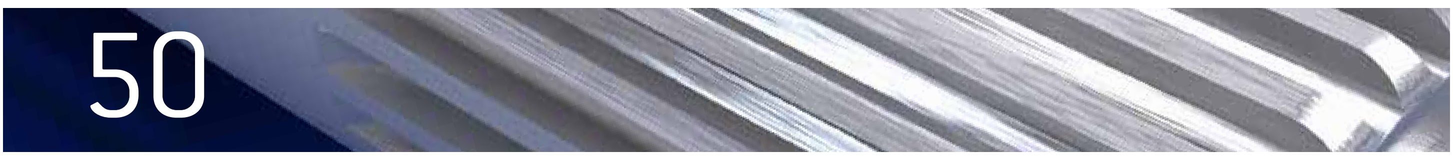

DEPARTMENTS

Spring/Summer 2015
Volume 4 / Number 1

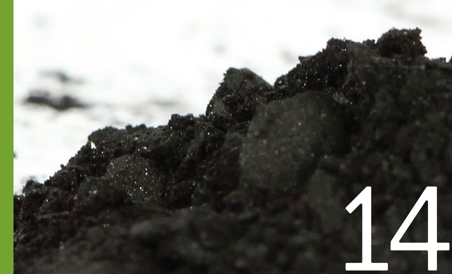

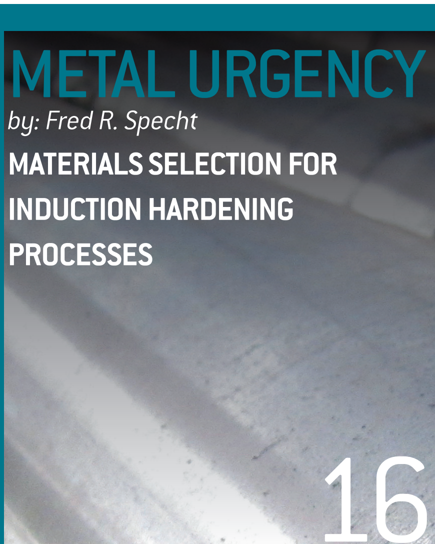

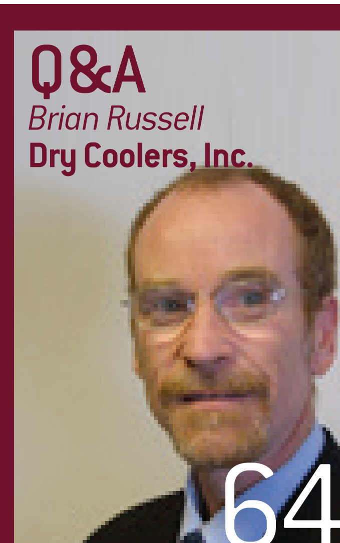

RESOURCES

Thermal Processing for Gear Solutions is published semi-annually by Media Solutions, Inc., 266D Yeager Parkway Pelham, AL 35124. Phone (205) 380-1573 Fax (205) 380-1580 International subscription rates: $105.00 per year. Postage Paid at Pelham AL and at additional mailing offices. Printed in the USA. POSTMASTER: Send address changes to *Thermal Processing for Gear Solutions* magazine, P.O. Box 1210 Pelham AL 35124. Return undeliverable Canadian addresses to P.O. Box 503 RPO West Beaver Creek Richmond Hill, ON L4B4R6.
Cover photo: Ipsen USA

LETTER FROM THE EDITOR

It's my pleasure to join the staff of *Thermal Processing for Gear Solutions* as the managing editor. This is a great opportunity for me to continue to have some connection to the heat treating and thermal processing industries in which I spent many years both working as a metallurgical engineer and serving in different editorial capacities on several magazines covering materials engineering and processing. There is a great deal of ongoing research and development in the areas of thermal processing and heat treating worldwide, and *Thermal Processing* aims to provide its readers with some of the latest developments, such as those in this issue.

Traditionally, gear design and heat treating process development for producing the required mechanical properties and other performance characteristics was advanced through experience and trial and error. This is time consuming, inefficient, and costly. With the development of powerful software, modeling and simulation of design and heat treatment continue to reduce the time necessary to reach the desired goals of engineers. Simulation techniques offer direct animation that provide detailed visualization of properties and high-speed process dynamics. Such tools enable developing tailored heat treating processes and materials for greater manufacturing flexibility. Modeling and simulation was identified recently in workshops conducted by the Thermal Manufacturing Industries Advanced Technology Consortium (TMI ATC) as one of the most important areas for further development.

This issue includes two examples of the use of modeling and simulation in process development. In the article "Stress Generation in an Axle Shaft during Induction Hardening," from DANTE Solutions, Fluxtrol and Dana Corp., electromagnetic modeling using Flux2D and thermal-stress modeling using DANTE are coupled to simulate induction hardening of an axle shaft. The simulation programs couple multiple physical phenomena involved including electromagnetic, thermal, metallurgical, stress and shape change. These computer-based studies enhance a designer's capabilities to predict the actual part performance from the induction hardening process.

Another example of the use of modeling to determine processing parameters is the article entitled "Time-Compressed Numerical Approach for Thermal Analysis of Preheating Process in Powder Metallurgy" from Ohio State University. In this work, a numerical method to simulate a heating cycle of powder material by means of a solid continuum model was developed. The analysis shows the influence of porosity on thermal behavior in the case of two equivalent numerical approaches, one using bulk material with powder thermal properties and the other using porous material with bulk thermal properties. A time-compression technique was developed that reduces the computational cost involved in thermal analysis of such long industrial processes.

The buzz for a number of years has been vacuum heat treating, and it is clear that this technology offers many benefits and advantages, and the use of vacuum heat treating continues to grow. But atmosphere heat treating isn't going away and gives the highest quality parts when controlled properly. This is illustrated in the article "Producing Quality Parts in an Atmosphere Furnace: How to Optimize Your Quenching and Carburizing Processes" from Ipsen USA.

The article discusses why when carburizing and through-hardening and quenching parts in a batch atmosphere furnace, it is essential to achieve uniformity of temperature and gassing, optimize the flow over components and aim for ideal quench speeds and heat extraction by using various high-performance systems, which enable producing high-quality parts with reduced distortion, as well as achieving competitive, overall manufacturing costs via heat treatment.

An article from Solar Atmospheres entitled "Enhanced Properties of 17-7 PH Stainless Steel" shows that vacuum heat treatment technology offers a unique processing advantage to achieving desirable properties in 17-7 PH stainless steel while producing bright, non-discolored parts cost effectively. Compared with conventionally processed 17-7 PH, Solar's three-step austenite conditioning, in situ cooling, and precipitation hardening process performed without breaking vacuum offers the user the benefit of reduced manufacturing costs owing to reduced pricing associated with the new in-situ vacuum heat treatment.

Finally, distortion of quenched parts is a major problem in heat treating where parts are quenched to obtain particular properties, and is especially of concern in parts requiring close tolerances so further processing such as machining and grinding isn't required. High-precision components such as automotive spiral bevel gears and aerospace quality bearing races can often distort appreciably during open tank oil quenching. Press quenching can help minimize the distortion of such components by using specialized tooling. This is discussed in the article entitled "Controlling Distortion in Heat Treatment through Press Quenching" by Art Reardon. The success of the technique depends strongly on a large number of variables including the knowledge, skill, and experience of the machine operator. Prior thermal history of the material is also demonstrated to be an important, and often overlooked, variable. We hope you enjoy this issue.

Ed Kubel
managing editor
Thermal Processing for Gear Solutions magazine
editor@thermalprocessing.com
(800) 366-2185 x205

Thermal processing for Gear Solutions

David C. Cooper
PUBLISHER

Chad Morrison
ASSOCIATE PUBLISHER

EDITORIAL
Stephen Sisk
EDITOR

Ed Kubel
MANAGING EDITOR

Anna Claire Conrad
ASSOCIATE EDITOR

SALES
Chad Morrison
ASSOCIATE PUBLISHER

Mike Barker
REGIONAL SALES MANAGER

CIRCULATION
Teresa Cooper
MANAGER

Kassie Boggan
COORDINATOR

Jamie Willett
ASSISTANT

ART
Jeremy Allen
CREATIVE DIRECTOR

Michele Hall
GRAPHIC DESIGNER

CONTRIBUTING WRITERS
JACK TITUS
FRED SPECHT
JIM OAKES
ZHICHAO LI
B. LYNN FERGUSON
ROBERT GOLDSTEIN
JOHN JACKOWSKI
VALENTIN NEMKOV
GREG FETT
AYMERIC GOLDSTEINAS
RENE ALQUICER
ART REARDON
S. SHLOK
R. SHIVPURI
DON JORDAN

Media solutions
PUBLISHED BY MEDIA SOLUTIONS, INC.
P. O. BOX 1987 • PELHAM, AL 35124
(800) 366-2185 • (205) 380-1580 FAX

David C. Cooper
PRESIDENT

Chad Morrison
VICE PRESIDENT

Teresa Cooper
OPERATIONS

UPDATE

New Products, Trends, Services, and Developments

Solar Atmospheres Renews Sikorsky Aircraft Approval

Solar Atmospheres, Inc. announced that it has renewed an approved supplier status with Sikorsky Aircraft Corporation with a 2-year certification. Solar is approved to provide heat treatment of titanium, and carburizing grade materials and aircraft grade steels in accordance with various AMS and Sikorsky specifications. In addition to maintaining current approvals, Solar also gained full approval for laboratory testing, metallography and micro hardness testing for Sikorsky products. Mike Moyer, Director of Sales at Solar Atmospheres, Inc. said, "Solar Atmospheres Inc. has been Sikorsky approved since the 1990s. Over the years, Solar's investment in R&D and process development has gotten the attention of Sikorsky and other prime aerospace companies, resulting in an expansion of our work scope. Solar's Low Pressure Vacuum Carburizing process is a perfect example of our ever-expanding capabilities and subsequent approvals."

For additional information, please contact Mike Moyer, Director of Sales at 215-721-1502 x1207, or mikem@solaratm.com, or go to the company's website at www.solaratm.com.

Companies wishing to submit materials for inclusion in Industry News should contact Anna Claire Conrad at editor@thermalprocesing.com.
Press Releases accompanied by color images will be given first consideration.

Carbolite Gero Representation in North America

The recent merger of Carbolite GmbH, the German sales organization of the British company Carbolite Ltd., and Gero Hochtemperaturöfen GmbH into Carbolite Gero GmbH & Co. KG has given rise to the availability of the Gero high temperature and vacuum furnace systems to North America for the first time. With over 30 years of furnace manufacturing under the direction of Roland Geiger, Gero is a well-established furnace manufacturing company in the European Union and is excited to offer their products to the North American market. Gero furnaces, specialized for heat treatment applications up to 3000°C and for vacuum and other modified atmospheres, are commonly used in Europe by companies in the aerospace, chemical, energy, and advanced materials sector as well as research and academia.

As a result of the merger, Verder Scientific, Inc., the United States subsidiary of Verder Scientific under which Carbolite Gero operates, now offers Retsch, Carbolite and Carbolite Gero equipment with fully trained product managers to address any and all inquiries. With this expanded product offering and professionally trained staff, Verder Scientific, Inc. is the main contact for your sample preparation and heat treatment needs.

For more information, contact Verder scientific, Inc. at info@verder-scientific.us or call (866) 473-8724.

Ajax TOCCO Supplies Induction Heater for FBE Coating System at L.B. Foster

Ajax TOCCO Magnethermic recently shipped a 4,500 kW, 12 pulse, Pacer II induction heating system to the L.B. Foster Coated Products pipe coating facility in Birmingham, AL. The installation of this advanced equipment marks a key development in L.B. Foster's capacity expansion plans.

The high-speed coating plant is capable of applying Fusion Bonded Epoxy (FBE) to 12.75 inch – 24 inch pipe in lengths up to 80 feet. The new Ajax TOCCO Magnethermic system provides progressive, in-line heating of the pipe prior to application of the FBE coating and features the ability to quickly change the line's inductors for differing pipe sizes to minimize production downtime. The L.B. Foster pipe coating facility is located on the site of American Steel Pipe.

For more information about Ajax TOCCO, go to www.ajaxtocco.com or contact the company at sales@ajaxtocco.com. For more information on L.B. Foster Company, go to www.lbfoster.com.

SECO/WARWICK Allied Pvt. Ltd. has installed single chamber vacuum hardening furnace with high pressure gas quenching facility for Jyoti Heat Treat Industries

The Vector™line furnace with high-pressure gas quench facility is ideally suitable for Vacuum Hardening in an oxygen free environment. Heating can be performed in vacuum as well as under convection with partial pressure. Quench pressure can be adjusted from 1.5 bar to a maximum of 10 bar. The Vector furnace installed at Jyoti can also be used for additional processes such as vacuum annealing, normalizing & tempering. The furnace has effective uniform hot zone size of 600x600x900 mm (24"x24"x36") & load capacity of 600 Kgs (1320 lbs.). The furnace complies with NADCA requirement and is equipped with an advanced PLC/HMI control system.

For more information on Jyoti Heat Treat Industries, contact the company by phone at +91 20 2712 8944. For additional information on the SECO/WARWICK Group, go to www.secowarwick.com.

Ipsen Kicks Off 2015 With Comprehensive Heat Treatment Course

Ipsen recently held their first Ipsen U class of 2015 in Cherry Valley, Illinois, allowing attendees to start the year with a broad overview of furnace equipment, processes, maintenance and more. Ipsen's three-day-course provides attendees with a hands-on approach to learning while receiving qualified tips and knowledge directly from the experts.

Participants in the February 2015 Ipsen U course came from across the country, including Colorado, Illinois, Michigan, Pennsylvania and Texas. Reflecting on the class, attendees found that it offered a "comprehensive overview of the general construction and mechanics of the furnace," as well as an in-depth look at "the furnace's hot zone and areas to focus on for preventive maintenance."

Throughout the course, attendees were able to:

- Learn about an extensive range of topics – from an introduction to vacuum furnaces and heat treating to furnace subsystems, maintenance and more
- View the different furnace components firsthand while learning how they affect other parts of the furnace and/or specific processes
- Take part in one-on-one discussions with Ipsen experts
- Participate in a leak detection demonstration
- Tour Ipsen's facility

Overall, Ipsen U allows participants to build and refresh their knowledge of heat-treating equipment and processes through applied learning.

For more information or to learn more and register for an upcoming 2015 Ipsen U course – April 7-9, June 2-4, August 4-6 or October 6-8 – at www.ipsenusa.com.

Special Vertical Airflow Cabinet Oven from Grieve

No. 814 is a 500ºF (260ºC), electrically-heated cabinet oven from Grieve, currently used for various plastic and metal part heat treating operations at the customer's facility. Workspace dimensions of this oven measure 22" W x 21" D x 85" H. 18 kW are installed in Nichrome wire tubular elements to heat the oven chamber, while a 750 CFM, 3/4-HP recirculating blower provides a vertical downward airflow to the workload.

This Grieve cabinet oven features 4" insulated walls, aluminized steel exterior and interior, three integral metal shelves, plus all safety equipment required by NFPA Standard 86 for handling flammable solvents, including a powered forced exhauster, airflow safety switch and purge tim.

Other controls on No. 814 include a fused disconnect switch, digital temperature controller and manual reset excess temperature controller.

For more information, please contact: THE GRIEVE CORPORATION, 500 Hart Road, Round Lake, Illinois 60073-2835 USA. Phone: (847) 546-8225. Fax: (847) 546-9210. Web: www.grievecorp.com. Email: sales@grievecorp.com.

MARK SALINE JOINS SINTERITE / C.I. HAYES AS GENERAL MANAGER

Gasbarre Products, Inc. is pleased to announce the hiring of Mark Saline as General Manager of Sinterite and C.I. Hayes. Mark is an accomplished manager with nearly 30 years of technical and business experience in the powder metallurgy industry. He has worked with all aspects of the manufacturing process, starting on the production floor and eventually into sales, engineering and management positions.

Mark is a Penn State graduate with two degrees: Materials Engineering and Business. Continuing education of professional development includes lean manufacturing, business training and Shainin technical courses. He is also an active member of the local Rotary Club. Sinterite and C.I. Hayes are furnace manufacturing companies within the Gasbarre Furnace Group. Sinterite designs, manufactures and services custom continuous belt and batch furnaces for sintering, steam treating, annealing, brazing and heat treating applications. Sinterite's quality design includes alloy and ceramic muffles, powder-handling equipment, custom fabrications, and the exclusively-manufactured HyperCooler, sinter-hardening system. Sinterite is located in St. Marys, Pennsylvania. C. I. Hayes offers a full line of vacuum and atmosphere furnaces capable of temperatures to 3000ºF. Belt, pusher, and walking-beam furnaces highlight our atmosphere line. Single chamber and modular furnaces, for batch and continuous production, are included in the Hayes' vacuum line. Modular vacuum furnaces feature isolated heating and quenching chambers. Endothermic, exothermic, and DA generators are also available. C.I. Hayes is located in Cranston, Rhode Island.

For more information on how Sinterite and C.I. Hayes can provide custom-engineered solutions for your specific thermal heating requirements and manufactured heat treating equipment, contact Bill Gasbarre at (814) 590-6282 or bgasbarre@gasbarre.com . Also visit the company's websites at www.sinterite.com and www.cihayes.com.

U. S. Steel Announces Construction of EAF And Tubular Products Coupling Facility in Alabama

United States Steel Corporation announced two capital investment projects valued at a total of $277.5 million. The first capital project is the construction of a technologically advanced electric arc furnace (EAF) steelmaking facility at its Fairfield Works in Birmingham, Ala., located in Jefferson County. The company will also construct a tubular products coupling facility at Fairfield Works to manufacture couplings with premium, semi-premium and American Petroleum Institute (API) connections for customers in the oil and gas industries.

The EAF is part of the company's larger transformation, The Carnegie Way, in which a large number of initiatives to improve the company's customer intimacy, operating flexibility, cost structure and raw materials position are being implemented. The tubular coupling facility is an integral part of the company's plan to develop and manufacture oil country tubular goods (OCTG) products with premium connections. The facility will feature four coupling cells to manufacture couplings for all of U. S. Steel's premium connections, including USS Liberty FJM®, USS-Patriot EBM™ and USS-Patriot TC™ connections, for customers in the energy industry.

Construction of the EAF will begin in the second quarter of 2015, with construction expected to be complete in the third quarter of 2016. The construction on the coupling facility is also anticipated to begin in the second quarter of 2015 and is expected to be complete in the first quarter of 2016. Throughout the process, U. S. Steel will continue to operate Fairfield Works' steelmaking and finishing operations to serve both flat-rolled and tubular customers in accordance with market requirements.

Additional information can be found at www.ussteel.com.

ASM International Convenes Discussion to Advance the Goals of the Materials Genome Initiative

A workshop report released by ASM International, Materials Park, Ohio through its Computational Materials Data Network outlined actions that professional societies can take to convene the materials community to drive the development of a materials data infrastructure aimed at transforming the way the materials community collaborates on materials and manufacturing innovation. By focusing on the development of a series of materials community workshops, the report offers an approach that can bring the community one step closer to the overall goal of the Materials Genome Initiative (MGI): a future where materials are created and implemented twice as fast an at a fraction of the cost that they are today.

ASM International convened the workshop that resulted in the Building the Materials Data Infrastructure: A Materials Community Planning Workshop report in January, which brought together representatives from more than a dozen professional societies to address the December 2014 Materials Genome Initiative Strategic Plan objective to "Identify Best Practices for Implementation of a Materials Data Infrastructure." The specific focus of the workshop was to identify a series of multiagency workshops that could engage the different components of the materials community to establish needs, identify barriers, and define methods to overcome them.

"This timely workshop provided valuable engagement across disparate materials communities into how to identify and overcome the challenges recently laid out in the 2014 Materials Genome Initiative

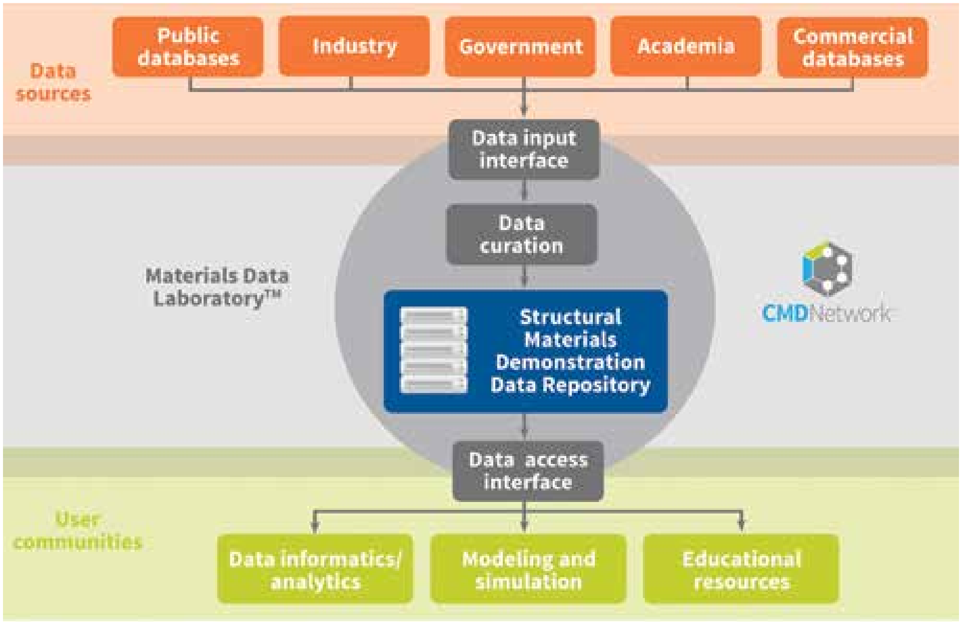

Strategic Plan," said Dr. James A Warren, Technical Program Director for Materials Genomics at the Material Measurement Laboratory of the National Institute of Standards and Technology.

Participants at the workshop built on an analysis of previous workshop results and studies to identify needs and outline a four-year timeline for future workshop-type activities that could address these needs. These activities fall into three broad categories—data management; data sharing; and education, training, and outreach—and include the following:

Data Management

- Establish a materials data quality roadmap by convening a broad scoping workshop supplemented by other subsequent workshops on specific data quality topics such as quality standards, uncertainty quantification, curation practices, and data gathering "codification."
- Develop a materials community data registry—a listing of databases—by leveraging experience with existing data registries in other fields, such as the Virtual Astronomical Observatory (VAO) Registry, through a series of working group activities.

Data Sharing

- Develop business models to encourage participation in the materials data infrastructure by conducting a series of forums with disparate materials communities.
- Identify connections between publishing articles and data through a series of publishing forums involving publishers, data generators, and other stakeholders.

Education, Training, and Outreach

- Develop data management workforce training through a robust set of workshop-type efforts, including communication and training in current tools and capabilities as well as curriculum development for both current materials professionals and those in undergraduate and graduate programs in universities in new and emerging areas.

Professional societies are uniquely positioned to lead many of these initiatives, as their ability to convene a range of materials experts across industry, academia, and national and federal laboratories is critical to bringing the Materials Innovation Infrastructure to fruition.

"The role of professional societies in supporting the development of the materials data infrastructure is a conversation that needs to continue in order to build a robust and effective system," said Scott D. Henry, Director of Content and Knowledge-Based Solutions at ASM International. "With access to a broad range of expertise as well as the ability to work across traditional boundaries, professional societies will continue to be a driving force toward a future of rapid and more efficient materials and manufacturing innovation."

To learn more about ASM International, visit www.asminternational.org

Cypress and Spansion complete $5 billion merger

Cypress Semiconductor Corp., San Jose, Calif., and Spansion Inc., Sunnyvale, Calif., have closed the merger of the two companies in an all-stock, tax-free transaction valued at approximately $5 billion. The newly combined company delivers microcontrollers and specialized memories for embedded systems.

Cypress has a broad, differentiated product portfolio, which includes NOR flash memories, F-RAM and SRAM, Traveo microcontrollers, the industry's only PSoC programmable system-on-chip solutions, analog and PMIC Power Management ICs, CapSense capacitive touch-sensing controllers, and Wireless BLE Bluetooth Low-Energy and USB connectivity solutions.

Spansion's flash memory, microcontrollers, mixed-signal, and analog products drive the development of faster, more intelligent and energy efficient electronics. Spansion is at the heart of electronics systems, connecting, controlling, storing and powering everything from automotive electronics and industrial systems, to highly interactive and immersive consumer devices.

The merger is expected to achieve more than $135 million in cost synergies on an annualized basis within three years, and to be accretive to non-GAAP earnings within the first full year after the transaction closes. The combined company will continue to pay $0.11 per share in quarterly dividends to shareholders.

For more information, go to www.cypress.com.

KNOWING TRUE CARBON POTENTIAL ENABLES ACCURATE PREDICTING CARBON DIFFUSION INTO THE PART

by Jim Oakes

THE RELATIONSHIP BETWEEN A CARBON-RICH ATMOSPHERE and its effects on low-carbon steel are well known. The evolution of carburizing led to in-situ monitoring of carbon-rich atmospheres to provide controllable parameters based on diffusion of carbon into a workpiece and simulation of carbon transfer and diffusion.

A continuing challenge is correlating in-situ sensor-based calculations with the actual carbon content of the furnace atmosphere. In-situ sensor technology measures oxygen levels and derives a carbon value from the partial pressure of oxygen inside the furnace compared with the partial pressure of oxygen in air. Knowing the oxygen level, the makeup of the prepared atmosphere, and the temperature enables predicting the carbon level of the atmosphere and, based on that value, predicting the diffusion of carbon into the workpiece.

Predicting the carbon level of the atmosphere involves many assumptions. For example, it is assumed that the part temperature is in equilibrium with the furnace temperature carbon is available from the amount of CO present in the prepared atmosphere, and the amount of hydrocarbon enriching gas used, which includes methane, propane, and methanol.

CARBON-POTENTIAL PITFALLS

If it is not known that there is a carbon potential issue, carbon levels produced could be higher or lower than planned. Both situations lead to undesirable results in the workpiece. Higher carbon, in the form of soot, not only delivers undesirable workpieces, but it also creates a harsh atmosphere for the furnace, which has a deleterious effect on lives of refractory, alloy furnace hardware, and sensors. Figure 1 shows excessive carbide formation in a carburized case of AISI 8620 low-alloy steel. Spherical carbides grow and join together due to high carbon levels forming carbide networks. These networks often form along grain boundaries while reducing mechanical properties. When soot builds up, the furnace should be burned out to prevent damage to furnace hardware.

Consider a "leaky" furnace. On one hand, air infiltrates the work zone, and the in-situ carbon probe gives a lower millivolt (mV) reading. Today's controls act on the sensor input and call for the output of the controller to add more enriching gas. If the correct mV, or carbon potential, is never achieved, enriching gas continues to flow, leading to an out-of-control situation, an unbalanced atmosphere, and potentially soot. High carbon levels can lead to retained austenite in the workpiece. In some cases, retained austenite transforms during part service, leading to failure from dimensional and metallurgical changes. Extreme cases of retained austenite lead to softness of the part surface. Figure 2 shows an example of an excessive amount of retained austenite caused by high carbon.

Some processes call for operating parameters (temperature and carbon set-point) at or just below the carbon-saturation limit in austenite. This level is determined by temperature and alloy composition. Operating a furnace at the saturation limit, leads to soot formation and nonuniform case depth. Therefore, strict process control parameters should be adopted.

On the other hand, a leaky furnace might never reach the sooting level, resulting in a light case, lower surface carbon content, and longer cycles, which impact production schedules. Carburizing at higher temperatures shortens cycle time, but can increase austenite grain size to undesirable levels.

Increasing carbon potential increases the rate of carbon transfer from the atmosphere to the workpiece. Despite the potential advantages of shorter cycle times at higher carburizing temperatures, proper control is essential, and care must be taken in the second stage of the process (diffuse, for example) to ensure achieving proper surface carbon.

During the diffuse stage, the rate of carbon transfer is limited by carbon diffusion in austenite, which is primarily determined by carburizing temperature and alloy composition. Austenitic carbon diffusion ultimately determines surface carbon if ample time is provided. Diffusion provides a desirable overall carbon profile, drives carbon to the required case depth, and begins the cooling process before quenching.

ABOUT THE AUTHOR: Jim Oakes is vice president of business development for Super Systems Inc. (SSi) where he is responsible for marketing and growth of various business segments and development of product-innovation strategies to meet customer needs. Jim has extensive experience in the heat treating and software/IT industries. He can be contacted at joakes@supersystems.com. Go to www.supersystems.com for more information.

Figure 1: Microstructure of carburized case where a high carbon potential resulted in excessive carbide formation.

Figure 2: Microstructure of carburized case containing about 30% retained austenite in a martensite matrix.

Tight process control is strongly recommended for all stages of the carburizing process to maintain proper atmosphere, reduce chances for error, and avoid out-of-control situations. Today, most heat treating furnaces are equipped with in-situ atmosphere monitoring, some redundancy, and automatic adjustment of the calculated carbon based on other inputs, such as gas analysis. At a minimum, furnace atmosphere should be verified using alternate gas analysis methods such as nondispersive infrared (NDIR), dew point, carbon wire, shim stock, and carbon bar.

MATERIALS SELECTION FOR INDUCTION HARDENING PROCESSES

by Fred R. Specht

INDUCTION HARDENING is the most common technique of the various types of applied energy processing. It uses alternating current that induces a magnetic field in a workpiece causing the workpiece to heat up to a certain depth below the surface. The piece is then quenched, which results in an increase in hardness within the heated area. The process is typically completed in a relatively short time. Final desired workpiece performance characteristics are determined by the hardness profile and induced stresses, which are influenced by the steel grade (chemical composition) and prior microstructure of the starting material.

The case hardness pattern produced by induction heating (Fig. 1) is a function of the inductor type and shape, as well as the heating method. Quenching or rapidly cooling the workpiece is accomplished by spray and submerged quenching, typically using water or a water-based polymer. Quench severity is controlled by the polymer concentration. Cooling rates are usually somewhere between those obtained with pure water and oil. In some special cases, compressed air is used to quench the workpiece. Some applications require through hardening where the entire piece is hardened and tempered.

MATERIAL SELECTION

Plain carbon steels are classified into four distinct series in accordance with the AISI system:

- The 1000 series are plain-carbon steels containing no more than 1.00% manganese
- The 1100 series are resulfurized (sulfur is added) carbon steels for machinability
- The 1200 series are resulfurized and rephosphorized for machinability
- The 1500 series have between 1.00 and 1.65% manganese

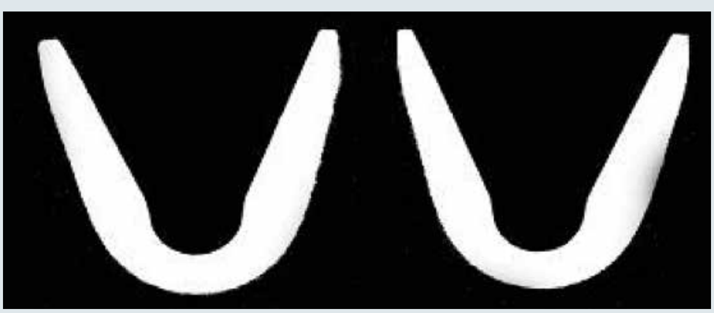

Figure 1: Hardened case pattern produced by induction hardening a gear tooth.

Carbon is the key to the hardening of steels. The carbon level of steel determines the maximum obtainable hardness (Fig. 2). The lower the carbon level, the lower the maximum as-quenched hardness that is achievable.

Steel grades commonly induction-hardened include 1045, 1050, 1144, 4140, 4150, 4350, 5150, and 8650. Some of these grades are cold drawn using very high reductions, which produce high tensile and yield strengths. Alloy steels require a quenched and tempered prior microstructure to optimize hardness and reduce the case-transition zone. Higher carbon content makes machining more difficult. Therefore, 1141 and 1144 grades are used where hardenability as well as ease of machinability is required. These steels are resulfurized, where the formation of sulfide inclusions significantly increase machinability.

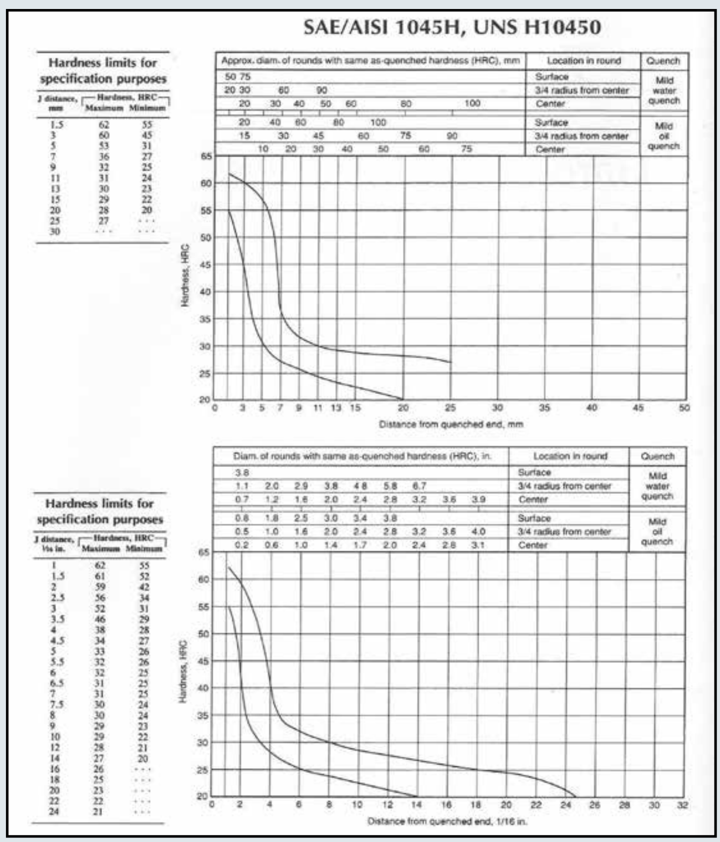

Hardness limits for specification purposes

J distance, mm	Hardness, HRC Maximum	Hardness, HRC Minimum
1.5	62	55
3	60	45
5	53	31
7	36	27
9	32	25
11	31	24
13	30	23
15	29	22
20	28	20
25	27	...
30	...	...

Hardness limits for specification purposes

J distance, 1/16 in.	Hardness, HRC Maximum	Hardness, HRC Minimum
1	62	55
1.5	61	52
2	59	42
2.5	56	34
3	52	31
3.5	46	29
4	38	28
4.5	34	27
5	33	26
5.5	32	26
6	32	25
6.5	31	25
7	31	25
7.5	30	24
8	30	24
9	29	23
10	29	22
12	28	21
14	27	20
16	26	...
18	25	...
20	23	...
22	22	...
24	21	...

Figure 2: Hardness limits of 1045 plain carbon steel.

ABOUT THE AUTHOR: Fred Specht is national sales manager of heat-treat products for Interpower Induction USA. To learn more about Interpower Induction USA's products and services, visit www.interpowerinduction.com.

AISI Designation	Description C	Composition, % Mn	Cr	Mo	Ni	Va
Carbon Steels						
10*xx*	*xx*	0.30–1.50	. . .	. . .	. . .	. . .
11*xx*	*xx*	1.30–1.65	. . .	. . .	. . .	. . .
15*xx*	*xx*	1.25–1.75	. . .	. . .	. . .	. . .
Alloy Steels						
41*xx*	*xx*	0.40–1.00	0.80–1.10	0.15–0.25	. . .	. . .
43*xx*	*xx*	0.45–0.80	0.40–0.90	0.20–0.30	1.65–2.00	. . .
52100	0.98–1.10	0.25–0.45	1.30–1.60	. . .	. . .	. . .
6150	0.48–0.53	0.70–0.90	0.80–1.10	. . .	. . .	0.015 min.
H-Steels						
4150H	0.65–1.10	0.65–1.10	0.75–1.20	0.15–0.25	. . .	. . .
Boron Steels						
10B*xx*	*xx*					
15B35	0.31–0.39	0.70–1.20	. . .	. . .	. . .	. . .
Stainless Steels						
416	0.15 max	1.25 max	12.0–14.0	. . .	. . .	. . .
420	Over 0.15	1.00 max	12.0–14.0	. . .	. . .	. . .
440C	0.96–1.20	1.00 max	16.0–18.0	0.75 max	. . .	. . .

The *xx* in the last two digits stands for the carbon content by weight. Steel 1045 has 0.45% carbon. Source: Ref 24

Figure 3: Classification of carbon and alloy steels.

A rule of thumb in steel grade selection is to select the grade with a carbon content that will produce the required hardness and mechanical properties for the application. For example, if a hardness of 40 HRC is needed, carbon content can be below 0.30%. However, if the required hardness is 60+ HRC, a carbon content greater than 0.50% is required. The use of lower carbon increases ductility and reduces the chances of quench cracking.

Induction hardened plain carbon steels have shallower case depths, and alloy steels can be hardened to higher hardness at greater case depths. The addition of a small amount of boron (0.001%) to low and medium carbon steels results in an increase in hardenability (Fig. 3). Charts showing different alloys and the relationship of hardness, machinability, and ease of grinding are available in the literature, and is an easy way to evaluate the manufacturing process. Steel suppliers have steel grade price charts with product forms available.

REFERENCES

- D.H. Herring, F.J. Otto, and F.R. Specht, Gear Materials and Their Heat Treatment, Industrial Heating, September, 2012.
- R.E. Haimbaugh, Practical Induction Heat Treating, ASM International, 2001.
- Properties and Selection: Irons, Steels, and High-performance Alloys, Vol 1, ASM Handbook, ASM International, 1990.

INTENSIVE QUENCHING CALLS FOR VERY HIGH COOLING RATES PT.II

by Jack Titus

INTENSIVE QUENCHING (IQ) is defined as cooling, usually using pure water, at a rate several times higher than the rate of conventional quenching. Fast, uniform part cooling reduces the probability of part cracking and distortion, while improving the surface hardness and durability of steel parts. Part I of this article (September 2014 *Thermal Processing*) discussed the history of the development of IQ, how it works, and how it compares with other quenching methods. This article covers IQ advantages and shows examples of parts that have been successfully produced using IQ.

Distortion resulting from quenching ferrous materials is caused by the non-geometrical transformation from austenite to martensite. Reduced distortion is achieved by:

- Quenching into hot oil; i.e., >250°F, or >120°C (moderate heat transfer)
- Press quenching in oil (high heat transfer with mechanical forced restriction)
- Quenching in hot salt bath (moderate to high heat transfer with interrupted cooling and no vapor barrier)
- High-pressure gas quenching, or HPGQ (moderate heat transfer, convection, with interrupted cooling)
- Intensive quenching, or IQ (extremely high heat transfer with interrupted cooling and no vapor barrier)

IQ is a patented, repeatable process that creates more uniform growth over the entire part geometry because the transformed case has a higher percentage of martensite (Figure 1). Growth uniformity is similar to that achieved with the white layer in nitriding.

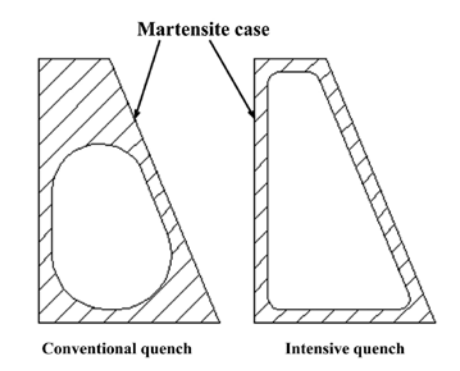

Figure 1: Compared with a conventional quenched part (left), intensive quenching creates more uniform growth over the entire part geometry (right) because the transformed case has a higher percentage of martensite.

Figure 2: Four 32-in. diameter spur gears carburized and intensive quenched in AFC-Holcroft UBQ batch carburizing furnace.

IQ ADVANTAGES

Oil, press, salt-bath, and high-pressure gas quenching methods are discussed in detail in the literature, but IQ might be considered counterintuitive, because quenching in water is associated with quench cracking. What is different about IQ?

Quench cracking is caused by non-uniform martensite transformation and/or high tensile stresses on the part surface. Intensive quenching forms a martensite shell on the part's surface by way of vapor-less, uniform high-velocity water. The shell expands, creating a compression ring around the hot core, and as the core cools and its volume shrinks, it "pulls" the martensitic shell into even greater compression. Because the temperature difference between the part surface and its core is much greater in IQ than in oil, salt, or gas quenching, the potential compressive stresses are magnified.

IQ provides an additional advantage for

Figure 3: Heavy truck pinion carburized and intensive quenched in AFC-Holcroft UBQ batch carburizing furnace

ABOUT THE AUTHOR: Jack Titus can be reached at (248) 668-4040 or jtitus@afc-holcroft.com. Go online to www.afc-holcroft.com. He is also the current "Hot Seat" columnist in *Gear Solutions* magazine.

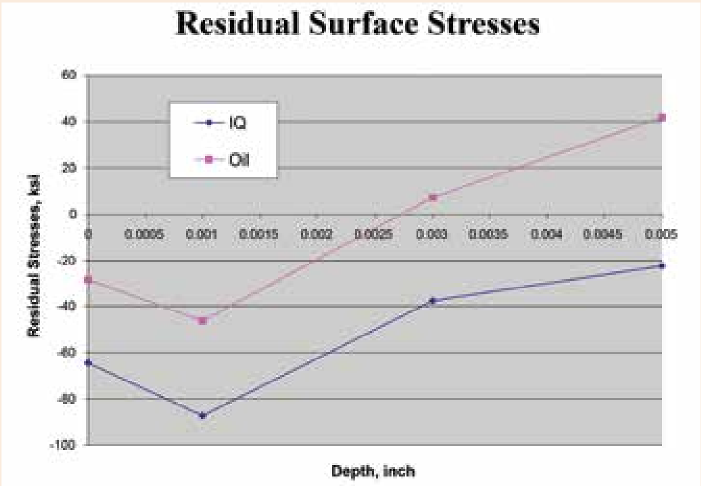

Figure 4: Distribution of residual stress between an oil-quenched and intensive quenched pinion.

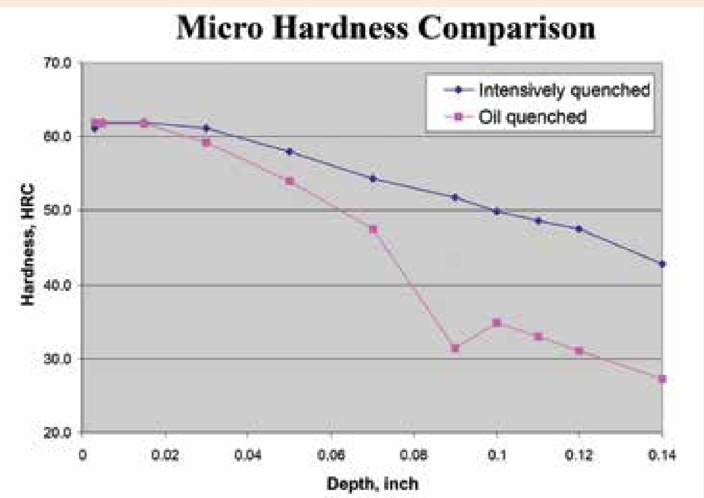

Figure 5: Example of depth of hardening that can be achieved by intensive quenching.

carburized parts by shortening carburizing time. Because IQ's heat transfer is so high, the ECD (effective case depth) is achieved using lower carbon levels. Typically, oil, salt, and gas quenching carburized alloy steels produce an ECD corresponding to a hardness of 50 HRC (Vickers 513) at a carbon level of 0.40%. Intensive quenching steel with the same carbon content produces a hardness of almost 56 HRC. In other words, the ECD can be achieved at 0.30% carbon, thus reducing the carburizing time. Therefore, this phenomenon has dramatically increased interest in the use of plain-carbon steels over alloy steels. In the majority of applications, the post temper surface hardness of 58 to 62 HRC is typical for carburized steels. The high quench severity of IQ enables neutral hardening of plain carbon steels; for example, IQ of AISI 1060 steel can achieve 61 HRC at over 95% martensite.

Another advantage of using IQ with plain carbon steels is the reduction of retained austenite. As the alloy content in steel increases, the martensite start and finish (Ms and Mf) temperatures are depressed, promoting an increase in retained austenite. Extremely fast quenching of 1060 steel (with no alloying additions) produces a simpler microstructure that limits the development of retained austenite. Carburized steel generally achieves 0.75 to 0.90% surface carbon, and carbon is one of the strongest austenite formers, followed by nickel, molybdenum, and manganese. If the surface carbon of plain-carbon steel can be kept lower, retained austenite can also be reduced.

Regarding my comparison in Part 1 to the market's acceptance of HPGQ—which in many cases requires that a steel's hardenability be increased—IQ's ultrahigh heat transfer promotes the opposite; that is, reduction in alloy content for many components. Gear teeth are designed to withstand impact and to endure high loads. Therefore, the core of gear teeth must be ductile enough to absorb deflection. Using plain- and low-carbon steels satisfies that requirement by limiting the hardened depth in gears having fine-pitch teeth, which today are difficult to carburize without hardening the tooth core. The only traditional solution available to avoid that issue is a long nitriding process.

A few years ago, AFC-Holcroft provided IQ Technologies a large 36 in. x 72 in. x 36 in. UBQ batch carburizing furnace with an 11,000-gallon capacity water quench tank for the purpose of achieving IQ quench velocities. Figure 2 shows an example of the size range that can be successfully quenched using IQ. Four 32-in. diameter spur gears were carburized and intensively quenched in the furnace. Due to the deep hardening of IQ, the carburizing cycle was reduced by 10 hours (about 33% of the time for conventional carburizing) to achieve the required ECD. The gears met the manufacture's specifications for distortion and hardness among other parameters, and have been in operation nearly three years.

Heavy truck pinions, helical gears, and internal gears were also carburized and quenched in the furnace system. Due to confidentiality agreements between IQ Technologies and test-part owners, most results are proprietary, but all parameters including dynamic testing were positive. Figures 3, 4, and 5 show some tests results from those pinions. Figure 4 shows the distribution of residual stress between oil-quenched and intensive quenched pinions. Figure 5 is an example of the depth of hardening that can be achieved by intensive quenching.

I believe that for IQ acceptance by the early and late majorities (see Figure 1, Part I), it should be integrated with an austenitizing process, whether carburizing or straight hardening, that is established, thereby providing a "perfect marriage" for industry. While quenching one gear at a time is ideal for maximum distortion control, it may not meet higher production requirements. When improved distortion and higher production is a necessity, two options to consider are the material and the process:

- Higher alloy steels are more expensive, but are deeper hardening and produce increased levels of distortion when quenched too fast
- Low-cost alloys require a faster quench, and that usually includes liquids.

The compromise is a liquid that is easier to live with, and that is water.

INEX Inc.

Pairing an advanced Silicon-Silicon Carbide material with a unique, cost-effective manufacturing process they pioneered more than 25 years ago, one Holland, New York-based company is solving the all-too-common occurrence of radiant tube failure.

By Stephen Sisk

When using conventional metal-alloy radiant tubes, failure is not just possible — it's a certainty. It's a costly reality that has long plagued heat treaters looking to maximize efficiency and productivity while streamlining costs.

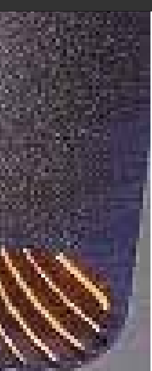

Recognizing this problem, INEX Inc., an advanced materials producer, developed a unique process to manufacture tubular forms made of Silicon Carbide (SiC), taking on the challenge to prove that failure of radiant tube heaters was not inevitable. The company focused its attention on this problem and in 1989 began producing Silicon - Silicon Carbide (Si-SiC) composite radiant tubes, which both outlast and outperform traditional metal-alloys.

"Typically, radiant tubes are made of nickel-chromium, or some people would say stainless steel," said Michael Kasprzyk, president of Holland, New York-based INEX Inc. "In heat treating furnaces all metal-alloy radiant tubes fail eventually. If the furnace operator is aggressive, the metal-alloy fails quickly in about 18 months. If run more conservatively, they may last several years. But eventually they all fail. Our advantage is a material that does not fail either thermally or chemically in heat treating environments. We replace a consumable tube with one made of Si-SiC that, at least in theory, could last forever."

Factors that affect the life of metal-alloy tubes include thermal creep, oxidation, and brittleness arising from carburization. These conditions vary depending on how each furnace is used, but failure will certainly occur at some point, according to Kasprzyk.

INEX Si-SiC tubes are immune to these factors, resulting in a much longer lifespan and reduced downtime.

"We're in the business of taking away headaches," Kasprzyk said. "Tube failure often ruins a furnace load, resulting in downtime, late deliveries, and costly

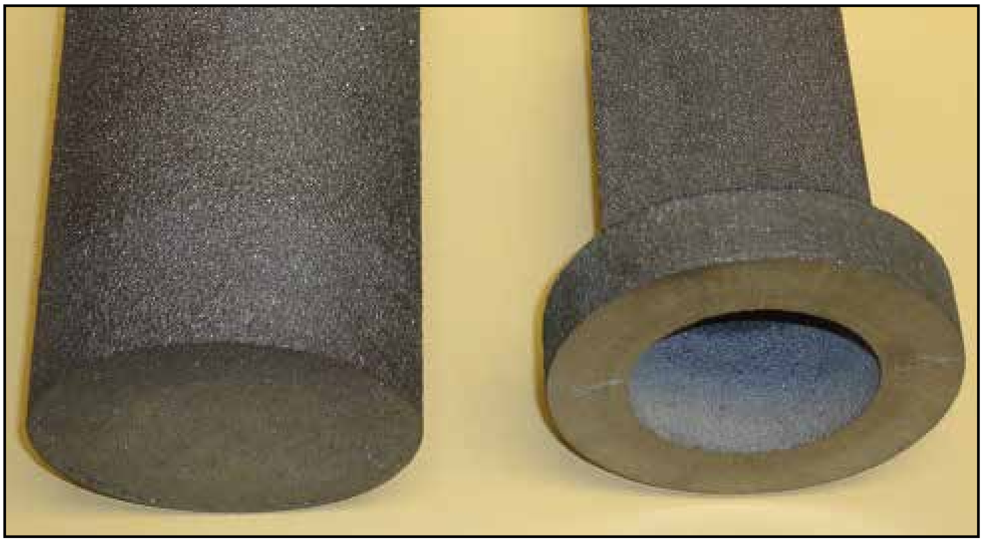

INEX COMPOSITE RADIANT TUBES	
Material Property	Data
Bulk density	2.85 g/cm^3
Apparent porosity	0%
Modulus of rupture	78 MPa
Compressive strength	580 MPa
Vickers hardness	SiC 25.000 MPa Si 9.000 MPa
Thermal expansion coefficient (20 -1000°C)	4.2 x 10^{-6} /°C
Thermal conductivity @ 100°C @1280°C	160 W/mK 24 W/mK
Specific heat @ 25°C @1280°C	600 J/kgK 1200 J/kgK
Maximum application temperature	2450°F (1340°C)

metal-alloy replacement. In addition, there is the cost of repair labor, and the lost opportunity to make money while the furnace is down. INEX radiant tubes offer a tremendous advantage to heat treaters."

Additionally, the material properties of Si-SiC allow more effective heat transfer, resulting in productivity gains of 25 percent and more. "The general rule of thumb in the industry is to limit heat flux to 55 BTU per square inch per hour for metal-alloy tubes," Kasprzyk said. "Si-SiC composite material is routinely used at 110 BTU per square inch per hour and higher, transferring twice the heat. That, in turn, means that the load can be ramped-up to temperature much more quickly, leading to a significant increase in throughput. In other words, more work can be done using the very same furnace. You can attempt to do the same thing with nickel-chrome alloy, but the tube life is drastically shortened. Si-SiC tube life is unaffected by its much higher heat release."

While INEX's radiant tubes are considered a premium replacement for existing metal-alloy products, Kasprzyk points out that the actual life-cycle cost is significantly less — especially when the productivity benefits are considered.

"Tube failure often ruins a furnace load, resulting in downtime, late deliveries, and costly metal-alloy replacement."

Additionally, INEX tubes are less costly than both domestic and foreign competitors offering other SiC radiant tubes thanks to its unique and cost-effective Si-SiC composite manufacture. That's a process-driven advantage. Replacing traditional metal-alloy tubes with INEX Si-SiC is a relatively simple process, as the tubes usually require only minor changes in mounting hardware.

"And there's not much we need to teach people about the product," Kasprzyk said. "Mostly users must consider that this is a brittle material — don't hit them with a hammer to make them fit. Other than that, there's not really a whole lot to retrofitting a furnace."

The greater challenge often comes in "opening the eyes" of furnace operators to the expanded opportunities of Si-SiC materials. "Everyone is accustomed to thinking they can only get so many pounds per hour or batches per day out of a furnace. We show them how they can get much more work done in the same time and footprint. Higher heat flux capability is key to furnace productivity and metal-alloy tubes cannot provide this."

INEX Inc. has nine employees at its offices and manufacturing facility in Holland, New York, and nearly 30 independent sales representatives throughout North America, Europe and Asia.

FOR MORE INFORMATION: Contact INEX Inc.'s composite radiant tubes, call (716) 537-2270, email inex@inexinc.net, or visit www.inexinc.net

Controlling Distortion in Heat Treatment Through Press Quenching

By Art Reardon

Press quenching is a specialized quenching technique that can be used to minimize the distortion of complex geometrical components during heat treatment. However, the success of this technique depends strongly on a large number of variables including the knowledge, skill, and experience of the machine operator as well as the prior thermal history of the material.

INTRODUCTION

Press quenching is a specialized quenching technique that may be utilized to minimize the distortion of complex geometrical components during heat treatment1. Distortion is routinely encountered in industrial heat treating operations, and is an especially important consideration where high accuracy, precision components are concerned. It can result from a wide variety of independent contributing factors. In press quenching these can include, among others:

(1) The quality and prior processing history of the material from which the part in question has been manufactured
(2) The prior thermal history and residual stress distribution contained within the part

(3) The generation of unbalanced thermal and transformation stresses induced by the quenching operation
(4) The grade of material and austenitizing temperature that is used
(5) Transfer time between the austenitizing furnace and the quenching machine
(6) The type, condition, quantity, and temperature of quenchant used
(7) Direction and selective metering of quenchant flow over the component
(8) Duration of the quench at various flow rates
(9) Locations of contact points on the component for applying external loads
(10) Magnitude of the forces applied for maintaining the required part geometry
(11) Proper quench die tooling design, set-up, and maintenance
(12) Pulsing methodology

DISTORTION ISSUES DURING QUENCHING

High precision components such as automotive spiral bevel gears and aerospace quality bearing races can often distort appreciably during open tank oil quenching. Press quenching can help to minimize the distortion of such components by utilizing specialized tooling for generating concentrated forces at key locations to constrain the movement of the component in a carefully controlled manner. It can be performed on a wide variety of components manufactured from both ferrous and non-ferrous based alloys. For example, a number of aluminum alloys are routinely press quenched. Common steel alloys that are press quenched include high carbon through-hardening grades such as AISI 52100 and A2 tool steel. Press quenching is particularly well suited for the processing of carburizing steel grades such as AISI 9310, 8620, and 3310.

Ideally, the transformation temperature should be the same throughout the entire cross-section of the component during quenching so that the material is capable of transforming in a uniform manner. However, in case carburized parts the martensite start transformation temperature (Ms) is not uniform throughout the entire cross-section of the part. During carburizing, a composition gradient is produced as carbon is diffused into the part surface. This results in a corresponding gradient in the transformation temperature near the surface that can promote or aggravate distortion issues in such components during quenching. Non-uniformities in the base material microstructure due to segregation or improperly normalized material can also contribute to this type of distortion. Thin walled components such as large diameter bearing races, are generally more susceptible to these distortion related issues than are relatively massive, compact geometries. Although press quenching cannot eliminate these effects, its use can help to minimize their contribution to the overall distortion that is produced during heat treatment.

The amount of distortion encountered depends strongly on the nature of the heat treating process that is used. In order to minimize distortion related issues during quenching, heat should be extracted from the component in as uniform a manner as possible. This can be difficult to achieve for parts that are designed with sudden changes in geometry with heavy or thick sections located adjacent to relatively thin sections on the same component. A good example of this is the teeth on a spiral bevel gear or pinion. The teeth have a greater surface area to volume ratio than the body of the gear or pinion, and due to their symmetrical nature and distribution the teeth have a tendency to distort by unwinding during quenching. As the work piece is submerged into the quenching medium, the teeth tend to cool and contract much more rapidly than the adjacent heavier sections. As a result of this varying quench rate, the teeth harden more rapidly and contract while the balance of the component is still in an expanded state. The outcome of quenching such components is the generation of temperature gradients and non-uniform transformation induced stresses. This particular issue can be addressed in press quenching by selectively directing the quenchant flow toward the thicker sections and baffling it away from the teeth in order to promote a more uniform quench. By implementing this important technique, lower levels of transformation-induced distortion can be achieved.

Figure 1. Example of a modern quenching machine. (Photograph courtesy of The Gleason Works, Rochester, NY).

PRESS QUENCHING MACHINES

A representative version of a standard quenching machine is depicted in Figure 1, and examples of the numerous parameters that may be adjusted during the course of a typical quenching cycle are shown on the machine's main control screen in Figure 2. During operation, the component to be quenched is removed from a separate furnace (usually a box, continuous rotary, or pusher type furnace) and is placed onto the

Figure 2. Control screen showing the various parameters that may be adjusted over the course of a typical quenching cycle. (Photograph courtesy of The Gleason Works, Rochester, NY).

Figure 3. Hot bearing race positioned on the lower die assembly of a quenching machine just before it is retracted into the machine for quenching. Note the segmented die tooling and individual slotted rings. The slotted rings may be independently adjusted to control the flow of oil over the part being quenched. (Photograph courtesy of The Gleason Works, Rochester, NY).

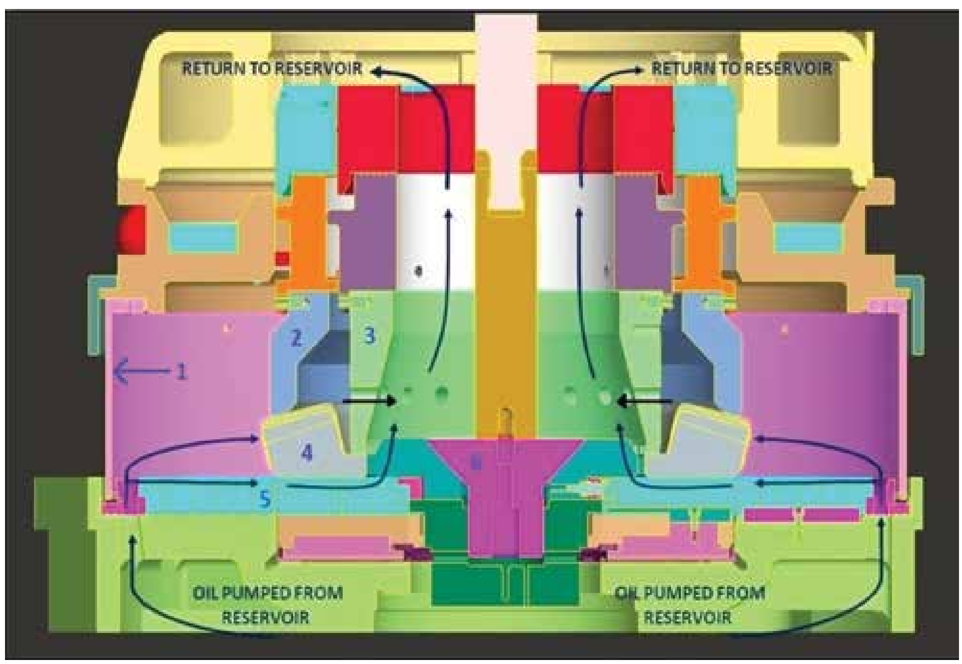

Figure 4. Schematic cross-sectional diagram illustrating the contact of the center expander and the inner and outer dies with the part during quenching. The various components labeled in the diagram are (1) the machine guard attached to the upper die assembly; (2) outer upper die; (3) inner upper die; (4) component undergoing quench; (5) lower die assembly; and (6) center expander cone. The oil flow path through the quench chamber is depicted by the flow line arrows. (Image courtesy of The Gleason Works, Rochester, NY).

tooling of the lower die assembly. A close up view of this die assembly is shown in Figure 3.

After the part is successfully loaded onto the lower die assembly, the machine is actuated and the part is retracted into the machine where it is centered below the upper hydraulic ram assembly. As the assembly descends the center ram actuates one or more internal expanders that make contact with the inner diameter of the component at the specified points to maintain roundness at these locations (see Figure 4). Each component of the ram assembly (the center expander, inner and outer dies) is controlled independently through three separate proportional valves. A predetermined pressure level is usually maintained by the expander throughout the quench cycle. The inner and outer dies are lowered to make physical contact with the upper surfaces of the component being quenched in order to control alignment, dish, and part flatness during the course of the quenching cycle. The flow of quench oil is then activated to quench the part.

Figure 4 illustrates an example of a quench oil circulation path that can be established within the quenching chamber. Oil is pumped into the quench chamber through apertures around the outside diameter of the lower die. As the chamber fills up surrounding the component, oil flows out of the top. If the tooling is properly designed, the direction of oil flow over the component can be adjusted to obtain the best overall results. The elongated apertures at the exit may be adjusted to restrict oil flow, or may be fully opened to maximize flow depending upon the requirements for the part in question. The lower dies are constructed from several different concentric slotted rings that may be rotated to provide full flow or to restrict oil flow to the underside of the part. These particular features can be finely adjusted to help minimize the degree of distortion attributed to uneven heat removal during quenching. Timed segments during the quenching cycle can also be utilized to vary both the oil flow rate and duration in

order to establish a well defined quenching recipe for a specific part design.

The oil quenching process itself may consist of up to three general stages: (1) the initial vapor blanket stage where the first oil to come in contact with the part is instantly vaporized and forms a vapor barrier that surrounds the part and acts as an effective thermal insulting layer; (2) the vapor transport stage where oil breaks through the vapor blanket resulting in more rapid heat transfer; and (3) the liquid stage where heat extraction occurs predominately by convective heat transfer. In order for uniform heat extraction to occur during the initial stages of quenching, the oil flow rates must be sufficient to prevent the formation of a vapor blanket. If vapor bubbles are allowed to form in areas around the surface of the component, uneven heat extraction will result that can lead to unacceptable hardness variations and distortion. After this initial quenching stage has been successfully eliminated, lower quenchant flow rates may be safely tolerated. The quenchant flow rate profile that is ultimately established for the part in question must be carefully selected so that the hardness and geometry requirements are satisfactorily met. Too slow of a quench rate will result in a slack quench, undesirable transformation products, and hardness variations. Too rapid of a quench rate could result in cracking and/or unacceptable part distortion. The establishment of an oil flow path around the part and selection of the proper oil flow rate are often determined using a trial and error process. Success frequently depends upon the knowledge, experience, and skill of the machine operator.

The average oil temperature for most press quenching operations typically falls somewhere within the range of approximately 75°F to165°F, depending upon the material in question, the nature of the quenching operation, the type of quench oil being used, and post heat treat property requirements. Average quench oil temperatures exceeding 140°F should generally be avoided as a precaution to prevent damage to the machine seals that are used to contain the quench oil. Proper and routine maintenance of the quench oil bath is an often neglected aspect of the press quenching process and can lead to unexpected variations in the hardening response of the materials processed in these types of systems. As the quench oil continues to be used, the oil additives gradually break down, and fine particulates can accumulate over time even if the oil is continuously filtered. If left undetected, this can lead to accelerated quench rates which can compromise the integrity of the oil quenching process.

A specific die tooling design configuration and machine set-up is required for each component that is press quenched. The use of expanding segmental dies are often employed to maintain bore size and roundness in bearing races and gears. If a component possesses a bore diameter that is physically too small to accommodate these segmental dies, a solid plug could be used instead to control the diameter and taper of the bore. The plug would simply be removed after quenching. When there are different locating surfaces on the lower die assembly it is

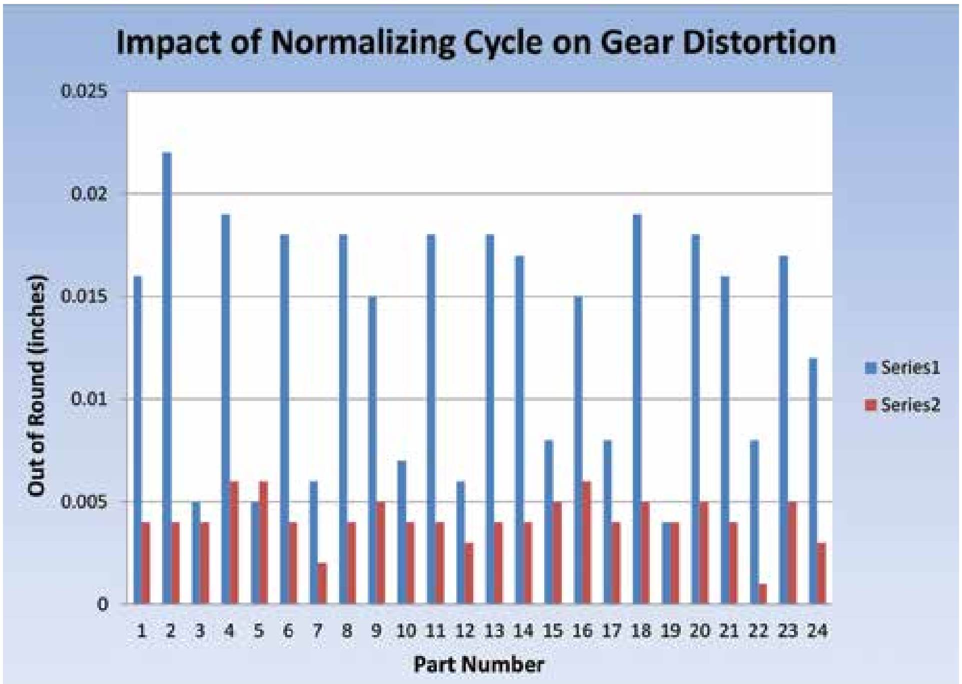

Figure 5. Out of round measurements on two different groups of case carburized AISI 8620H gears after press quenching and tempering. These gears originally measured approximately 13.75 inches in diameter. There were 24 gears evaluated per group, and each group was normalized using different cycles (see the text for a description of these cycles). The numbers that appear on the horizontal axis in this chart each represent two gears; one gear randomly selected from Series 1 (blue) and one gear randomly selected from Series 2 (red). Note the dramatic improvement in out of round on the Series 2 gears.

imperative that the dimensions between these surfaces be held to a close tolerance from piece to piece. Failure to adhere to this rule may result in unwanted distortion and/or inconsistent results. Contracting dies are also available to maintain the geometrical tolerances for the outside diameter of components where this is a critical factor. A good example of this are gears that incorporate thin web sections in conjunction with relatively heavy sections for gear teeth, bosses, and bearing diameters. Gears used in aerospace applications such as helicopter gear assemblies often incorporate several of these features which may cause them to contract unevenly during quenching. This problem can be effectively remedied by the application of compressive loads on the outside surface of the component during press quenching.

It should also be noted that the inner and outer dies are typically pulsed during quenching to maintain the geometry of the part and to minimize distortion. The pulse feature periodically eases the applied pressure exerted by the inner and outer dies, allowing the component to contract normally as it cools while still maintaining

“Press quenching can help minimize distortion by using specialized tooling to generate concentrated forces at key locations to constrain component movement in a controlled manner. It is used on a wide variety of ferrous and nonferrous components.”

the desired part geometry. If this feature was not incorporated (and on some of the older machines it isn’t available), the stresses that would be induced from frictional contact between the die assembly and the component would not allow it to contract normally as it cools. Pulsing effectively reduces this frictional contact, and avoids distortion related issues due to eccentricity and out-of-flatness. The pulsing technique keeps the dies in contact with the part throughout the entire quenching cycle, but allows the pressure to be released and then re-applied approximately every two seconds. The inner and outer dies are typically cycled in this manner. However, the expander pressure is not normally pulsed.

CASE STUDY

The dimensional tolerances achieved during quenching are strongly dependent upon the various factors that can contribute to part distortion, as mentioned previously. The prior thermal history and residual stress distribution contained within the part can contribute significantly to distortion related issues during heat treatment, and this is certainly true during press quenching, as well. A case study that clearly illustrates this point was conducted on a number of automotive gears that were manufactured from AISI 8620H, a chromium-nickel-molybdenum case carburizing steel that is commonly designated for use in gearing applications. The outside diameter of these machined gears measured approximately 13 3/4 inches prior to austenitizing and press quenching. They were processed on two separate furnace loads. For the first set of gears, which were designated Series 1, the normalizing temperature that was used was 1700ºF. These gears received a single normalizing cycle. The second set of gears, labeled Series 2, was normalized twice in succession. The first normalizing cycle they received was identical to that used for the Series 1 gears. For the second normalizing cycle, the temperature was raised to 1750oF. Each group of 24 gears was subsequently processed through a gas carburizing furnace using an endothermic atmosphere at a temperature of 1700ºF to generate effective case depths in the range of 0.040 to 0.055 inches. The gears were all cooled to room temperature after carburizing was completed. They were then reheated to the austenitizing temperature of 1570ºF, and individually press quenched.

The resulting distortion that was measured on the outside diameter of these gears in terms of out of round is shown in Figure 5. Examination of this chart reveals that the gears normalized once at 1700oF (Series 1) exhibited substantially greater amounts of distortion in terms of out of round than the gears which were normalized twice using a final temperature of 1750ºF (Series 2).

SUMMARY

Press quenching is a specialized quenching technique that may be utilized to minimize the distortion of complex geometrical components during heat treatment. It is a versatile and time proven technique that can accommodate a wide variety of material grades and component geometries. The success of this technique depends strongly on a large number of variables. Some of the more important among these variables include the knowledge, skill, and experience of the machine operator. In this investigation, the prior thermal history of the material was also demonstrated to be an important, and often overlooked, variable, as well.

REFERENCES

1. Arthur C. Reardon, “Press Quenching”, in ASM Handbook, Volume 4a, Steel Heat Treating Fundamentals and Processes, J. Dossett and G. Totten, Editors, ASM International, Nov. 2013

ABOUT THE AUTHORS: Dr. Reardon is currently employed as the Corporate Metallurgist for The Gleason Works in Rochester, New York. He earned his bachelor’s degree in physics and mathematics in 1986 at the State University of New York College at Oswego, and later earned his M.S. in mechanical and aerospace sciences, and his Ph.D. in materials science at the University of Rochester. He is an experienced professional in materials science, engineering, and metallurgy with extensive experience in research and development, alloy design, process metallurgy, mechanical engineering, material selection, and customer technical support. Dr. Reardon has worked in industry for over 20 years; more than ten years were spent working as a senior process metallurgist in the steel production industry where he led projects in the melting, forging, rolling, finishing, and inspection operations. In this role he also provided metallurgical support for the annealing and heat treating operations; this included processing of a large number of 300 and 400 series stainless steels, valve steels, tool steels, high speed steels, and a variety of other specialty steel grades. He worked closely with the members of R&D on the design and development of state-of-the-art alloys using both traditional air-melt and powder metallurgy processing techniques. Dr. Reardon also worked as an Adjunct Assistant Professor in the L.C. Smith College of Engineering at Syracuse University where he taught a junior level engineering course entitled Materials, Properties, and Processing for nine consecutive years. He earned his professional engineering license in the discipline of metallurgy, and is licensed in the states of Colorado, New York, Pennsylvania, and Wisconsin. He has numerous technical publications in refered scientific journals spanning subjects from low temperature physics and fracture mechanics to the simulation of atomic solidification processes, laser theory, and astrophysics. He has been a member of ASM International since 1988, and currently serves as a member of the ASM International Technical Books Committee. He authored the chapter on press quenching that appears in the ASM Metals Handbook Volume 4a. He also authored the book Metallurgy for the Non-Metallurgist, second edition, which was published by ASM International in November of 2011. This book received the prestigious award of Outstanding Academic Title by Choice Magazine in January 2013, and is currently in its fourth printing.

Producing Quality Parts in an Atmosphere Furnace: How to Optimize Your Quenching and Carburizing Processes

By Aymeric Goldsteinas and Rene Alquicer

Heat treatment plays a crucial role when adding value to the parts produced. When used properly, the carburizing and quenching processes can help achieve ideal results in atmosphere furnaces.

Throughout the manufacturing process, heat treatment is consistently viewed as a critical step for adding value to the parts produced. A part expensively manufactured by melting, hot rolling or forging, annealing, rough machining, teeth cutting and grinding is of little or no value without final heat treatment to produce the required metallurgical and mechanical properties. Additionally, without reliable, repeatable heat treatment, it is impossible to achieve competitive overall manufacturing costs.

The cost for a manufacturing step that adds such a high value is only a fraction of the total production costs – generally about 5 percent. However, this increases to about 15 percent of the costs per part if post-treatment process steps such as cleaning, blasting, straightening, and grinding are taken into account. Therefore, a noticeable reduction of manufacturing costs is only possible by minimizing the distortion of parts. Factors that influence distortion, such as melting, forming, uniformity of microstructure and hardness, positioning of parts in the heat treat load, uniformity of heating, carburizing, and heat extraction during quenching, must be optimized to consistently produce quality parts in batch atmosphere furnaces.

Producing quality parts requires properly carrying out the carburizing and quenching processes and using applicable modern technology. From optimizing controls and quenching systems to the benefits of establishing temperature and gassing uniformity, here are some tips highlighting how to make the most of your processes and atmosphere furnace.

CARBURIZING: THE IMPORTANCE OF UNIFORMITY

Gas carburizing in atmosphere furnaces and low pressure carburizing in vacuum furnaces are commonly used industrial carburizing processes, both with the same aim of uniformly carburizing all parts in a workload to the same surface carbon content and to the same case depth.

Atmosphere carburizing consists of different process steps. It is necessary to understand these steps to achieve repeatable, uniform carburizing:

- **Gas reactions:** generation of carburizing gas components in the furnace atmosphere
- **Convective gassing:** transport of carbon-containing molecules in the gaseous phase to the component

ATMOSPHERE Q&A – A FIRSTHAND LOOK AT IPSEN'S ATLAS

Q: Ipsen's newest atmosphere furnace is the ATLAS single-chain model. What type of atmosphere furnace is the ATLAS, and what does that mean for users?

A: Ipsen's single-chain ATLAS is a batch-type, integral-quench furnace. This single-chain, in-out-style furnace has a load size of 36" x 48" x 38" (W x L x H) and features all of the ATLAS's latest technological advantages, as seen in Figure 1. The single-chain model is configured for maximum compatibility and utilizes the same push-pull chain loader as the industry standard, allowing it to integrate into existing lines for any brand of atmosphere furnace with ease.*

When it comes to the atmosphere furnace market, Ipsen has always been a strong leader with one of the largest atmosphere furnace installation bases in the U.S. – several thousand since we were founded in 1948. In fact, our founder, Harold Ipsen, was a pioneer in the development of integral-quench, batch-atmosphere furnace technology.

Fig. 1: Ipsen's ATLAS – a single-chain, in-out-style batch atmosphere furnace

Although we have an established atmosphere base, Ipsen believes that innovation drives excellence. For Ipsen, a key part of innovating is listening to the specific needs and challenges of our customers and then providing ideal solutions that meet those needs. As we focus on the continuous improvement of our atmosphere products, we have dedicated significant resources toward gathering input from our customers and heavily researching industry needs.

This focus and research – as well as our experienced team of engineers working on research and development – allow us to tailor our products and services so we can provide our customers with optimum equipment they can trust and rely on for full-scale solutions.

Q: Where is the ATLAS single-chain model manufactured for the North American market?

A: The ATLAS single-chain model is manufactured in the United States at our facility in Cherry Valley, Illinois. Our extensive U.S. Field Service network provides support for atmosphere heat-treating furnaces, including parts, service, retrofits, training and more.

Q: What are some of the advantages of manufacturing the ATLAS single-chain model in the United States?

A: One of the main advantages is providing our customers with prompt, timely service and support. When customers are deciding on what equipment to invest in, we've found one of the factors they consider is the location of the manufacturing and service network facilities.

With locations across the United Sates, we're able to deliver spare parts, perform maintenance and more, all while minimizing companies' downtime. In addition, our comprehensive on-hand stock inventories comprise more than 2,000 items, ensuring our customers quickly receive the required parts and components needed to maintain their heat-treating equipment.

Q: Does Ipsen offer entire atmosphere systems?

A: Yes, Ipsen's batch furnace systems are comprised of several components – sealed-quench furnaces, temper furnaces, washers and loaders. These complete atmosphere systems provide users with a high level of flexibility as they can execute different thermal processes in each sealed-quench furnace, as well as expand the system for larger production needs and future increases in demand.

Q: What are a few of the ATLAS's unique features?

A: If I had to sum it up, I would say the ATLAS's most unique core features include:

- The ability to integrate into existing atmosphere furnace lines (any brand)*
- Intelligent controls with predictive process capabilities – Carb-o-Prof
- A compact footprint
- Ease of maintenance, thanks to a plug-type heat fan assembly, shelf-mounted quench oil heaters and oil circulation pump, safety catwalks and more

- An efficient combustion system, which provides energy and cost savings
- Variable speed quench agitation, allowing users to achieve and maintain better quenching control
- Uniform quenching, resulting in minimized distortion and high part quality

Q: How do you consistently get good results out of your equipment?

A: Well, first it's important to understand there are several factors that contribute to high-quality parts – the biggest is temperature uniformity. This is why we engineered the ATLAS to efficiently maintain:

- Temperature uniformity
- Atmosphere uniformity
- Uniform quenching
- Precise and consistent control of the carbon potential

Q: You mention that the ATLAS provides uniform quenching. Can you expand on this?

A: Achieving uniform quenching can only be accomplished with a sufficient and uniform flow of oil around the part. To accomplish this, you need an efficient quench system design.

As such, the ATLAS features TurboQuench™, a modern oil-quenching system with an agitation system that produces a uniform and adjustable flow of oil throughout the load. By using high oil flow velocity, users can achieve a uniform cooling rate on the part's entire surface area, resulting in uniform surface and core hardness with low distortion.

Q: In summary, when working with batch atmosphere furnaces – such as Ipsen's ATLAS – what are some of the most essential things to consider?

A: hen working with batch atmosphere furnaces – especially when you are carburizing – it's essential that the furnace is capable of:

- Achieving tight temperature uniformity
- Maintaining consistent carbon potential
- Quenching uniformly
- Controlling the quench rate

Why is this important? Because having these capabilities allows you to be more competitive by consistently and economically producing high-quality parts with reduced distortion.

*Compatible with most single-chain, in-out-style atmosphere furnace lines

- **Diffusion transport:** transport of carbon-containing molecules through the boundary layer (v = 0) at the component surface
- **Dissociation and adsorption:** dissociation of molecules at the component surface
- **Absorption:** taking up of carbon by the component surface
- **Diffusion:** transport of carbon into the component

There are various gas reactions that occur in the carburizing atmosphere. Taking into consideration the steps listed above, ideal carburizing conditions exist when temperature and gassing uniformity, flow over the components, and fast reaction kinetics occur evenly throughout the treatment chamber. Achieving ideal conditions in these areas positively influences carburized component quality.

How to Ensure High-Quality Parts: Temperature Uniformity

A uniform temperature is essential for ensuring the production of quality parts with the required carburized depth. Efficient batch atmosphere furnaces, such as the Ipsen ATLAS, should maintain a temperature uniformity of at least ±13 °F (±7 °C) in the heat chamber. This ensures that all parts in the load are at the required austenitizing temperature upon completion of the heating phases.

Efficient burners – like Ipsen's Recon III Burners – can enhance the heating in batch furnaces. These burners are single-ended recuperative tubes (SERT) fitted with special ceramic inner tubes. The burners increase thermal efficiency up to 75 percent by recovering heat from exhaust gases and reducing time to recovery of the hot zone temperature. With low noise levels, high durability, low maintenance, and easy installation, these modern burners provide ideal heating while optimizing gas consumption. Reliability comes from excellent furnace design. For example, if one of the burners is down in the middle of a cycle, the other burners are adaptive and compensate to maintain excellent uniformity throughout the chamber.

However, achieving temperature uniformity is not possible without improved gas flow over the components. This requires a well-planned circulation system to achieve excellent flow around components and, thus, maintain temperature uniformity.

How to Ensure High-Quality Parts: Gassing Uniformity

PPositive convective properties produce excellent temperature uniformity within the load area, improved heat transfer to the load and homogenous process atmosphere. Figure 2 illustrates how the combination of minimum temperature deviation within the load area and homogenous process atmosphere results in minimized case depth deviations throughout the load.

CARB-O-PROF® – BOOSTING EFFICIENCY WITH INTELLIGENT CONTROLS

Ipsen's Carb-o-Prof combines more than six decades of knowledge and expertise in a single controls system, and it is specially designed for the computation and execution of the complete carburizing and quenching cycles, as well as other heat treatment processes. Overall, it provides the flexibility needed to measure and analyze your equipment and processes with ease. This analysis can be used to refine and adjust the settings and parameters of your equipment to enhance your process, thus improving part quality.

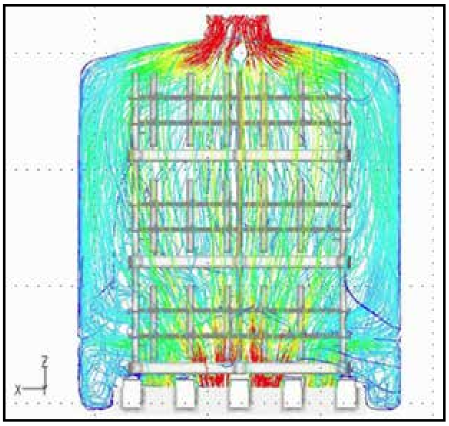

Fig. 2: Representation of the fluid flow lines in a treatment chamber

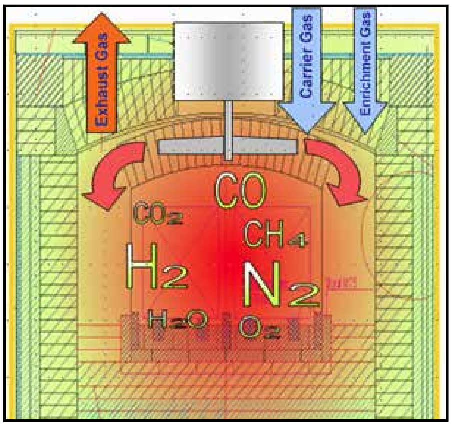

Fig. 3: A furnace atmosphere during gas carburizing

The unique, reliable software consists of user-friendly, flexible controls and straightforward user prompts and color menus. Other features include an extensive recipe database, an adaptive C-profile control and a time- and cost-saving simulation function.

RECIPE DATABASE

Programmed with hundreds of available recipes, the database allows the most important recipe information to be registered via a quick, simple input. Faulty inputs are prevented by appropriately limiting the input range, thus maintaining a safe operation and avoiding excessive consumption. As a result, recipes are generated in an easy, consistent manner that focuses on the carburizing/hardness results and prevents input errors.

SIMULATION WITH C-PROFILE OPTIMIZATION

A standard feature of Carb-o-Prof is its simulation function. Essentially, it computes the material's expected carbon profile according to the entered parameters and displays the results in both tabular and graphical forms, as demonstrated by Figure 5. The profile can then be reevaluated and parameters adjusted if necessary. This allows users to review process results for their specific load immediately after generating the potential recipe, all without having to carry out the actual run. Without having to run a test load beforehand, no valuable parts, time, and resources are wasted.

C-PROFILE CONTROL

Using pre-specified target parameters, such as surface carbon content, carburizing depth, and core carbon content, Carb-o-Prof defines a target carbon-content curve in the shape of a smooth S-form. As a result, parts in the same load have both consistent case depth and hardness, which is repeated load after load.

Fig 5: Example of a simulated test run conducted using Carb-o-Prof software.

Continuous introduction of carrier gas and controlled additions of the enriching gas result in a furnace atmosphere capable of producing carburized parts with the specified weight percent of surface carbon and to the specified case depth with highly repeatable results, as shown in Figure 3.

Intuitive control software, such as Ipsen's Carb-o-Prof system, assists in maintaining balance by regulating, documenting, and archiving the carburizing process in atmosphere furnaces. In the instance of a power outage or other unforeseen events, the software adapts the process to the changing circumstances, preventing the potential waste of parts and resources. Even before processing a load, users can generate a potential recipe and immediately review process results using the advanced simulation software.

Specifically, the software monitors and controls uniformity of the carbon level in the atmosphere which, through supervision, maintains a tolerance of ±0.05 % C for the

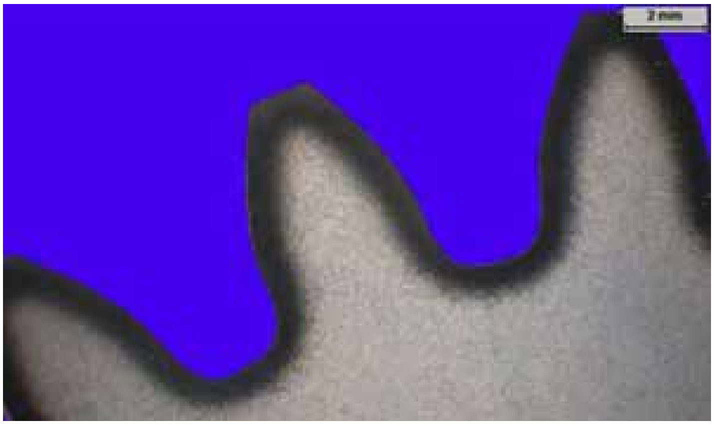

Fig. 4: Uniform surface carburizing of a gear wheel

workpiece surface carbon content. This consistency of the atmosphere's carburizing effect results in uniform carburizing of the surface layer, as shown in the example of a gear wheel in Figure 4.

When striving for uniform carburizing, it is important to remember that temperature and gassing uniformities are interrelated because it is difficult to meet one parameter without influencing the other. Beyond temperature and gassing uniformity, the next critical step is optimizing the quenching process.

Quenching – The Importance of Oil Flow

Older quench systems for batch atmosphere furnaces used to possess little flexibility in varying the quench intensity. Experience shows that optimizing and producing a uniform quench in oil is possible. The implementation of these techniques produces a more uniform hardening of parts – especially gear components – with improved microstructure and reduced distortion. Adapting the quenching intensity of quench systems to meet the requirements of different components – specifically hardenability and minimal distortion – have also led to the increased production of quality components.

Modern oil quenching systems, like Ipsen's SuperQuench and TurboQuench™, have an all-encompassing agitation system, which produces a uniform oil flow through the load section, as well as uses an adjustable oil flow rate. In addition, using the timing control of the agitator enables the achievement of a cooling curve closer to the ideal cooling curve, as seen in Figure 6. This feature increases the efficiency and flexibility of oil-quench systems and makes hardening of low-alloy materials and thicker cross sections possible.

In addition, the realization of complex quench cycles is easily done with the proper control software. The program creates a quench cycle by assessing section size, material type, load density, temperature, and the type of quench oil.

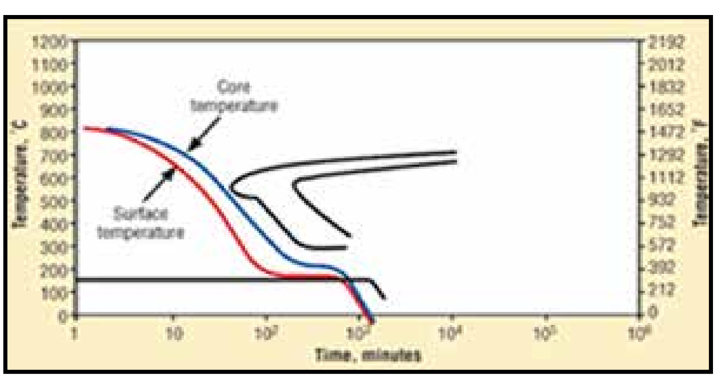

Fig. 6: Representation of an ideal cooling curve with a high cooling rate to start and a cooling rate reduction when entering the martensitic phase.

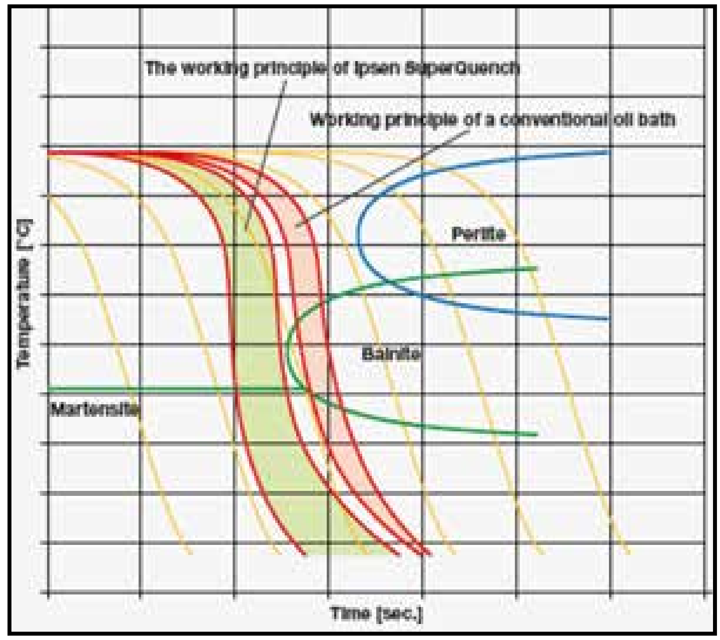

Fig. 7: Comparison of SuperQuench's working principle (left) to that of a conventional oil bath (right)

How to Achieve Ideal Quench Speed and Heat Extraction

The goal of uniform heat extraction over the entire surface of the part is only possible with an equal flow of oil around the entire part. While this situation is possible with simple parts, it is difficult with complex part geometries, yet still achievable with an efficient quench system.

It is important to be aware of the vapor phase, also known as the Leidenfrost effect. This phenomenon occurs when a liquid in near contact with a mass significantly hotter than the liquid's boiling point forms an insulating vapor film that keeps the liquid from boiling rapidly. As the vapor film randomly breaks down, the nucleate boiling phase starts and is characterized by a high cooling rate. The final stage is the convection phase.

One way to prevent the difficulties associated with the vapor phase is by using media like salt and gas, which do not evaporate. However, their cooling rates in the upper temperature region are usually not sufficient for low-alloy and plain carbon steels. Therefore, the objective is to optimize oil quenching in such a way that it reproduces an ideal cooling curve.

Assuming use of a high-performance quench oil, which is typical in today's sealed-quench furnaces, a high oil flow rate best achieves a high, uniform cooling rate on the entire surface area of a part. This speeds up the breakdown of the vapor film in areas of less flow, producing a more uniform, faster quench.

Higher oil flow rates considerably improve the uniformity of heat extraction. Depending on the thickness of the part and the hardenability of the respective steel, the flow rate can also result in further improvement in part quality.

How to Reduce Distortion

Goals for a distortion-optimized quenching are:

- Uniform heat extraction over the entire surface of the part
- Uniform heat extraction on every part within a load
- Material- and part-adapted timing to control quench intensity

These goals are realized throughout the quenching cycle. The first part of the quenching cycle uses a maximum oil flow that quickly breaks down the vapor film and achieves high heat extraction in the nucleate boiling phase, which prevents the formation of ferrite and pearlite. The second

TURBOQUENCH™ – ACHIEVING PRECISION LOAD AFTER LOAD

Regardless of whether you are quenching bulk or very dense loads, Ipsen's TurboQuench™ system tackles even the most challenging alloy by reducing the spread of hardness values, thus maximizing the parts produced per load. With a vertical oil pump, four VFD-controlled agitators, eight oil heaters and an optimized plenum and baffle design, the TurboQuench system produces a uniform, adjustable flow of oil throughout the load. These comprehensive features ensure a reduced footprint, ease of maintenance, increased oil bath control and the ability to integrate into existing pits while maintaining the proper load-to-oil ratio.

Overall, the TurboQuench system allows the entire load to be reliably, uniformly, and quickly quenched, resulting in optimum quenching and minimal distortion. Paired with the efficient heating system of the ATLAS, the powerful but flexible TurboQuench system ensures users achieve precision, load after load, even for the most varied and demanding materials.

part of the quenching cycle reduces the cooling rate to allow temperature homogenization between the surface and core before martensite transformation starts. This equalizes thermal and transformational stresses, thus producing less distortion. As Figure 7 demonstrates, these modern innovative systems enable users to achieve optimized performance and produce quality components compared to a conventional oil bath.

CONCLUSION

When carburizing/through hardening and quenching parts in a batch atmosphere furnace, it is essential to achieve uniformity of temperature and gassing, optimize the flow over components and aim for ideal quench speeds and heat extraction by using various high-performance systems. This enables producing high-quality parts with reduced distortion, as well as achieving competitive overall manufacturing costs via heat treatment.

In addition, using modern technology enables users to achieve ideal end results for the carburizing/through-hardening and quenching processes. In the end, the enhanced design and control of such technologies, as well as using the tips provided to produce quality parts positively impacts your processes.

ABOUT THE AUTHORS: Rene Alquicer is Manager – Atmosphere Products. Rene Alquicer joined Ipsen in 2009 as an International Sales Manager for Latin America. Now, as Ipsen's Manager for Atmosphere Products, his primary focus is the development and sale of Ipsen's batch atmosphere product lines. Alquicer possesses a vast amount of experience, having received his bachelor's degree in mechanical engineering and his master's degree in international business from the Universidad De Las Americas in Mexico. He also spent 14 years working for international companies in varied roles, including mechanical engineering, project management and sales.

Aymeric Goldsteinas is Product Development Manager. Aymeric Goldsteinas joined Ipsen in 2009 as Product Development Manager where his primary focus is developing innovative furnace- and process-related solutions. Through his extensive work in vacuum carburizing, high-pressure gas quenching, hardening, sintering and more, he is able to provide in-depth technical support and expertly analyze industry trends. Goldsteinas received his doctorate from the National Polytechnic Institute of Toulouse (INP) in Grenoble, France and graduated from the University of Marseille in France with a master's degree in chemistry and technology. For more information contact Rene Alquicer at 800-727-7625, ext. 2695 (+1-815-332-2695) or Rene.Alquicer@IpsenUSA.com, or visit www.www.IpsenUSA.com.

A Time-Compressed Numerical Approach for Thermal Analysis of Preheating Process in Powder Metallurgy

By S. Slock and R. Shivpuri

Here, a numerical method is used to simulate a heating cycle of a powder material through the use of a solid continuum model. This time-compressed approach to thermal modeling can be useful to accurately predict the homogenization time required to reach a particular temperature and the powder densification.

INTRODUCTION

Recent developments have been made in the field of powder metallurgy of materials to obtain advanced properties as compared to conventional manufacturing of materials for various applications. Powder metallurgy offers several advantages like improved strength and dimensional stability resulting in near net-shape products. Development of powder metallurgy techniques has resulted in new primary and secondary fabrication routes for semi-finished products. Numerous consolidation methods have been implemented to produce components with superior microstructure and mechanical properties [1]. Properties and performance of these powder metallurgy components rely heavily on the type of manufacturing process selected. One such manufacturing process in powder metallurgy is solid-state sintering.

Solid-state sintering is a widespread technique used in the powder metallurgy of ceramics, metals, and superalloys. It is a phenomenon that involves densification of the powder at high temperatures below its melting point with or without

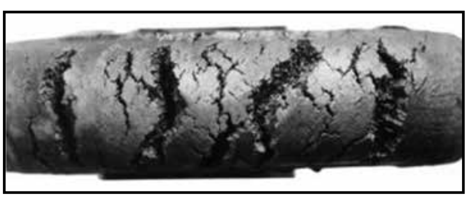

Figure 1: Surface cracks on nickel-based superalloy powder billet.

the application of external pressure to obtain a consolidated green compact with good strength [2]. This thermal treatment imparts strength and integrity. Sintering consists of three steps—the initial stage when neck formation begins, the intermediate stage when pores interconnect, and the final stage when pores become disconnected thereby forming a consolidated material [3]. Pressure-less sintering involves heating the powder to a high temperature for a long time such that the powder consolidates due to homogenized densification obtaining good green strength. The thermal evolution during pressure-less sintering depends on the inherent thermal properties of the powder such as thermal conductivity and heat capacity. In addition, densification is strongly dependent on the temperatures involved during sintering. These thermal properties are different for the powder as compared to bulk material [4]. Porosity in the unconsolidated powder has a major effect on the thermal and mechanical behavior. As these pores act as thermal insulators, the material in the powder form exhibits different heat transfer compared to a continuum bulk material with no pores. Heat transfer in porous media can occur by conduction through base material, convection from surrounding atmosphere and radiation through pores. Conduction is the dominant process of heat transfer during sintering in vacuum at relatively lower temperatures where radiation is not much [5]. Powder size and pore size also have an effect on the heat transfer. Finer powder has more surface area to volume ratio and hence would have better heat transfer resulting in enhanced thermal conductivity. Thus, it is important to analyze powder mesh size and distribution during preheating cycles as they affect thermal evolution and mechanical properties. In order to obtain homogenization in terms of heating and densification throughout the material, sintering time can take place for several days depending on the size and shape of the product. Hence, such manufacturing processes are time consuming and costly. Based on literature on sintering curves for superalloys (Graph 1), the accuracy of temperature predictions can be a determining factor to predict the densification of powder. Even a small variation in temperature prediction with respect to the real case can result in an incorrect densification prediction. Non-uniform temperature distribution, in the preheated component can, results in thermal stresses that lead to cracks near the outer surface as shown in the figure below (Figure 1).

As heat transfer takes place from the surface to core, the surface reaches the desired temperature much faster than the core. This results in a density variation as seen in the graph for superalloys (Graph 1). The surface tends to densify much faster than the powder in the core resulting in significant difference in mechanical properties. Powder consolidation and bonding occurs rapidly near the surface while the core is still unconsolidated and porous even after several hours of preheating. For example, in case of preheating IN718 superalloy powder billet in the temperature range between 1300°C and 1330°C, minute temperature difference between the core and surface can result in large variation in density ranging from 63% to 95%. This variation can lead to non-uniform mechanical properties that adversely affect the performance of the component. Thus, it is important to achieve homogenization throughout the powder component to obtain uniform thermal and mechanical properties

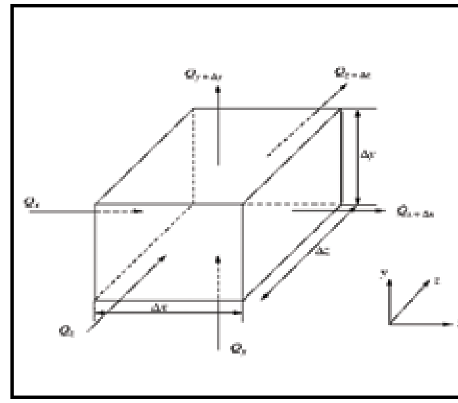

Figure 2: A differential control volume for heat conduction.

thereby eliminating critical defect issues arising due to inhomogeneity.

Hence, modeling and simulation of such processes are crucial to understand the sintering kinetics and effect of temperature on densification phenomena for various powder materials. This can help in determining optimum thermal treatments necessary for achieving uniform/desired properties for further processing. Models that represent and connect this discrete nature of particulate media to bulk continuum macroscopic properties can be useful in predicting how powdered materials behave during a sintering thermal cycle. Various thermo-mechanical equations have been developed that calculate thermal and mechanical properties of powder from bulk properties as a function of porosity correlating to experimental results [2]. Hence, it is important to understand the thermal behavior of powdered materials and develop computational models that can predict the thermal evolution accurately during sintering and provide results within few minutes while the actual process takes several days.

Prior computational applications explored the possibility of predicting the thermal behavior of a metal undergoing a thermal or thermo-mechanical working cycles. These kind of analyses represent the classical numerical calculation of thousands of processes and could be consid-

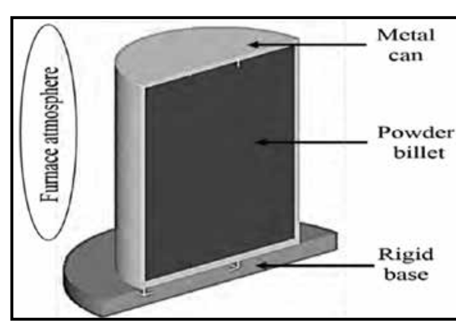

Figure 3: Cut section of powder billet filled in metal can.

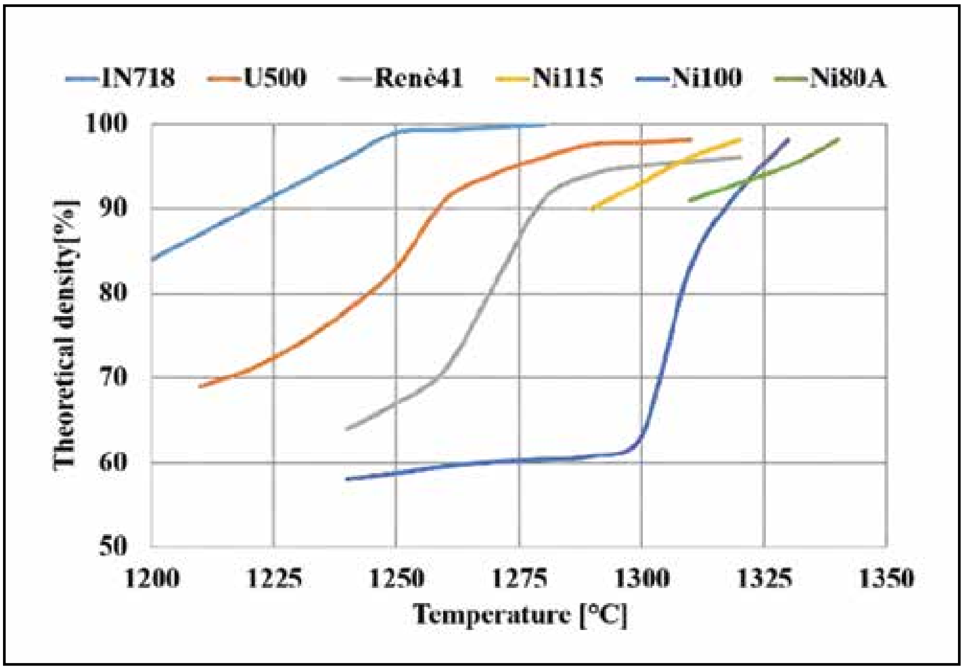

Graph 1: Sintering curves for different superalloys [1].

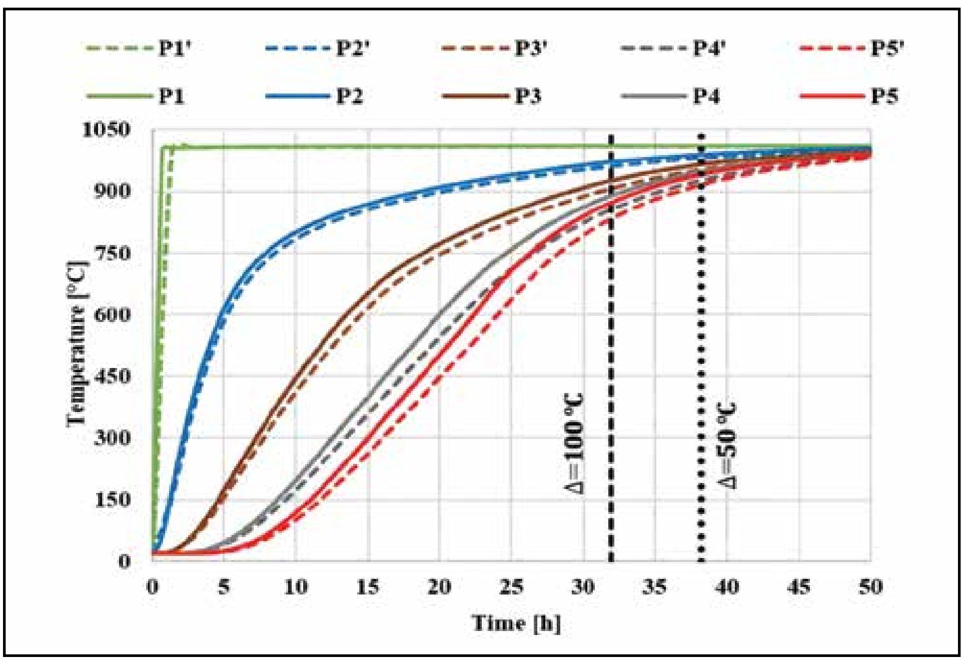

Graph 2: Temperature point tracking for radial points of billet comparing 70% (P1' to P5') to 100% density (P1 to P5).

ered like a standard in the actual state-of-art of FEM models. However, the classical numerical approach may create issues in terms of computational cost and time, especially when long processes are simulated. This severely limits the scope of investigations of critical physical mechanisms. A good help may come from the timestepping techniques, which allow the user to compress the real process time by means of simple mathematical considerations accelerating the temporal behavior of the material. In this case, it is possible to reduce computational time drastically maintaining a good quality of results and coherent physical characteristics of the solution.

The critical part is to explore and acquire proper knowledge to relate mathematical form of parameters within the numerical model to response of the code. It often happens that the governing equation depends on several factors with each one having its own weight inside the formula due to its dependence from linear or derivative forms. It means that a value change of a parameter can produce different effects on the final result of the computation because of different error sensibility of mathematical operators and their coupling.

Szabò [6] investigated the numerical solution of the one-dimensional heat conduction equation by applying Dirichlet and Neumann boundary conditions in order to obtain a good numerical result. The space was discretized by applying the linear finite element method while the theta-method was used for the time discretization. The core of the work was to select theoretically the correct time step size in FEM for the original physical phenomenon to be analyzed.

Tronel and Fichtner [7] focused on timestepping optimization during both coupled and non-coupled thermal and mechanical analysis. The timestepping optimization itself was described with its various possible variants and applied to solve numerical examples. The procedure allows the reduction of computation time by a significant factor when compared to standard uniform timestepping. The study reported in this paper is based on a simulation campaign having the aim of predicting the thermal evolution of a metal powder during a sintering process. This kind of industrial process takes several days to be completed and a quick numerical prediction is often needed to help select the desired process parameters.

The simulation campaign was conducted by using the time-compression method in order to obtain a reduction of calculation time. During the simulation campaign, the influence of different coefficients concerning the heat transport phenomena were studied with respect to accuracy of the numerical result, and the numerical issues arising from the FEM code. The aim of this study is to find the best way to simulate this kind of process without compromising the physics of sintering phenomena.

HEAT TRANSFER CALCULATION

Heat transfer is the section of science concerning the energy transportation between bodies having a temperature difference [8-11]. This energy transport is classified in three different mechanisms: conduction, convection and radiation and all of them are generally present in a real physical problem [12].

The aim of the calculation is finding the temperature distribution inside the material bodies undergoing to the heat exchange phenomena. The knowledge of temperature distribution within the material may be used to determine the thermal stress. By deriving the conduction equation inside a

Cartesian coordinates system and applying the energy conservation criteria to a differential control volume (Figure 2), the temperature distribution in the medium is obtained.

Once this temperature distribution is known, the heat flux at any point within the medium, or on its surface, may be computed by means of Fourier's law (Eq. 1).

$$q_x = -k\frac{dT}{dx} \qquad [1]$$

where k is the thermal conductivity. By applying the Taylor series expansion (Eq. 2), limited to first order, to the control volume (Figure 2) it results in the following:

$$\begin{cases} Q_{x+dx} = Q_x + \dfrac{\partial Q_x}{\partial x}\Delta x \\ Q_{y+dy} = Q_y + \dfrac{\partial Q_y}{\partial y}\Delta y \\ Q_{z+dz} = Q_z + \dfrac{\partial Q_z}{\partial z}\Delta z \end{cases} \qquad [2]$$

Considering heat generation in the control volume (Eq. 3).

$$G\Delta x\Delta y\Delta z \qquad [3]$$

and the rate of change in energy storage (Eq. 4)

$$\rho\Delta x\Delta y\Delta z c_p\frac{\partial T}{\partial t} \qquad [4]$$

where ρ is the medium density and c_p is the specific heat capacity, it is possible to write the thermal energy equilibrium of the control volume (Eq. 5).

$$\begin{gathered} G\Delta x\Delta y\Delta z + Q_x + Q_y + Q_z = \\ \rho\Delta x\Delta y\Delta z c_p\frac{\partial T}{\partial t} + Q_{x+dx} + Q_{y+dy} + Q_{z+dz} \end{gathered} \qquad [5]$$

Considering the Taylor series expansion (Eq. 2) the previous equation (Eq. 5) can be written as (Eq. 6).

$$\begin{gathered} G\Delta x\Delta y\Delta z - \frac{\partial Q_x}{\partial x}\Delta x - \frac{\partial Q_y}{\partial y}\Delta y - \frac{\partial Q_z}{\partial z}\Delta z = \\ \rho\Delta x\Delta y\Delta z c_p\frac{\partial T}{\partial t} \end{gathered} \qquad [6]$$

The total heat transfer in a tri-axial system can be represented as (Eq. 7).

$$\begin{cases} Q_x = -k_x\Delta y\Delta z\dfrac{\partial T}{\partial x} \\ Q_y = -k_y\Delta x\Delta z\dfrac{\partial T}{\partial y} \\ Q_z = -k_z\Delta x\Delta y\dfrac{\partial T}{\partial z} \end{cases} \qquad [7]$$

Considering heat transfer (Eq. 7) and control volume, the heat conduction equation for a stationary system in Cartesian coordinates can be expressed as below (Eq. 8).

$$\begin{gathered} \frac{\partial}{\partial x}\left[k_x\frac{\partial T}{\partial x}\right] + \frac{\partial}{\partial y}\left[k_y\frac{\partial T}{\partial y}\right] + \frac{\partial}{\partial z}\left[k_z\frac{\partial T}{\partial z}\right] + \\ G = \rho c_p\frac{\partial T}{\partial t} \end{gathered} \qquad [8]$$

In the previous equation k is the thermal conductivity of the considered material, which can be expressed as a following tensor (Eq. 9).

$$\begin{bmatrix} k_{xx} & k_{xy} & k_{xz} \\ k_{yx} & k_{yy} & k_{yz} \\ k_{zx} & k_{zy} & k_{zz} \end{bmatrix} \qquad [9]$$

The previous general form for thermal conductivity can be simplified by means of a one-directional form. This approach is common for such materials in which the thermal behavior is considered like isotropic. The equation below represents thermal diffusivity for isotropic materials (Eq. 10).

$$\frac{\partial^2 T}{\partial x^2} + \frac{\partial^2 T}{\partial y^2} + \frac{\partial^2 T}{\partial z^2} + \frac{G}{k} = \frac{1}{\lambda}\frac{\partial T}{\partial t} \qquad [10]$$

Where thermal diffusivity $\lambda = {}^{k}/\rho c_p$. For porous media with isotropic behavior, negligible effects come from radiative transfer, viscous dissipation and pressure work. By assuming the local thermal equilibrium and parallelism of heat conduction between solid and fluid atmosphere, as well as a constant porosity we can write the thermal transport equation for both the solid (Eq. 11) and liquid phases (Eq. 12).

$$(1-\varphi)(\rho c)_S \frac{\partial T_S}{\partial t} = (1-\varphi)\nabla \cdot (k_s \nabla T_S) + (1-\varphi) q_S^{vol} \qquad [11]$$

$$\varphi(\rho c_p)_F \frac{\partial T_F}{\partial t} + (\rho c_p)_F v \cdot \nabla T_F = \varphi \nabla \cdot (k_F \nabla T_F) + \varphi q_F^{vol} \qquad [12]$$

The subscripts *S* and *F* refer to the solid and fluid phases respectively, φ is the porosity of the material, *c* is the specific heat capacity of the solid phase, c_p is the specific heat at constant pressure of the fluid phase, *k* is the thermal conductivity, q_f^{vol} is the heat production per unit volume in W/m^3[9, 13] and *v*= φ*V* is the Dupuit-Forchheimer relationship. In this case, it can be observed that there is a linear relation between density and physical thermal properties.

If we consider same temperature for both solid and fluid phase in the previous equations (Eq. 11, Eq. 12) we obtain the following general equation (Eq. 13).

$$(\rho c)_M \frac{\partial T}{\partial t} + (\rho c_p)_F v \cdot \nabla T = \nabla(k_M \nabla T) + q_M^{vol} \qquad [13]$$

Where:

$$\begin{cases} (\rho c)_M = (1-\varphi)(\rho c)_S + \varphi(\rho c_p)_F \\ k_M = (1-\varphi)k_S + \varphi k_F \\ q_M^{vol} = (1-\varphi)q_S^{vol} + \varphi q_F^{vol} \end{cases}$$

FEM HEAT TRANSFER ANALYSIS

The basic equations and the FE formulation for heat transfer analysis arise from the energy balance equation that can be expressed for isotropic materials as below.

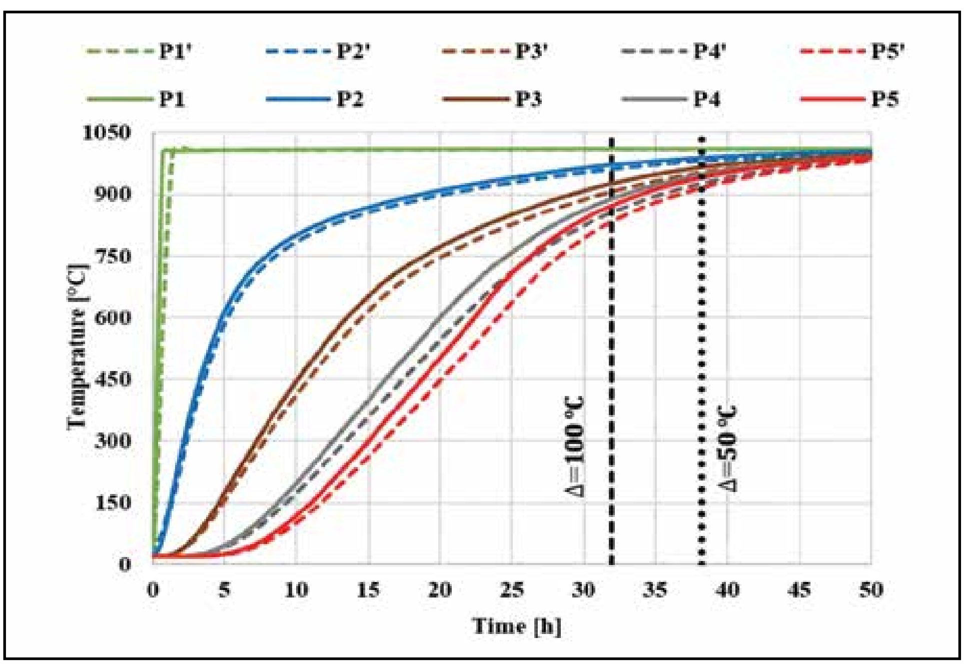

Graph 3: Temperature point tracking for axial points of billet comparing 70% (P6' to P10') to 100% density (P6 to P10).

$$K_s T_{,ii} + \dot{r} - \rho c_p \dot{T} = 0 \qquad [14]$$

Where K_s is the thermal conductivity, $T_{,ii}$ is the Laplace differential operator for temperature, $K_s T_{,ii}$ represents the heat transfer rate, $\rho c_p \dot{T}$ is the heat generation rate and the term represents the internal energy rate. The previous equation (Eq. 14) shows the general approach in case of thermo-mechanical analysis in which the heat generation coming from the plastic deformation (Eq. 15) has to be considered.

$$\dot{r} = K\sigma_{ij}\dot{\varepsilon}_{ij} \qquad [15]$$

In the previous equation (Eq. 12) *K* is the heat generation energy coming from that fraction of mechanical work transformed into heat. For metals, this portion is assumed as 90%, while the remaining 10% is consumed by the microstructural changes.

By using the divergence theorem and considering the volumetric integrals, the energy balance equation (Eq. 14) can be written as follows:

$$\int_V k_1 T_{,ii} \delta T dV - \int_V k\sigma_{ij}\dot{\varepsilon}_{ij}\delta T dV + \int_V \rho c_p \dot{T} \delta T dV - \int_{S} q_n \delta T dS = 0 \qquad [16]$$

Where S_q is the boundary surface and q_n represents the normal heat flux across that surface:

$$q_n = k_1 T_{,n} \qquad [17]$$

The previous equation can be solved only if the boundary temperature field (Eq. 18) is known.

$$T = \sum_{\alpha} q_\alpha T_\alpha = N^T T \qquad [18]$$

$$Q = \int_V k(\bar{\sigma}\dot{\bar{\varepsilon}})N dV + \int_{S_r} \sigma\xi(T_e^4 - T \ldots + \int_{S_t} h(T_e - T_s)N dS + \int_{S_c} q_f N \ldots \qquad [19]$$

The first term on the right side of the equation (Eq. 16) represents the heat coming from the plastic deformation work. The second term represents the heat coming from radiation of environmental medium, in which σ is the Stefan-

Boltzmann constant ξ and is the surface emissivity. The third term is the heat coming from convection phenomenon from the body surface to environmental medium, in which h is the heat convection coefficient. The last term is the heat transferred between bodies in contact [5].

The previous analysis is correct when bulk materials are used. However, for porous media, the energy balance equation has to be defined properly as below (Eq. 20).

$$k_R T_{R,ii} - \rho_R c_R \dot{T}_R + kY_R \dot{\bar{\varepsilon}}_R = 0 \qquad [20]$$

Where the subscript R denotes the equivalent quantities of a porous material within a continuum formulation, k_R and c_R apparent thermal properties derived from the bulk material. By assuming this hypothesis, it is possible to adopt the same mathematical procedure for non-porous materials as for a solid.

The physical behavior of porous material takes place by conduction through rigid base, and convection and radiation phenomena through pores. Depending on the size of pores, the convection can be considered as negligible while the contribution of radiation can be neglected if temperature is low. This signifies that conduction plays a major role.

However, porosity can have complex effects on thermal properties of the material and such aspects are studied extensively by assuming simplified hypothesis.

By assuming heat flow to be unidirectional, pore distribution equal in all directions and thermal properties homogeneous, Im and Kobayashi [14] proposed a linear equation linking the thermal conductivity of powder material to the base bulk material (Eq. 21).

$$\frac{k_R}{k_b} = 1 - \frac{(1-P)\left(1-\frac{k_v}{k_b}\right)}{1+\frac{k_v}{k_b}\frac{P}{1-P}} \qquad [21]$$

Here, k_R is the apparent thermal conductivity depending on both the volume fraction of pores and the thermal conductivity ratio between bulk material and air inside cavities; k_b is thermal conductivity of the base bulk material; k_v is thermal conductivity of the pores and P is the porosity of the volume fraction of voids. By introducing the apparent density p_R of porous material as well as its specific heat, c_R it is possible to obtain the internal energy change relation (Eq. 22)

$$\rho_R c_R V_R \frac{dT_R}{dt} = \rho_b c_b V_b \frac{dT_b}{dt} + \rho_v c_v V_v \frac{dT_v}{dt} \qquad [22]$$

p is the density, c is the specific heat, V is the volume and the subscripts R, b and v are related to porous material, base bulk material and pores respectively.

POWDER-BULK THERMAL RELATIONSHIP

As explained previously, this kind of analysis is related to the thermal physical properties of bulk base material as well as powder characteristics. In particular, the major thermal parameters are directly related to density value of powder when the considered material is assumed as isotropic. By following this logic, the simulation campaign was split into two main approaches for thermal analysis. The first one considers the billet as a powder having 70% packing density and a thermal characterization (in terms of thermal conductivity and heat capacity) of the bulk base material. The second one considers the billet as

bulk base material having 100% of density and a thermal characterization of the powder. Thermal data of the material for these two density cases was carried out by means of theoretical relationships, considering the following equations (Eq. 23) for calculating thermal conductivity and heat capacity of the powder material starting from the bulk base material and directly dependent on amount of porosity [4].

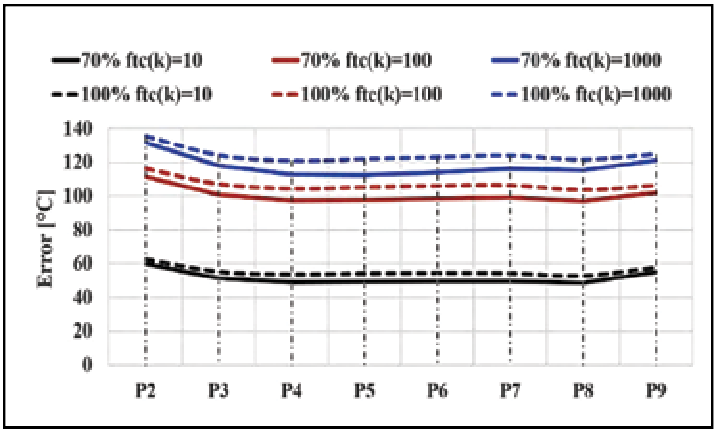

Graph 4: Average error for each point tracking of the simulation campaign with 70% and 100% density and compressed time as function of thermal conductivity k.

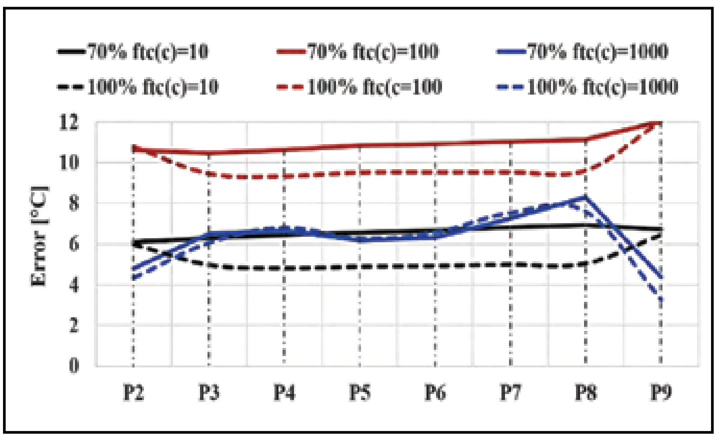

Graph 5: Average error for each point tracking of the simulation campaign with 70% and 100% density and compressed time as function of heat capacity c.

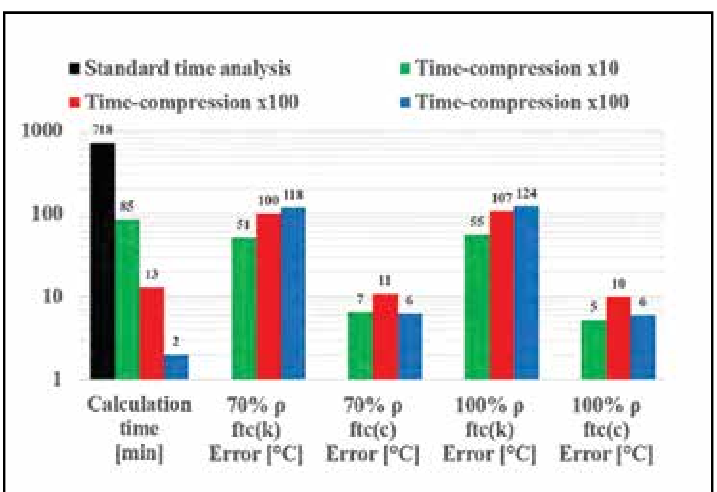

Graph 6: Comparison between benchmark simulation and time compressed campaign with 100% density and heat capacity time-compression factor.

$$\begin{cases} k_P = k_B \cdot (1-P)^{\alpha} \\ c_P = c_B \cdot (1-P)^{\beta} \end{cases} \quad [23]$$

Where:

- k_p is the thermal conductivity of the powder material;
- k_B is the thermal conductivity of the base bulk material;
- c_p is the heat capacity of the powder material;
- c_B is the heat capacity of the base bulk material;
- P is the porosity value of the considered powder material

α and β are coefficients depending on the material.

However, thermal conductivity and heat capacity of bulk material depend on temperature as shown in the following equation (Eq. 24).

$$\begin{cases} k_B = k_0 + k_1 T + k_2 T^2 \\ c_B = c_0 + c_1 T + c_2 T^2 \end{cases} \quad [24]$$

Where:

- k_0 is the thermal conductivity of the bulk material at room temperature;
- c_0 is the heat capacity of the bulk material at room temperature;
- k_1, k_2, c_1, c_2 are coefficients depending on the material.

Time-Compression Factor Determination

Each simulation was accompanied by the use of different level of time-compression in order to make the process faster by 10, 100 and 1000 times respectively. Each compression factor was obtained by simple mathematical considerations on energy balance equations (Eq. 10, Eq. 14) for pure thermal case. The Fourier equation (Eq. 10) was considered for and simulation objects (Eq. 25) and furnace atmosphere (Eq. 26) separately.

$$\nabla^2 T = \frac{1}{\lambda_{mat}} \frac{\Delta T}{\Delta t} \quad [25]$$

$$\nabla^2 T + \frac{G}{k_{furn}} = \frac{1}{\lambda_{furn}} \frac{\Delta T}{\Delta t} \quad [26]$$

Where λ_{mat} is thermal diffusivity of material when solid simulation objects are considered, while k_{furn}, λ_{furn} and G are thermal conductivity, thermal diffusivity and convection coefficient of furnace atmosphere respectively.

In the case of solid continuum objects, if real temperature variation ΔT_{real} is assumed to be equal to simulated temperature one ΔT_{sim} and Laplace spatial operator $\Delta^2 T$ is considered as constant (due to constancy of geometries), the Fourier equation (Eq. 25) can be written as below (Eq. 27).

$$\frac{\Delta t_{real}}{\Delta t_{sim}} = f_{tc} = \frac{k_{sim}}{k_{real}} \cdot \frac{\rho_{real}}{\rho_{sim}} \cdot \frac{c_{real}}{c_{sim}} \quad [27]$$

Where is the time-compression factor for simulation. In this way, a linear relation between simulated time and real time of the process is obtained. It is sufficient to change the value of diffusivity parameters inside the numerical code to obtain a speeding of simulated time with a compatible result with respect to standard time simulation. If density is the same for both standard (real) and compressed time (simulation) approach, the equation (Eq. 27) can be written as below (Eq. 28).

$$f_{tc} = \frac{k_{sim}}{k_{real}} \cdot \frac{c_{real}}{c_{sim}} \quad [28]$$

The equation above (Eq. 28) considers thermal conductivity having no dependence of temperature. However, thermo-physical properties of materials in general do have temperature dependence, as shown by thermal conductivity and heat capacity equation (Eq. 24).

When the same logic is applied to the furnace atmosphere (Eq. 26), it has to be considered that, due to the simulation ambient in which a heating atmosphere is simulated by means of boundary condition for the solid simulated objects, physical variables of furnace medium can be neglected. The only parameter that needs to be taken into account is the convection coefficient *G*, which regulates the energy flux per time unit. It means that, every time that a specific time-compression factor has to be used, the value of *G* has to be multiplied by the same factor in order to obtain the same amount of energy going into solid bodies during the simulation.

Thus, the time-compression method can be affected by changing *k*, *c* and *G* parameters. Considering that the time-compression method changes the ratio between temperature and time, the effect and the accuracy of results may vary as functions of thermal material properties, which can be constant, linear or quadratic functions of temperature (Eq. 24). Keeping in mind this dependence, the effect of thermal conductivity on accuracy of results was considered in the time-compression approach by using a linear dependence between f_{tc} , k , c and G as shown in the table below (Table 1) which summarizes the thermal parameter set-up for each time compressed simulation.

CASE STUDY

An experimental campaign* was conducted on preheating of a nickel-based superalloy powder with 60 - 80% packing density in order to find the optimal set-up for homogenization. Results were carried out by tracking the thermal evolution of powder with the help of thermocouples placed inside the metal can at different locations, as represented in (Figure 4). To replicate the thermal evolution of superalloy powder during this experimental process, a simulation campaign was carried out using the implicit lagrangian code DEFORM3D™ with a multi-body approach considering the main object (superalloy powder as billet) placed inside a metal can and in contact with a rigid base (Figure 3). The material of the can is assumed different with respect to the rigid base. The main objective of this simulation campaign was to calculate homogenization time required by superalloy powder during the preheating stage with the best ratio between quality of prediction and computation costs. It is well known that long preheating cycles are necessary for superalloy powders due to their thermo-mechanical properties, to achieve homogenization and green strength, especially for further processing involving large aerospace components[1]. In order to verify the capabilities of numerical code, the first approach in simulation was to model the powder like porous material using a continuum solid body having the same density of experimental powder and thermal properties of bulk material. The results of this first approach showed that the code was not able to match the thermal evolution observed during experiments. The reason for this discrepancy can be attributed to the in-built material definition. In fact, the experimental material data (in terms of thermal properties) captures the true physical nature and effects of powder size and distribution throughout the

can. Based on this experimental evidence, another approach in which the solid continuum body is modeled like bulk material having thermal properties of powder was considered. This new simulation required to know the thermal conductivity and heat capacity of powder material [4] and, based on experimental data, it was found that the considered superalloy powder showed a linear dependence of thermal properties on density (Eq. 23). The results of both 100% and 70% density simulations, in terms of temperature point-tracking in the same positions (Figure 4) of thermo-couples in the experimental test, showed a difference between the two cases with respect to radial (Graph 2) and axial directions (Graph 3). The full density simulation, in which the material has powder thermal properties, matched the thermal evolution of experimental can accurately. Hence, it was considered as the "benchmark" simulation.

The whole simulation campaign was carried out using the same numerical parameters, as below:

- Time step: 5 sec;
- Double symmetry plane;
- Min element size: 0.3 mm
- Max element size: 0.9 mm
- Billet mesh element number: 32770;
- Can mesh element number: 14200;
- Base mesh element number: 11700.

However, it is very difficult to run this kind of simulation in real time, as it requires a very long calculation time (days) with high calculation costs. In this scenario, it was useful to use the time-compression method to significantly reduce calculation time. This means that all simulation objects have to be considered with respect to the time-compression factor equations (Eq. 28). Depending on the thermal parameter selected to obtain a proper value, thermal conductivity or heat capacity c of all materials built in the model have to be modified. The same consideration has to be done for the convection coefficient G related to the furnace atmosphere and heat exchange coefficient H between each couple of simulated objects. The relation between these coefficients and time-compression factor is always linear, as shown in the table below (Table 1).

To simplify the simulation campaign chart (Table 1), all thermal parameters were grouped as shown in the following wording (Eq. 29).

$$\begin{cases} K' = k_B, k_C, k_{RB} \\ C' = c_B, c_C, c_{RB} \\ K'' = k_P, k_C, k_{RB} \\ C'' = c_P, c_C, c_{RB} \end{cases} \qquad [29]$$

- k_B is the original thermal conductivity of bulk material for the billet;
- k_P is the original thermal conductivity of powder material for the billet;
- k_C is the original thermal conductivity of the can;
- k_{RB} is the original thermal conductivity of the rigid base;
- c_B is the original heat capacity of bulk material for the billet;
- c_P is the original heat capacity of powder material for the billet;
- c_C is the original heat capacity of the can;
- c_{RB} is the original heat capacity of the rigid base.

NUMERICAL RESULTS AND DISCUSSION

The results of all simulations were compared to show the effects and consequences of each approach with respect to the benchmark simulation

Time – compression factor f_{tc}	Thermal parameters				
	Convection coefficient - G / Mutual heat exchange coefficient - H	70% density (Billet with bulk data)		100% density (Billet with powder data)	
		Thermal conductivity k	Heat Capacity c	Thermal conductivity k	Heat Capacity c
1	G, H	K'	C'	K''	C''
$10\,f(k)$	$10G,$	$10K'$	C'	$10K''$	C''
$10\,f(c)$	$10H$	K'	$10^{-1}C'$	K''	$10^{-1}C''$
$10^2 f(k)$	$10^2G,$	$10^2K'$	C'	$10^2K''$	C''
$10^2 f(c)$	10^2H	K'	$10^{-2}C'$	K''	$10^{-2}C''$
$10^3 f(k)$	$10^3G,$	$10^3K'$	C'	$10^3K''$	C''
$10^3 f(c)$	10^3H	K'	$10^{-3}C'$	K''	$10^{-3}C''$

Table 1: Simulation campaign matrix

(experimental result). In particular, the analysis was focused on the error between temperature predictions in the selected points (Figure 4). The final aim is to select the best way to simulate a long process like pre-heating of superalloy powder in few minutes without compromising on accuracy of predictions.

The following graphs represent the temperature evolution along radial (Graph 2) and axial (Graph 3) directions comparing standard time simulations for the case having 100% density with powder thermal data and 70% density with bulk material thermal data. This first comparison (Graph 2, Graph 3) is useful to show the difference in temperature prediction of the billet coming from the use of two equivalent computational logics.

Point-tracking coming from the use of 70% density material with bulk thermal properties differs from curves coming from 100% density material with powder thermal characterization, which represents the most accurate prediction if compared with the experimental plot.

In previous graphs, the vertical reference lines show the time at which temperature difference is 100 °C and 50 °C between the surface and the core of billet, radially (Graph 1) and axially (Graph 2). This can be useful to calculate the homogenization time required for entire billet to reach a desired temperature based on the given application. It must also be noted that thermal behavior of billet depends on the geometry of powder-filled can.

The two approaches can be considered identical according to energy balance equation (Eq. 14) and equation (Eq. 23), relating the thermal properties of bulk material to powder and assuming it to be a linear function (with a and β equal to 1). However, thermal relationship between bulk

and powder may not always be linear for different materials as the a and β parameters vary between 1 and 2 [4]. This has an effect on temperature prediction.

In the case of time-compressed simulations, the results showed a strong relation between thermal parameter used for time-compression factor (Eq. 28) and the accuracy of predictions. The previous graph (Graph 4) shows a variability of the error between 58 °C and 135 °C using time-compression as function of thermal conductivity. The quality of the prediction is similar in both 70% and 100% density simulations. In the same way, the average errors for temperature prediction of each point tracking between the benchmark simulation and the compressed-time campaigns as function of heat capacity were plotted (Graph 5). The results show that the error on temperature prediction is much lower than the previous cases, with a variation between 4 °C and 12 °C and a reduced variability with respect to different values of time-compression factor.

Considering the previous graph (Graph 5), it appears clear that the best quality in temperature prediction is reached by 100% density and compression factor equal to 10 as function of heat capacity. However, the results of both simulations having the maximum time-compression as function of c represent the best compromise between computation costs and quality of prediction.

It appears clear that the time-compression as function of heat capacity provides more accurate results in both 100% and 70% density cases with respect to the simulation campaigns in which the f_{tc} factor is function of thermal conductivity (Graph 4). This can be explained using the energy balance equation (Eq. 14) in which thermal conductivity is related to Laplace differential operator for temperature, while heat capacity is related to the derivate of temperature with respect to time. The use of time-compression method does influence the derivate function of temperature in the energy balance equation (Eq. 14).

If time-compression as function of c is used, the balance of equation is maintained. However, if time-compression as function of k is used, a different space propagation of thermal wave is obtained as space distribution of temperature has to be maintained in all cases. It can also be correlated to (Eq. 24), where thermal conductivity for the powder was assumed to be a linear function of temperature, neglecting the higher order terms.

Finally, considering the calculation time for different cases, the time-compression method allows a strong time reduction, up to two orders of magnitude, as shown in the graph below (Graph 6). A wider range of error with a variability of several degrees amongst the points considered in the billet is observed in case of thermal conductivity, when compared to heat capacity.

In this panorama, the simulation with 100% density of billet and time-compression factor as function of heat capacity showed the best consistency and minimal error throughout the billet. It must be noted that error in thermal predictions increases with increased time-compression factor using thermal conductivity, while it remains stable when heat capacity is used. This proves that it is possible to carry out, in few minutes, a good prediction of thermal evolution for a densification stage without any limitation in case materials having very different densification curves (Graph 1), where an imprecise estimation in temperature levels could determine the occurrence of defects and, as consequence, the inability to complete the production cycle.

CONCLUSIONS

A numerical method to simulate a heating cycle of a powder material by means of a solid continuum model is proposed. The analysis shows the influence of porosity on thermal behavior in the case of two equivalent numerical approaches, one using bulk material with powder thermal properties and the other using porous material with bulk thermal properties. A time-compression technique is developed that reduces the computational cost involved in thermal analysis of such long industrial processes. The influence of each thermal parameter on the prediction of time-compressed simulations is analyzed and a proper setup is obtained with the best ratio between accuracy of results and computational time. This time-compressed approach to thermal modeling can be useful to accurately predict the homogenization time required to reach a particular temperature, along with the powder densification at any given instant based on the application.

REFERENCES

[1] Gessinger, G. H., 1984, Powder metallurgy of superalloys, Butterworths.

[2] Olevsky, E. A., 1998, "Theory of sintering: from discrete to continuum," Materials Science & Engineering R-Reports, 23(2), pp. 41-100.

[3] German, R. M., 1996, "Sintering - Theory and practice."

[4] Montes, J. M., Cuevas, F. G., Cintas, J., and Muñoz, S., 2012, "Thermal Conductivity of Powder Aggregates and Porous Compacts," Metallurgical and Materials Transactions A, 43(12), pp. 4532-4538.

[5] Kobayashi, S., Oh, S. I., and Altan, T., 1989, "Metal Forming and the Finite-Element Method."

[6] Szabó, T., 2009, "On the Discretization Time-Step in the Finite Element Theta-Method of the Discrete HeatEquation," Numerical Analysis and Its Applications, S. Margenov, L. Vulkov, and J. Waśniewski, eds., Springer Berlin Heidelberg, pp. 564-571.

[7] Tronel, Y., and Fichtner, W., 1999, "Optimal Time Stepping in the Thermo-mechanical Finite Element Simulation of IGBTs Modules," Technical Proceedings of the 1999 International Conference on Modeling and Simulation of Microsystems Chapter 8: Numerics, Algorithms, pp. 334 - 337.

[8] Sukhatme, S. P., 1992, "A Text Book on Heat Transfer."

[9] Bejan, A., 1993, "Heat Transfer."

[10] Holman, J. P., 1989, "Heat Transfer."

[11] Incropera, F. P., and Dewitt, D. P., 1990, "Fundamentals of Heat and Mass Transfer."

[12] Lewis, R. W., Nithiarasu, P., and Seetharamu, K. N., 2004, "Fundamentals of the Finite Element Method for Heat and Fluid Flow."

[13] Bejan, A., and Nield, D. A., 2013, "Convection in porous media."

[14] Im, Y. T., and Kobayash, S., 1986, "Coupled thermoviscoplastic analysis in plain-strain compression of porous materials," Advanced manufacturing processes, 1, p. 269.

ABOUT THE AUTHORS: Dr. Shivpuri has been a faculty at OSU since 1986. At OSU, Dr. Shivpuri has won the 1997 Harrison Faculty Award for Excellence in Engineering Education and several Lumley Research Awards. Dr. Shivpuri has advised over 100 master theses and doctoral dissertations, and published over 300 research articles in refereed publications. Dr. Shivpuri is elected fellow of ASM International, ASME, CIRP (International Academy for Production Engineering) and SME. Dr. Shivpuri was the 2001 President of NAMRI (North American Manufacturign Research Institute). He is a Magnet Professor with the FIA (Forging Industry Education and Research Founation), and is active in proessional and trade associations such as AIST (Association of Iron and Steel Technology), ITA (International Titanium Association), NADCA (North American Die Casting Association).

Shlok Sundaresh was a graduate research associate at The Ohio State University in Columbus, Ohio, at the time of publication. He is currently a process engineer at TS USA of HEF USA.

Enhanced Properties of 17-7 PH Stainless Steel

By Don Jordan

Solar Atmospheres developed a unique process for heat treating 17-7 PH (precipitation hardening) stainless steel using vacuum furnace technology. This process enhances the tensile ductility of the steel while maintaining its very high tensile strength.

BACKGROUND

Precipitation-hardening (PH) stainless steel grade 17-7 PH is classified as a semiaustenitic stainless steel used extensively in aerospace and finding new applications in the medical industry. The material is most often used in sheet and strip form with springs, clips, and bellows being widely produced. The high alloy content of 17-7 provides excellent corrosion resistance, which is an attractive attribute to the medical industry.

After annealing at a temperature of 1950°F, 17-7 remains austenitic on cooling to room temperature. It is soft and ductile in this "Condition A" state, and can be fabricated similar to other austenitic stainless steels (e.g., 304). After fabrication, a sequence of thermal treatments significantly strengthens the steel by first transforming the austenite to martensite, which is further strengthened by precipitation hardening. Transformation from austenite to martensite is achieved by mechanical deformation (metallurgically classified as a strain-induced phase transformation) for the highest obtainable strengths. However, this phenomenon is not discussed herein. This article shows that attractive properties with enhanced ductility other than those classified as "standard PH conditions" can be routinely obtained and, in doing so, offer a unique processing advantage using vacuum heat treatment.

Transforming austenite to martensite in 17-7 starts with a heat treatment called austenite conditioning. What actually occurs is the austenite becomes destabilized by the precipitation of carbon. Two standard temperatures used for austenite conditioning are 1400°F and 1750°F. The martens-

Property	Condition A (a)	Condition T (b)
Tensile Strength, ksi	130	145
Yield Strength, ksi	40	100
Elongation %	35	9

Table 1: Mechanical properties of 17-7 PH for different thermal treatments, (a) Annealed (b) Austenite conditioned at 1400°F.

Property	TH 1050 (a)	950 (b)
Tensile Strength, ksi	200	230
Yield Strength, ksi	185	220
Elongation %	9	6
Hardness, HRC	43	48

Table 2: Typical room temperature mechanical properties of aged 17-7PH, (a) Condition T material aged 1050F for 1.5 h (b) Condition R material aged 950F for 1 h.

Condition	Tensile Strength, ksi	Yield Strength, ksi	Elongation %
TH 1050, Heat 1	208	201	4.5
	207	203	4.7
	209	205	4.7
SH 950, Heat 1	219	200	10
	221	202	9.5
	219	203	9.5
TH 1050, Heat 2	195	190	5
	200	195	5.5
	199	193	4.8
SH 950, Heat 2	209	191	10
	210	192	9.5
	211	195	10

Table 3: Mechanical properties of 17-7 PH Condition SH 950 and standard Condition TH 1050

ite start (Ms) and finish (Mf) temperatures vary depending on what treatment is used. Treatment at 1750°F precipitates less carbon than at 1400°F, and, as such, requires lower cooling temperatures to complete the martensite transformation. Cooling to a temperature below -90°F is specified for complete transformation, after which the steel is in Condition R. More carbon precipitates with the 1400°F treatment, which raises the Mf temperature to about 60°F, resulting in Condition T. Martensite transformation considerably increases the typical yield strength of the steel in Condition T over the annealed Condition A state, as shown in Table 1.

Following martensite transformation, 17-7 PH is further strengthened by a low temperature precipitation hardening treatment (also termed aging). The industry standard is to age Condition R material at 950°F for one hour, resulting in an end condition of RH 950. Condition T material is aged at 1050°F for 90 minutes, resulting in an end condition of TH 1050. Typical room temperature mechanical properties are listed in Table 2. Very high strength properties are obtained. TH 1050 provides more ductility at a reduced strength level.

INVESTIGATION

This study was conducted to develop a three-step heat treatment process that could be performed in a vacuum furnace without breaking vacuum between the austenite conditioning step and precipitation hardening step normally required to adequately cool parts for martensite transformation. This is highly desirable because it can be difficult to maintain 17-7 in a bright condition (no discoloring from oxidation) during the precipitation hardening treatment after breaking vacuum and exposing parts to ambient temperature and lower during cooling for martensite transformation. Working with the medical industry, the aim was to develop a new in-situ process where desirable mechanical properties could be consistently obtained. Once accomplished, a new medical device design could be based on the established set of mechanical properties and the medical company would benefit from reduced costs due to reduced pricing associated with the new in-situ process. As a baseline, the new mechanical properties and microstructural characteristics were compared with standard Condition TH 1050, the most common condition specified in industry.

Review of literature on the subject of precipitation-hardening stainless steels re-

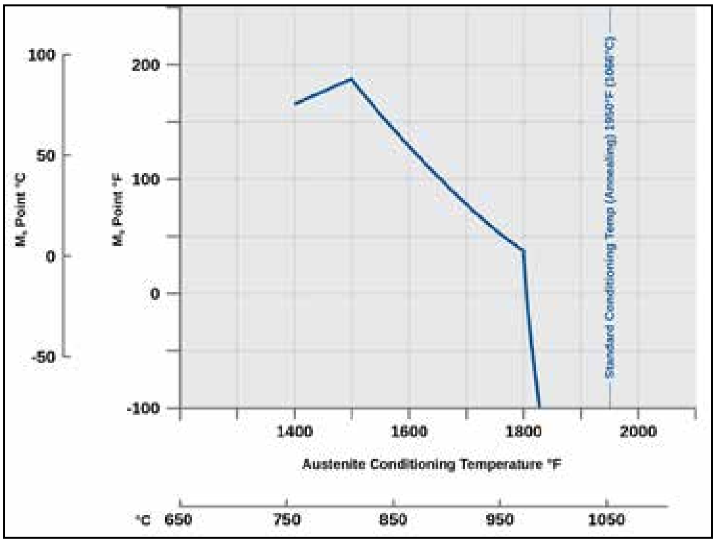

Figure 1

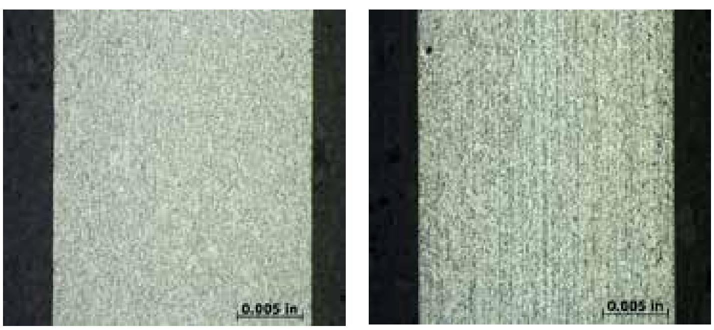

Figure 2

veals interesting data, which was the principal reason for initiating the study. AK Steel published a graph showing how the Ms temperature varies with austenite conditioning temperature, as seen in Figure 1.

Postulating that raising the Ms temperature will also raise the Mf temperature, an austenite conditioning temperature of 1500°F was chosen as the experimental starting point. Given that a 1400°F conditioning temperature requires cooling to 60°F to complete martensite transformation, it was extrapolated from the Ms curve that conditioning at 1500°F could produce a Mf at 80°F (provided the conditioning time allowed for adequate carbide precipitation). This higher Mf temperature is ideal for processing 17-7 PH at Solar Atmospheres in a vacuum furnace due to an advanced cooling system innovation installed on one of Solar's HL-57 size furnaces (36 in. 48 in. 30 in.). This technology can cool the workload down to 80°F from the estimated Ms of 185°F within one hour, which is the time limit recommend for Ms to Mf for Condition T. In this state, Solar coined the term Condition S.

The 17-7 PH material in Condition TH 1050 is overaged a fair amount, while in Condition RH 950, it is only slightly overaged (900°F produces maximum strength but minimum ductility). It is also known with 17-7 PH that maximum transformation of austenite to martensite equates to maximum strength. Given that the true Mf for the newly chosen conditioning temperature of 1500°F is not established, it was decided to select a precipitation hardening temperature of 950°F considering that this would produce higher strength than a 1050°F age, but not minimum ductility even if fully transformed like Condition R. Table 3 shows the tensile properties of the new Solar heat treatment Condition SH 950 compared to standard Condition TH 1050 that was heat treated by Solar with 17-7 of the same heats of steel.

SH 950 produced comparable yield strength, higher tensile strength, and, on average, twice the ductility of TH 1050. This is all carried out in a three-step heat treat process without breaking vacuum for martensite transformation cooling, resulting in bright, non-discolored parts. Evaluation of the microstructural quality revealed SH 950 was superior to that of TH 1050. Figure 2 shows the microstructure of both conditions. SH 950 shows considerably less delta ferrite stringers than TH 1050, which is believed due to the higher austenite conditioning temperature for a longer time used for SH 950. Delta ferrite is inherent to 17-7 PH, and is not detrimental in the quantity revealed, but less is considered better, resulting in better transverse tensile properties.

SUMMARY

Grade 17-7 PH stainless steel is widely used in the industry due to its attractive combination of properties including very high spring-like strength, good ductility, and excellent corrosion resistance. However, to obtain these properties, it must be heat treated in a more controlled manner than many other alloys. Even within these controlled parameters, flexibility exists to obtain attractive properties other than those classified as standard PH conditions. This study showed that vacuum heat treatment technology offers a unique processing advantage to cost-effectively achieve desirable properties while producing bright, non-discolored parts.

A three-step process consisting of austenite conditioning, in situ cooling, and precipitation hardening was performed without breaking vacuum resulting in a new condition of 17-7 PH that Solar Atmospheres coined SH 950. Compared with the most common condition of 17-7 PHproduced (TH 1050), Condition SH 950 shows comparable yield strength, higher tensile strength, and, on average, twice the ductility. The microstructure of SH 950 also is superior with respect to the presence of a lower amount of delta ferrite stringers. These results were obtained with two separate heats of steel, which is encouraging because 17-7 PH is quite sensitive to chemical composition variations in obtaining consistent mechanical properties. A similar outcome on another heat or two of steel indicates that a new medical device design, or a material change to 17-7 PH for an existing design, could be based on the newly established range of mechanical properties. This would provide the benefit of reduced manufacturing costs due to reduced pricing associated with the new in-situ vacuum heat treatment process for 17-7 PH stainless steel.

ABOUT THE AUTHOR: Don Jordan is the vice president of technology and corporate metallurgist for Solar Atmospheres, Inc., in Souderton, Pennsylvania. He manages the R&D Technology Group at Solar Atmospheres whose mission is to expand Solar's technical capabilities in all facets of vacuum heat treatment technology. The group has specific interests in thermochemical surface treatments and has developed processes for vacuum carburizing, vacuum gas nitriding, and solution nitriding of martensitic stainless steels and titanium alloys. While Solar Atmospheres services every major market, the R&D work of the article's topic was done specifically with the medical industry in mind. For more information, go to Solar's website at www.solartm.com, call 800.347.3236, or email Solar at info@solaratm.com.

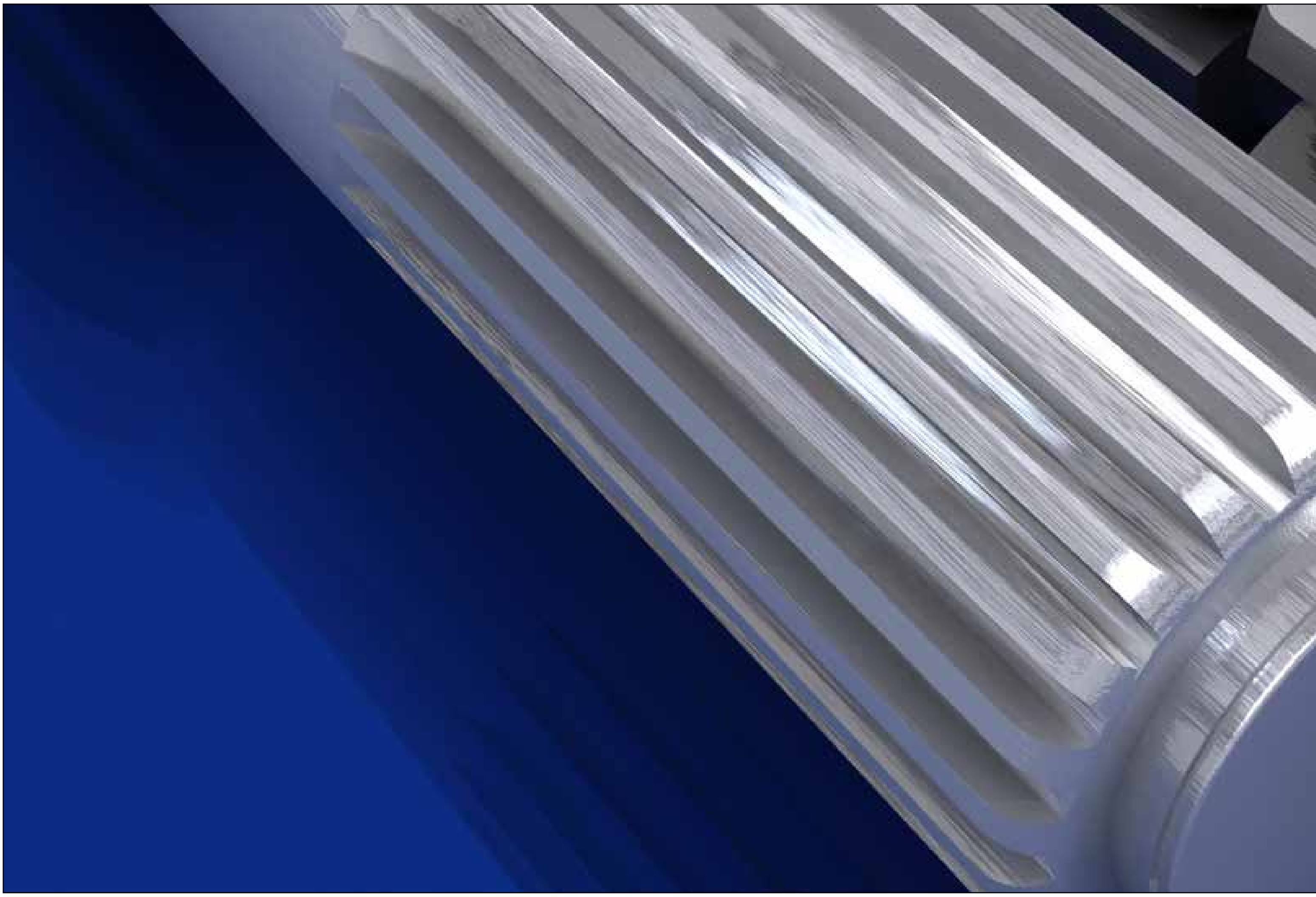

Stress Generation in an Axle Shaft during Induction Hardening

By Zhichao Li, B. Lynn Ferguson, Andrew Freborg, Robert Goldstein, John Jackowski, Valentin Nemkov, and Greg Fett

Compressive residual stresses are developed in the surface of an axle shaft during induction hardening, which further enhance its high-cycle fatigue performance. This article discusses the importance of the residual stress to high-cycle fatigue performance of an axle shaft under torsional loading.

INTRODUCTION

Induction hardening of steel components offers a fast heating rate, high efficiency, and the ability to heat locally. Induction hardening is a highly nonlinear multi-physical process with electro-magnetics, temperature, phase transformation, stress, and shape changes all occurring in the component. Compressive residual stress in the hardened case is beneficial to the high-cycle fatigue performance. Note however that material response to induction heating is not intuitive due to the highly nonlinear and transient phenomena of the hardening process, so predicting the final properties of a component after induction hardening is challenging. During hardening, magnetic properties change throughout the process, affecting thermal distribution and microstructure. Coupling these phenomena to reach the end properties after treatment requires state-of-the-art technology. Development of finite element analysis (FEA) has matured for both electromagnetic and thermal-stress modeling to include phase transformations during induction hardening, which are applied to understand and solve industrial problems [1-4]. FEA incorporates mechanical properties and residual stresses which are then imported to a loading model to analyze the mode and location of fatigue failures [5-6].

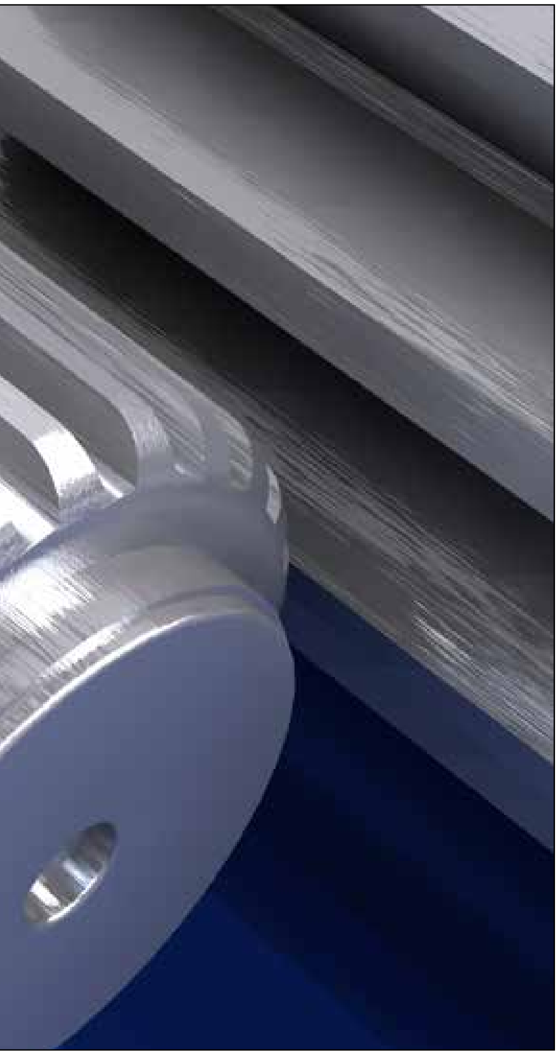

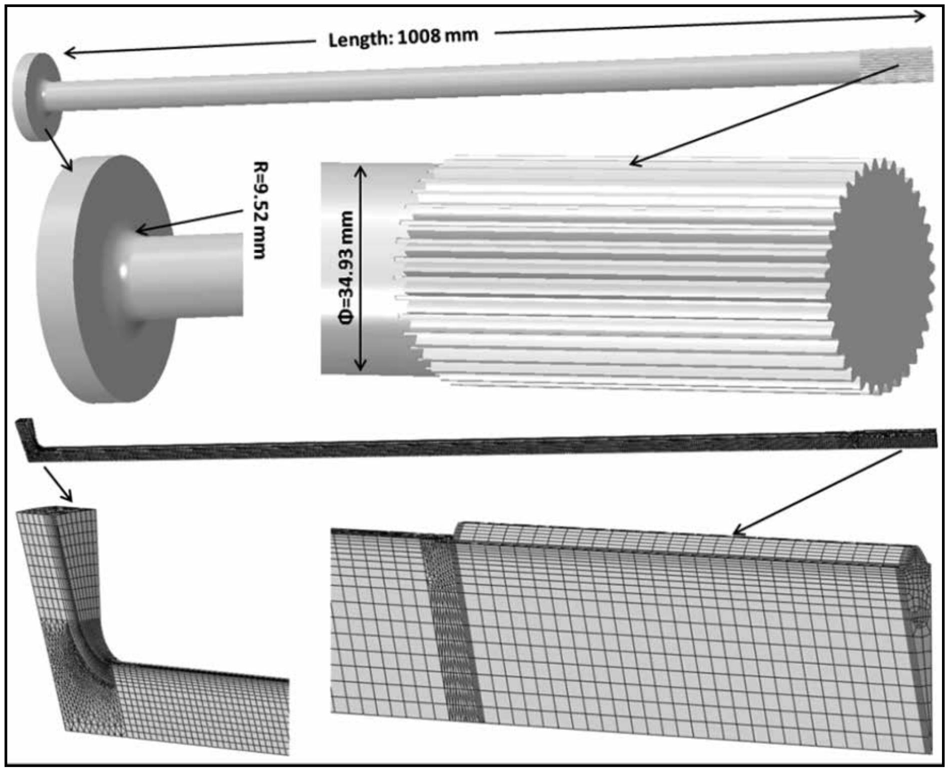

Figure 1: (a) CAD model, and (b) single spline tooth FEA model of full-float truck axle shaft

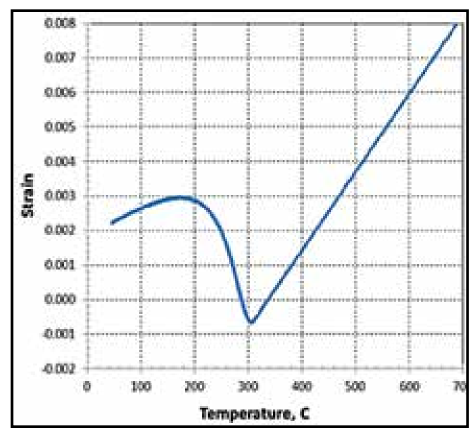

Figure 2: Dilatometry strain curve of martensite transformation for AISI 1541 during continuous cooling

Modeling studies have led to the development of simulation techniques to predict electromagnetic and thermal effects, coupled with structural changes to predict a hardness pattern [7]. DANTE is a commercial FEA based software developed to model heat treatment of steel components, including furnace heating with liquid and gas quenching, and induction hardening with spray quenching [8-9]. An investigation of stress and distortion modeling of a simple case of ID and OD hardening of a tubular product has been reported [10]. Taking the modeling to the next step required studying a common industrial component with a more complex geometry subjected to external stresses in service, such as a full-float truck axle shaft with dimensions typical to those manufactured by Dana Corp. The axle shaft, a common automotive component, enables comparing simulation results to desired axle shaft properties. Results are compared with typical performance criteria for the case chosen. The ultimate goal of this ongoing study is to produce results representative of actual part performance. Because DANTE was not developed to model electromagnetic physics of induction heating, Flux software is used, and power distributions in terms of time and part geometry are imported into DANTE for phase transformation, stress and distortion analyses. Predicted residual stresses after heat treatment are then imported into a torsion load model to determine the effect of the residual stresses on shear crack initiation.

DISCUSSION OF PART, FEA MODEL AND HEAT TREATMENT

Truck Axle Shaft Geometry and FEA Model

Axle shafts are surface hardened for durability to prevent failure in service. Hardening is commonly performed using induction scanning. How the process is performed affects resulting stresses and distortion. The main concerns during induction hardening of truck axle shafts over 1 m long are bowing distortion and axial growth. Bowing distortion can be minimized using proper inductor design, high quality process controls and structural support mechanisms. Excessive heat internal to the shaft is the main contributor to this problem, which can be evaluated by simulation. Change in length is affected by both shaft heating and cooling rates. A simplified CAD model of a full-float truck axle shaft from Dana Corp. is shown in Figure 1(a).

Shaft dimensions are 34.93 mm diameter by 1008 mm long with a 9.52 mm fillet radius between the 104.5 mm diameter by 16.5 mm thick flange; the spline has 35 teeth. Figure 1(b) shows the finite element mesh of a single tooth sector used for DANTE thermal, phase transformation, and stress analyses. Fine surface elements are used to effectively catch thermal and stress gradients in the surface.

The axle shaft is made of AISI 1541, and the nominal chemical composition is used in the modeling study. Phase transformations are involved in both induction heating and spray quenching processes. During induction heating, the part surface transforms to austenite. During spray quenching, austenite transforms to martensite mainly, with a small

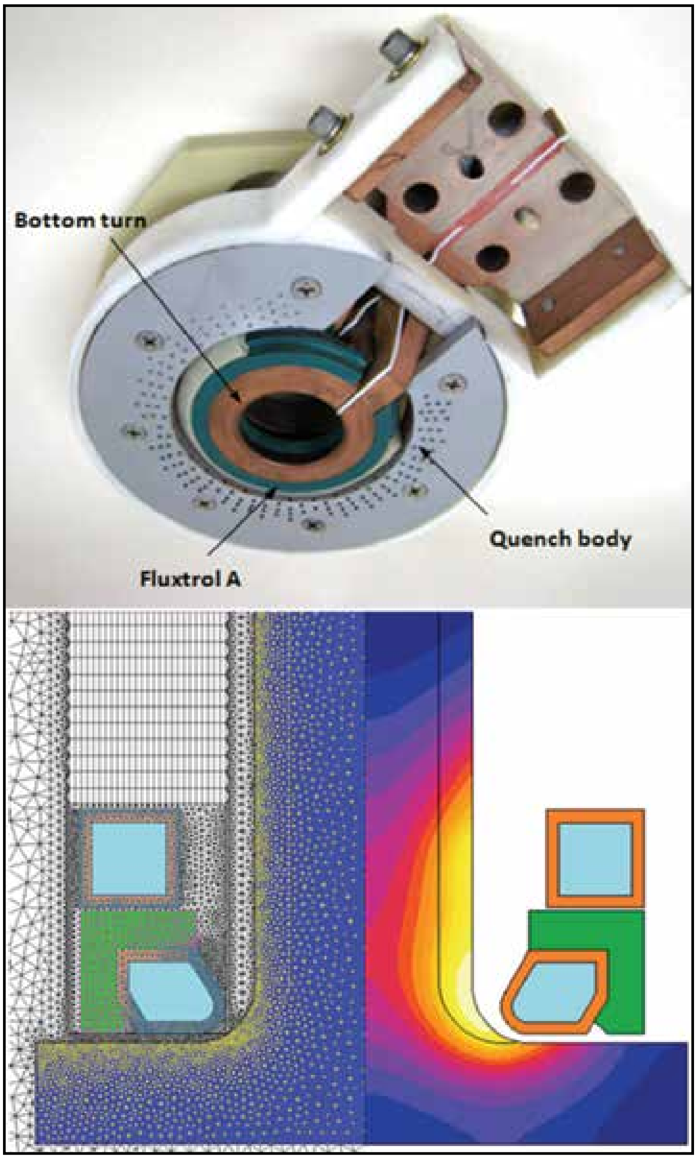

Figure 3: (a) Full assembly of a two-turn shaft scan coil with quench body, (b) fillet area of shaft modelled with Flux 2D

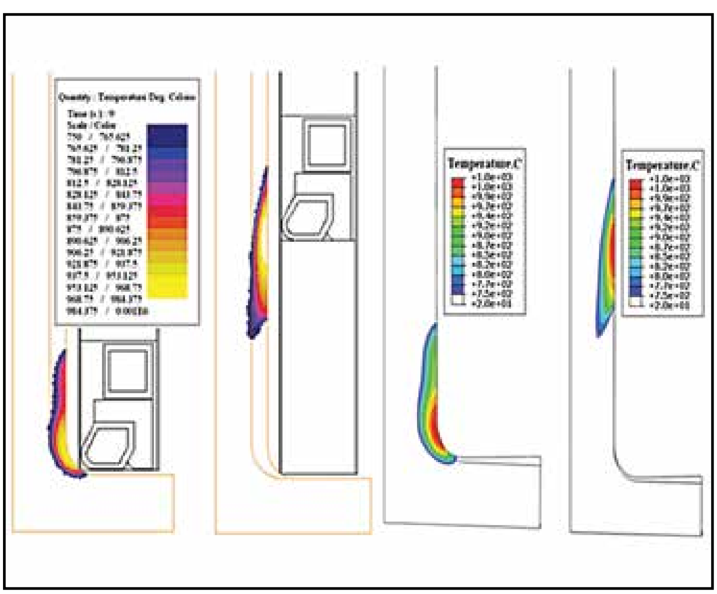

Figure 4: Temperature distributions predicted by Flux and DANTE. (a, c) at the end of 9 s dwell, and (b, d) at the end of 16.5 s from the start of induction heating

amount of diffusive phases, such as ferrite, pearlite and bainite. Accurate descriptions of phase transformations and mechanical properties of individual phases are required for thermal stress analysis [11]. Dilatometry is a key method for acquiring such data. Figure 2 shows a dilatometry strain curve during martensitic transformation under continuous cooling. The dilatometry strain curve provides the martensitic transformation start temperature (Ms), martensitic transformation finish temperature (Mf), transformation strain, and coefficients of thermal expansion (CTE) for both austenite and martensite. Due to the high cooling rate from the spray quench after induction heating, the martensitic transformation is the main phase transformation type in this case study.

Heat Treatment Process

During heat treatment, the axle shaft is positioned vertically in the induction hardening unit, with the flange on the bottom of the fixture. The distance between the inductor and the spray is 25.4 mm. The process starts with a 9 s static heating period on the flange/fillet, followed by scanning with an inductor travel speed of 15 mm/s. After scanning for 1.5 s, scan speed is decreased to 8 mm/s and remains at this speed. Power is turned off after an additional 119.65 seconds; this occurs before the end of shaft is austenitized. Spraying continues after inductor power is turned off to complete transformation of the austenitized section of the shaft to martensite.

INDUCTOR DESIGN AND MODELLING OF POWER DENSITY

It is critical not only to meet the hardened case depth requirement, but also prevent excessive heating in regions such as the flange, core and shaft end. Too much heat in these regions increases the possibility for cracking, and can also lead to excessive distortion. Minimum case depth requirement for the axle shaft is 5.4 mm, and the case depth is defined by a hardness of 40 HRC.

The inductor must be carefully designed to prevent cracking and excessive distortion. A machined two-turn coil with a magnetic flux concentrator was chosen and configured using Flux2D. Inductor optimization steps were followed [12]. An example of a fully assembled coil of this style is shown in Figure 3(a).

The view is from the bottom of the coil. The bottom turn is profiled to help drive heat into the radius. The profile design is guided to provide the most amount of heat in the radius, while preventing a bulged heating pattern in the base of the shaft or on the flange. Flux concentrator Fluxtrol A was applied to the bottom turn to further assist in driving heat into the radius, and partially shield flux from coupling with the shaft to prevent a bulged pattern. The top turn is required to aid in the scan process by widening the heat zone on the shaft, enabling a faster scan speed. In Figure 3(a), the green material is Fluxtrol A, surrounded by a grey quench body assembly. A quench body is mounted to the coil, which sprays quenchant about 25.4 mm below the coil. The quench is described in Flux2D by a heat transfer coefficient. The finite element mesh used to model the axle shaft by Flux2D is shown in Figure 3(b), with a predicted temperature distribution focusing on the flange and the fillet regions.

POWER DENSITY MAPPING FROM FLUX2D TO DANTE

The shaft material is magnetic, and the power density distribution changes greatly when the temperature exceeds the Curie point. The inductor frequency is 10 kHz, which is a common operating frequency of the Dana induction machines used for this class of parts. A difference in skin heating effect is observed during the scan of the shaft.

The portion of the shaft above the bottom turn has a high skin effect because it is below the Curie temperature. The bottom turn provides more intensive heating, which drives the case depth and results in a deeper penetration of power at its heat face. Specifically, Flux2D calculates when to turn off power at the end of the process by determining the temperature profile as the coil approaches the edge of the spline.

Different finite element meshes are used for the Flux2D and DANTE models due to different physics and accuracy requirements. Power densities in the axle shaft predicted by Flux2D are imported and mapped into DANTE. Temperature distributions predicted by Flux2D and DANTE at various times of the process are compared, as shown in Figure 4. The temperature profiles predicted from the two packages have reasonable agreement.

INDUCTION HARDENING PROCESS MODELING

As described, the first step of the induction hardening process is a 9 s dwell, during which time the inductor is stationary and there is no spray quenching. Next, the inductor moves up with a speed of 15 mm/s for 1.5 s, then drops to 8 mm/s and spray quenching is initiated. Spraying then continues for the duration of the process. Power and temperature distributions are stable during scanning period over most of the shaft length. Figure 5 shows a snapshot of temperature, austenite, martensite, axial stress, and hoop stress at 16.5 s during induction hardening process using heat transfer boundary condition of 12 kW/m2·C. During spraying quenching, the austenite layer transforms to martensite. Figure 5(e) is a snapshot of an in-process hoop stress distribution, which intuitively shows the effects of thermal gradient and phase transformation. The predicted nodal displacements in Figure 5 are magnified ten times to clearly show shape change. The same inductor power is applied to the spline region, and power is turned off after 130.15 s of total process time before the end of the spline section is austenitized.

Cooling rate has a significant effect on residual stresses obtained from quench hardening, and a detailed study of the cooling rate effect is given in [13-14]. For a heat transfer coefficient of 12 kW/m2·C, the residual stresses and axial distortion after induction hardening are shown in Figure 6. The highest tensile stress in the axial direction is located at the centerline of the shaft above the flange. Predicted axial residual stress is 750 MPa compression on the shaft surface, and the predicted hoop residual stress is 540 MPa compression. The magnitude of axial residual stress is higher than that in the circumferential direction. The effect of these stresses on shear crack generation is discussed later. Predicted axial growth is about 1.7 mm, as shown in Figure 6(c). Axial displacement in the shaft is not linearly distributed along the axis, because it is not stabilized during early scanning process of the shaft.

LOW TEMPERATURE TEMPERING PROCESS AND TORSION LOAD MODELING

After induction hardening, the shaft is furnace tempered at 175° C for 1 h to improve the ductility and toughness of the hardened case. The change in residual stress from tempering is shown in Figures 7 and 8 for both the axial and circumferential directions. The magnitude of stress reduction caused by tempering is approximately 15%. During tempering, brittle as-quenched martensite transforms to more ductile tempered martensite, sacrificing some hardness and strength. Microstresses concentrated on grain boundaries and interfaces between the matrix and the carbides are also effectively reduced.

The magnitude of residual stress in the axial direction is higher than that in the circumferential direction, which is true for both the as-quenched and tempered conditions. Away from the flange and the shaft splines, the residual stress distribution along the shaft is relatively uniform. Selecting a straight line of points starting from the shaft surface, residual stresses before and after tempering are compared in

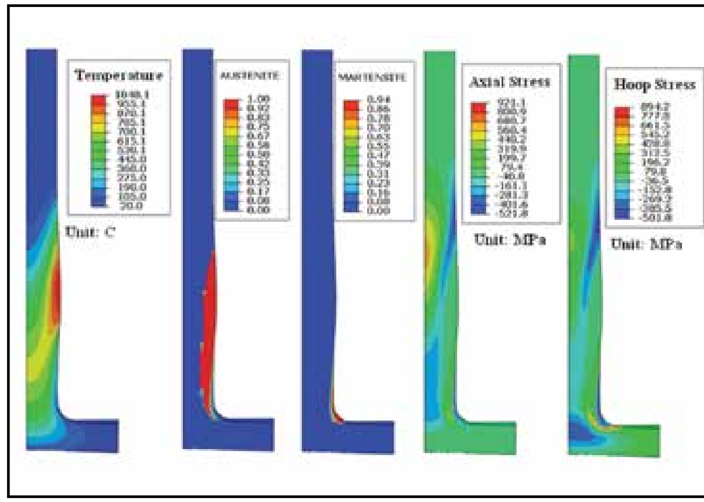

Figure 5: (a) Temperature, (b) austenite fraction, (c) martensite fraction, (d) axial stress, and (e) hoop stress distributions at the end of 16.5 s in the induction hardening process. (heat transfer coefficient = 12 kW/m2·C)

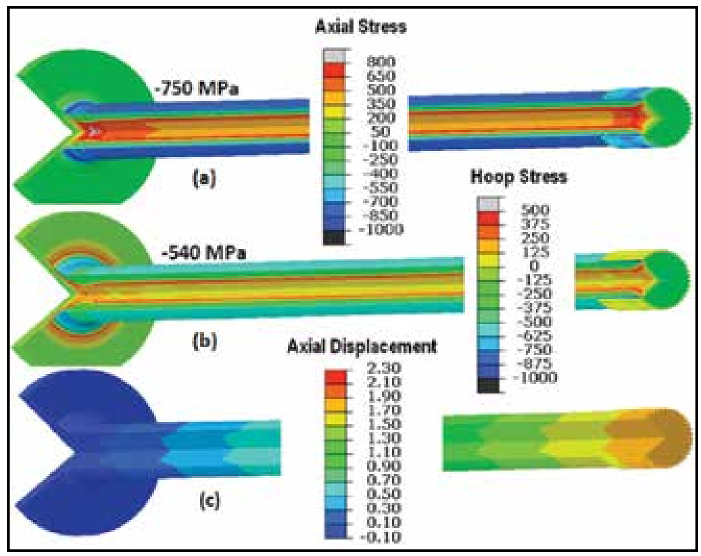

Figure 6: Predicted results after induction hardening with a heat transfer coefficient of 12 kW/m2·C. (a) Axial stress (unit: MPa), (b) Hoop stress (Unit: MPa), and (c) Axial displacement (Unit: mm)

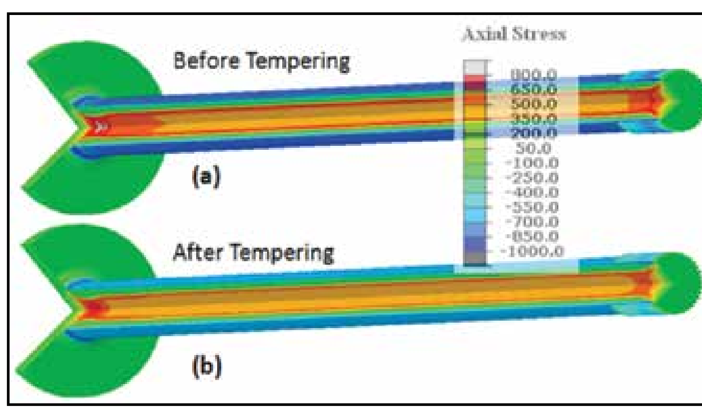

Figure 7: Comparison of axial residual stress before and after tempering

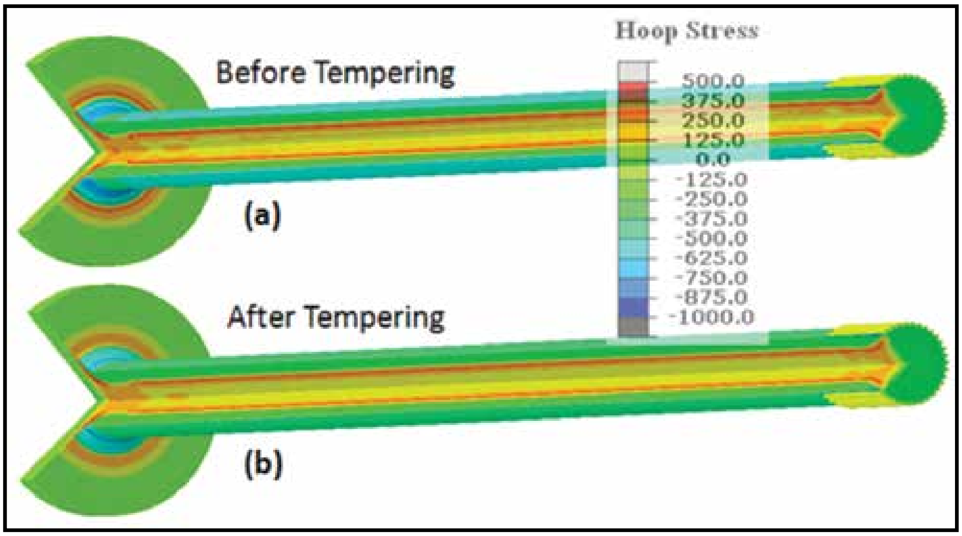

Figure 8: Comparison of hoop residual stress before and after tempering

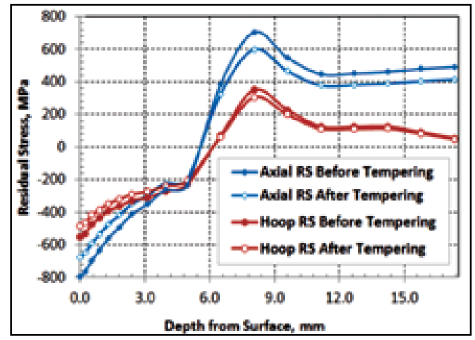

Figure 9: Comparison of residual stress in terms of depth before and after tempering

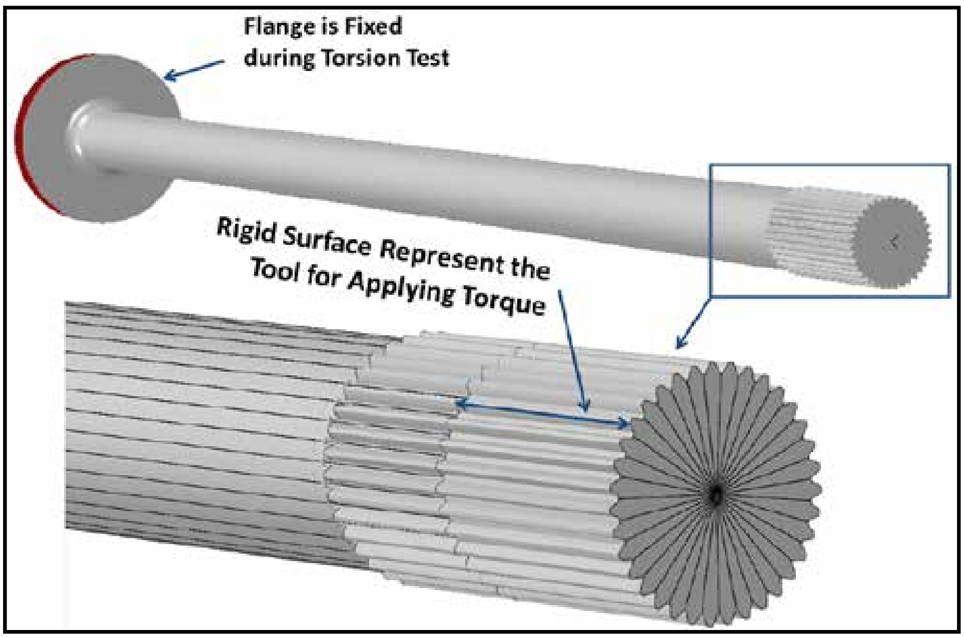

Figure 10: Torsional loading model and the mechanical boundary conditions

Figure 9. The x-axis of Figure 9 represents the depth of the point from the shaft surface, and the y-axis represents the magnitude of residual stresses in both axial and circumferential directions. A positive stress value indicates tension, and a negative value indicates compression. After tempering, residual compression in the axial direction is reduced from 750 to 675 MPa. Residual compression in the circumferential direction is reduced from 550 to 485 MPa.

The stress state after the tempering process is imported to a loading model to analyze stresses in the axle shaft during overload and torsional fatigue tests. To mimic loading conditions and constraints from the torsion fixture, the OD of the flange is constrained in the model, as shown in Figure 10. A rigid surface is used to represent the tool applying a torsion load to the splines of the axle shaft. In this model, the rigid surface covers approximately one half of the spline in the axial direction of the axle shaft.

Reported torsional yield strength from overload tests by DANA is 6,090 N·m, and the reported high cycle fatigue limit (2 million cycles) is 2,768 N·m. During the fatigue test, a fully reversing load (R = -1) is applied, and several fatigue test points are shown in Figure 11. The dotted line is a fitted S-N curve of the fatigue test results, with 2,768 N·m as the endurance limit.

In this study, the loading model assumes the axle shaft remains in the elastic region, with a maximum applied torsion load of 6,000 N·m. The Young's modulus in the model is 207 GPa and the Poisson ratio is 0.3. Two loading conditions are selected from modeling results. The 6,000 N·m torque load is slightly below the material yield strength, and 3,000 N·m represents a condition slightly above the fatigue limit. Rotational displacements under these torsional load conditions are shown in Figure 12. The maximum torsion displacement under 6,000 N·m torque is about 9.27 mm, and under 3,000 N·m torque is 4.64 mm. While in the elastic range, torsion displacement is related linearly to the applied torque, which is independent of the residual stresses.

Predicted shear stresses under the two specific loads are shown in Figure 13. Shear stress generated during torsion is independent of the incoming residual stress state. The magnitude of shear stress obtained from induction hardening is negligible, so it has no impact on shear stress generated during torsion testing. The magnitude of the shear stress does have a linear relationship to applied torque.

Figure 14 shows typical fracture surfaces for high-cycle fatigue and overload tests. During a high-cycle fatigue test conducted under a pure torsional load, the crack initiates on the shaft surface. The crack initially grows in the longitudinal direction for several millimeters, then propagates at an angle of 45 degrees. During the overload test, cracks initiate either on the shaft surface or spline surface. The fixture used to apply torsional load to the spline can affect the magnitude of concentrated stress in the spline. For example, if the fixture covers the spline in the axial direction, the crack most likely will not initiate on the spline surface.

Compressive residual stresses obtained from induction hardening benefit high-cy-

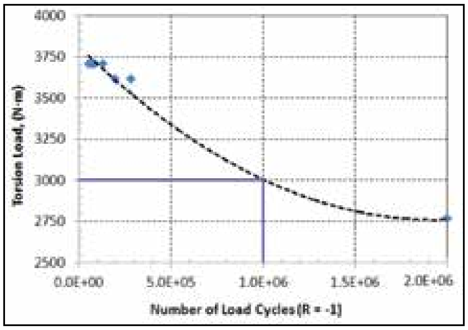

Figure 11: Fatigue test results and fitted S-N curve

cle fatigue performance of the axle shaft. As shown in Figure 13, predicted shear stresses from the induction hardening models are negligible, and shear stresses under torsion load are the same whether residual stresses from the hardening process are or are not considered. Figure 15 shows the calculated maximum principal stresses under torsion load conditions of 3,000 and 6,000 N·m.

If incoming residual stresses are not considered, the maximum principal stress on the shaft surface is about 720 MPa under the torsional yield load of 6,000 N·m, as shown in Figure 15(c). The stress magnitude is predicted to be 150 MPa on the surface when residual stresses are taken into account. For the high cycle fatigue test under pure torsion load, crack initiation and growth is directly related to the maximum principal stress instead of shear stress. Figures 15(b) and (d) show that the maximum principal stress is located at the case/core interface instead of the shaft surface. With a 6,000 N·m torque load, the magnitude of the tensile stress under the surface is about 750 MPa when accounting for the incoming residual stress state.

During either overload testing or fatigue testing under pure torsion, shear stress is generated in the shaft. Selecting a reference point on the surface of the shaft, the direction of the generated shear stress in the longitudinal and circumferential directions is shown schematically in Figure 16. Without considering residual stresses from the hardening process, axial stress and hoop stress are both zero. Therefore, shear stress is the only stress contributing to cracking. The directions of principal stresses generated by the shear stress are ±45 degrees, and maximum principal stress in the +45 degree direction is the direct cause of the fracture. The factors become more complicated with the existence of residual stresses. Figure 16 rep-

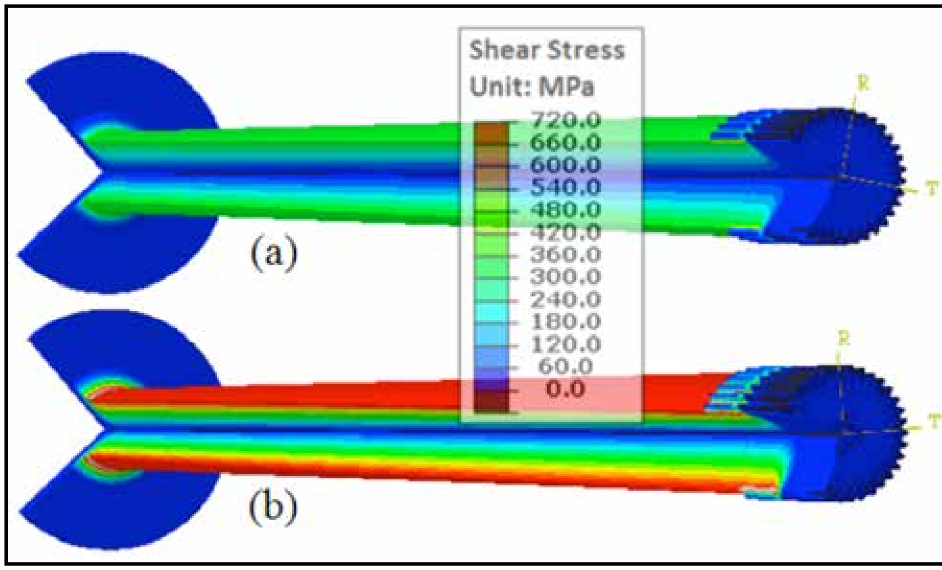

Figure 13: Shear stress (unit: MPa) under torsion loads: (a) 3,000 N·m, (b) 6,000 N·m

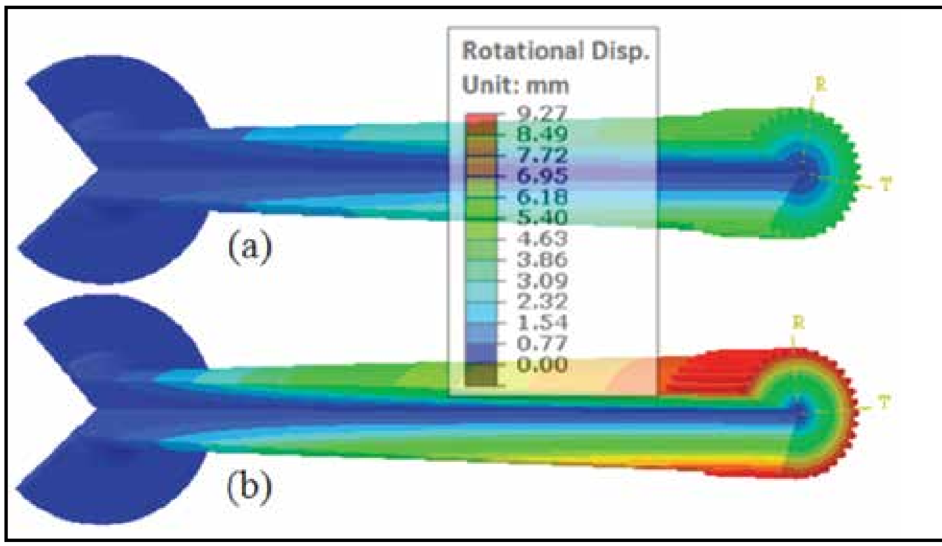

Figure 12: Rotational displacements under torsion loads (unit: mm): (a) 3,000 N·m, (b) 6,000 N·m.

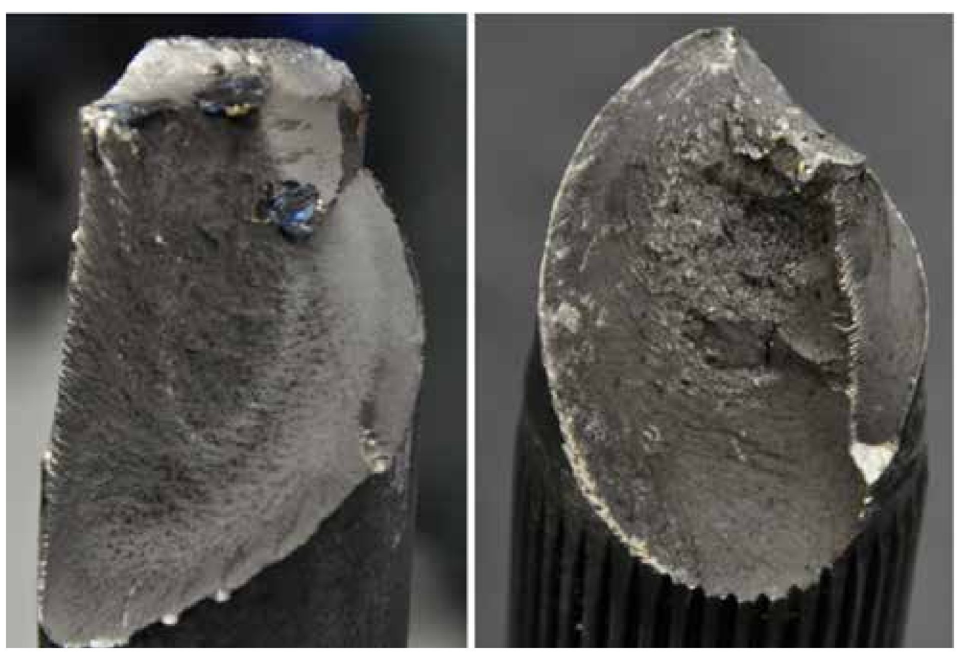

Figure 14: Fracture surface of the axle shaft. (a) Fatigue crack, and (b) Overload crack.


THINK
OUTSIDE
THE
BOX
Stor-Loc®
Modular Drawer System
MADE BY AMERICAN CRAFTSMEN IN THE USA
WWW.STORLOC.COM
1-800-786-7562
1-800-STORLOC

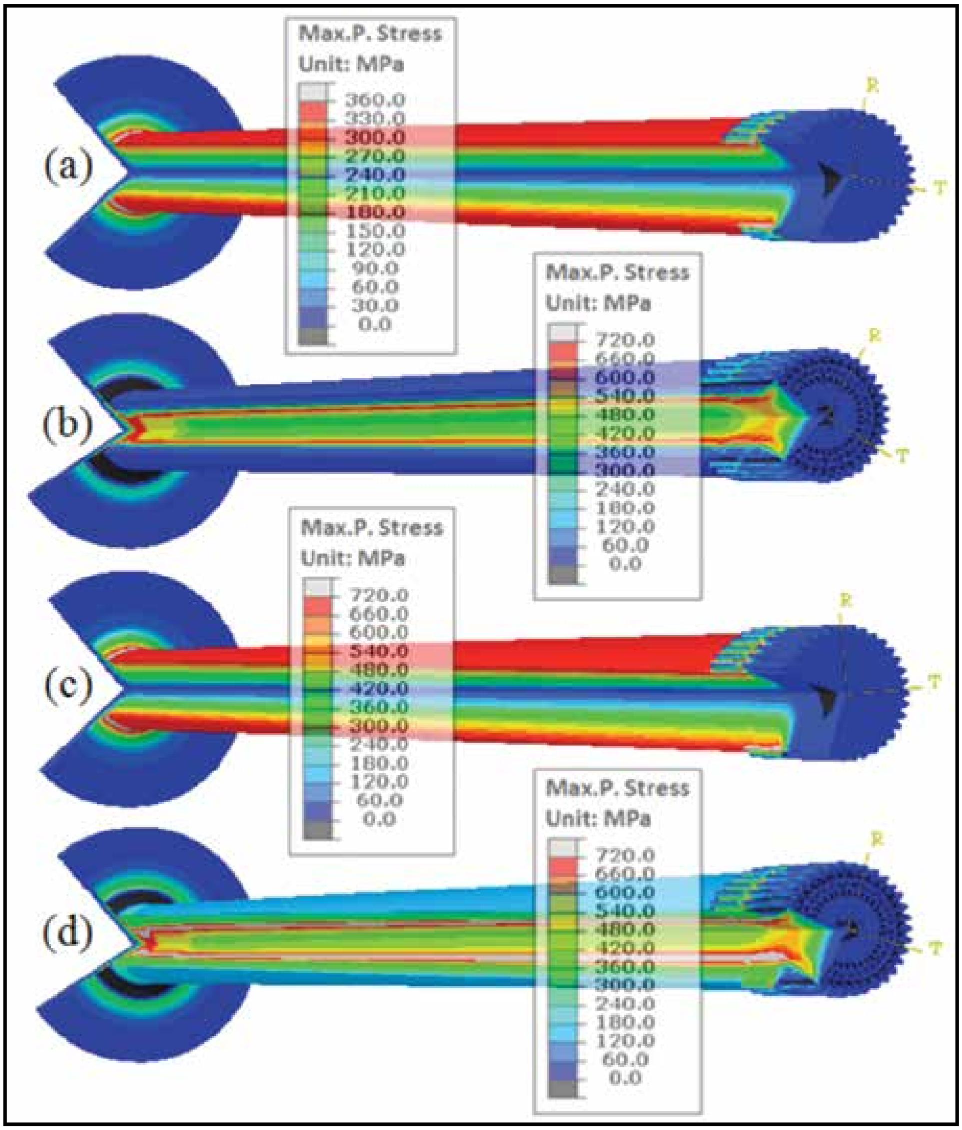

Figure 15: Effect of residual stress from induction hardening on maximum principal stress (unit: MPa) under (a) 3,000 N·m torsion load without considering induction hardening residual stress, (b) 3,000 N·m torsion load considering induction hardening residual stress, (c) 6,000 N·m torsion load without considering induction hardening residual stress, and (d) 6,000 N·m torsion load considering induction hardening residual stress.

resents the stress state of a surface point on the shaft, including residual stresses in both circumferential and axial directions, as well as the shear stresses from the torsion load. Compressive residual stresses reduce the magnitude of tensile principal stress as shown in Figure 15, which is why compressive residual stresses benefit high-cycle torsion fatigue performance. During overload testing, residual stresses are eliminated by plastic deformation, and compressive residual stresses are not expected to benefit the ultimate strength of the axle shaft.

Principal stresses generated in approximately a 45 degree angle are calculated, and results are plotted in terms of the torsion load. The curve with hollow round marks represents the principal stress without residual stresses from induction hardening; the magnitude of principal stress as a function of the torsion load is linear. With compressive residual stresses, the principal stress is about 475 MPa lower, as shown by the curve with diamond marks in Figure 17, and the relationship between principal stress and the torsion load is not linear, especially under lower torsion loads.

The reason for the nonlinear relationship between principal stress and torsion load is because of the change in direction of the principal stress. Figure 18 shows a plot of direction of principal stress vs. torsion load. It shows the effect of the residual stress can be significant on the facture angle.

CONCLUSIONS

The electromagnetic modelling using Flux2D and thermal-stress modelling using DANTE are successfully coupled to simulate the inducting hardening process of an axle shaft. The power mapping process from Flux and DANTE is validated by directly comparing the temperature profiles predicted by the two packages. The residual stresses predicted from the induction hardening model are imported to a low-temperature tempering model, and the magnitude of the stress decrease is approximately 15%. The residual stresses from the tempering model are imported to a loading model to estimate the stresses for high cycle torsion fatigue and overload testes. The loading models have shown clearly how the residual stresses from the induction hardening benefit the fatigue performance.

REFERENCES

[1] G. Goldstein, G.,V. Nemkov, V.,and J. Jackowski, J. (2009) Virtual Prototyping of Induction Heat Treating. , 25th ASM HTSeat Treating Society ConferenceConf., 2009.

[2] D. Ivanov, D., Markegard, L., Asperheim, J., and Kristoffersen, H.et al., “Simulation of Stress and Strain for Induction-Hardening Applications”, Journal J. Matls. Engrg. and Perf., published online, July 18, 2013.

[3] B. Ferguson, B., and W. Dowling, W., “Predictive Model and Methodology for Heat Treatment Distortion”, NCMS Report #0383RE97, 1997.

[4] V. Warke, R. Sisson, and M. Makhlouf, FEA Model for Predicting the Response of Powder Metallurgy Steel Components to Heat Treatment, Mater. Sci. Eng., A, 518(1–2), p 7–15, 2009.

[5] Z. Li and B. Ferguson, Computer Modeling and Validations of Steel Gear Heat Treatment Processes using Commercial Software DANTE, J. Shanghai Jiaotong Univ. (Sci.), 16(2), p152-156, 2011.

[6] B. Ferguson, A. Freborg, and A. Li, Residual Stress and Heat Treatment – Process Design for Bending Fatigue Strength Improvement of Carburized Aerospace Gears, J. of HTM. , Härterei-technische Mitteilun, 62(6), 2007, p 279-284, 2007.

[7] Z. Li, Z., Ferguson, B., and Goldstein, G., Nemkov, V., Jackowski, J., and Fett, G.et al., “Modeling Stress and Distor-

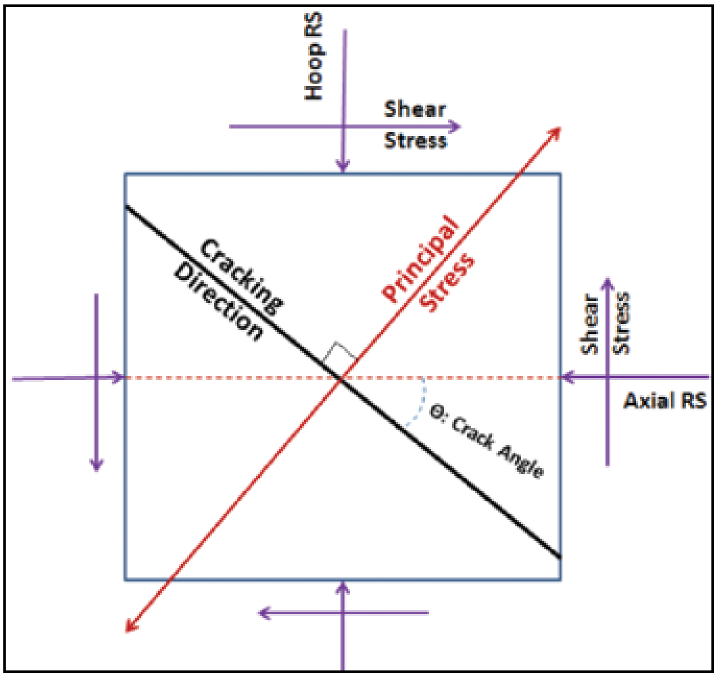

Figure 16: Schematic plot for analyzing the effect of residual stresses on crack generation

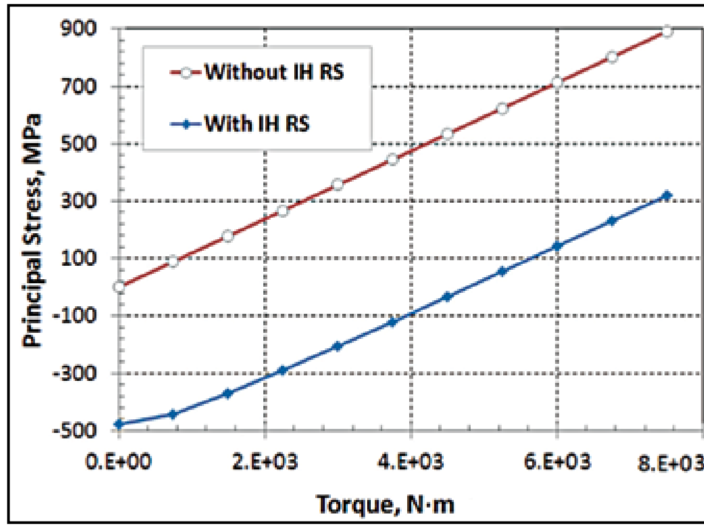

Figure 17: Effect of residual stress from induction hardening on the principal stress dominating shear cracking

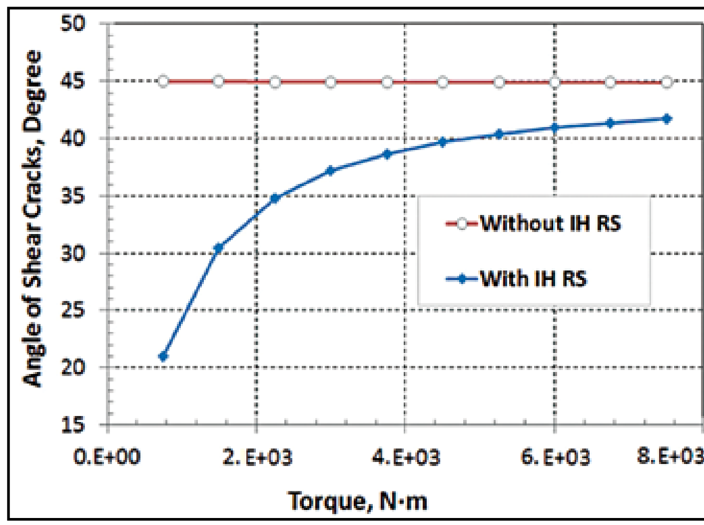

Figure 18: Effect of residual stress from induction hardening on the angle of shear cracking.

tion of Full-float Truck Axle during Induction Hardening Process", 27th ASM HTS eat Treating Society Conference., 2013.

[8] D. Bammann, D., et al., "Development of a Carburizing and Quenching Simulation Tool: A Material Model for Carburizing Steels Undergoing Phase Transformations", Proceedings Proc. of the 2nd Intl.ernational Conf.erence on Quenching and the Control of Distortion, November (1996), pp. 367-375, Nov. 1996.

[9] B. Ferguson, B.,A. Freborg, A., andG. Petrus, G., "Software Simulates Quenching", Advanced Materials and Processes, H31-H36, Aug.ust (2000).

[10] V. Nemkov, V., G. Goldstein, G., and J. Jackowski, J. (2011). Stress and Distortion Evolution During Induction Case Hardening of Tube. , 26th ASM HTSeat Treating Society Conf.erence, 2011.

[11] Z. Li, Z., B. Ferguson, B., and A. Freborg, A., "Data Needs for Modeling Heat Treatment of Steel Parts", Proc.eedings of Materials Matl. Science Sci. & Technology Tech. ConferenceConf., 2004, pp. 219-226, 2004.

[12] R. Goldstein, R.,V. Nemkov, V., and R. Madeira, R., (2007). Optimizing Axle-Scan Hardening Inductors. , Industrial Heating, December Dec. 2007.

[13] B. Ferguson, B.L.,A. Freborg, A.M.,and Z. Li, Z., "Probe Design to CharactrizeCharacterize Heat Transfer during Quenching Process", Proceedings Proc. of 6th International Quenching and Control of Distortion ConferenceConf., Chicago, Illinois, September 9-13, 2012, pp. 792-801, Sept. 2012.

[14] A. Banka, A., Franklin, J., Li, Z., Ferguson, B.L., and Aronov, M.et al., "Applying CFD to Characterize Gear Response during Intensive Quenching Process", Proceedings Proc. of the 24th ASM HTS eat Treating Society ConferenceConf., September 17-19, 2007, pp. 147-155, 2007.

ABOUT THE AUTHORS: Dr. B. Lynn Ferguson, a graduate of Drexel University, is president of DANTE Solutions, Inc., formerly known as Deformation Control Technology, Inc., a company he founded in 1982. His career has focused on the broad field of mechanical metallurgy, with a concentration on thermal and mechanical processing of metals. Over the past 20 years, he has been primarily involved with analysis of the metallurgical events that take place during heat treatment of steel parts, including prediction of distortion, residual stress, and the evolution of microstructural phases. He has published more than 70 technical papers, authored many sections of various ASM handbooks, co-authored one book, and been an instructor in several sponsored short courses. He is a Fellow of ASMI, Alpha Sigma Mu, and IFHTSE. Dr. Zhichao (Charlie) Li is a chief engineer at DANTE Solutions, Inc. located in Cleveland, Ohio. Dr. Li's areas of expertise include design optimization, finite element modeling, fatigue life characterization and analysis, metal forming and heat treatment. Dr. Li's main focus at DANTE is on heat treatment software development, technical support, and consulting services on heat treatment process improvement using computer modeling.

EQUIPMENT

Contact *Thermal Processing for Gear Solutions* at 800-366-2185 to list your equipment.

Heat Treat Equipment – REF #101
Phone: 734-331-3939 • Fax: 734-331-3915
Email: john@heattreatequip.com
Website: www.heattreatequip.com

Summit Products, Inc. – REF #102
65 Greenside Drive, Grand Island, NY 14072
Phone: 716-867-4312 • Fax: 716-867-4312
Email: summit@roadrunner.com

The W.H. Kay Company – REF #103
30925 Aurora Road, Cleveland, OH 44139
Phone: 440-519-3800 • Fax: 440-519-1455
Email: sales@whkay.com
Website: www.whkay.com

Park Thermal – REF #104
257 Elmwood Ave #300, Buffalo, NY 14222
Phone: 905-877-5254 • Fax: 905-877-6205
Email: jmistry@parkthermal.com
Website: www.parkthermal.com

BATCH OVENS & BOX TEMPERING FURNACES
8" 18" 8" Lucifer Elec. 1250 F. **REF #103**
12" 16" 18" Lindberg Elec. 1200 F. **REF #103**
12" 16" 18" Lindberg (3) Elec. 1250 F. **REF #103**
12" 18" 12" Lucifer Elec 1250 F. **REF #103**
14" 14" 14" Gruenberg -Solvent Elec. 450 F. **REF #103**
15" 24" 12" Sunbeam (N2) Elec. 1200 F. **REF #103**
19" 19" 19" Prec.Scientific Elec. 617 F. **REF #103**
20" 18" 20" Blue-M (2) Elec. 400 F. **REF #103**
20" 18" 20" Blue-M (2) Elec. 400 F. **REF #103**
20" 18" 20" Blue-M (Inert) Elec. 600 F. **REF #103**
20" 18" 20" Despatch (Solvent) - 2 Avail Elec. 650 F. **REF #103**
20" 18" 20" Blue-M Elec. 800 F. **REF #103**
20" 18" 20" Blue-M Elec. 1200 F. **REF #103**
20" 20" 20" Grieve Elec. 500 F. **REF #103**
20" 20" 20" Michigan/Grieve Elec. 1000 F. **REF #103**
20" 20" 20" Grieve Elec. 1250 F **REF #103**
24" 24" 36" New England Elec. 800 F. **REF #103**
24" 26" 24" Grieve Gas 500 F. **REF #103**
24" 36" 24" Demtec (N2) Elec. 500 F. **REF #103**
24" 36" 24" Grieve Elec. 850 F. **REF #103**
24" 36" 24" Paulo Gas 1250 F. **REF #103**
25" 20" 20" Blue-M Elec. 650 F. **REF #103**
25" 20" 20" Blue-M Elec. 650 F. **REF #103**
25" 20" 20" Blue-M - Inert Elec. 1100 F. **REF #103**
25" 20" 25" Gruenberg Elec. 500 F. **REF #103**
26" 26" 38" Grieve (2) Elec. 850 F. **REF #103**
28" 24" 18" Grieve Elec. 350 F. **REF #103**
28" 48" 28" Wisconsin (3) Elec. 800 F. **REF #103**
30" 30" 30" Hevi-Duty Elec. 1500 F. **REF #103**
30" 38" 48" Gruenberg (2) M21 Elec. 450 F. **REF #103**
30" 48" 22" Dow Elec. 1250 F. **REF #103**
34" 19" 33" Poll.Ctrls Burnoff Gas 900 F. **REF #103**
36" 36" 35" Despatch Elec. 400 F. **REF #103**
36" 36" 120" Steelman Elec. 450 F. **REF #103**
36" 48" 36" Grieve Elec. 350 F. **REF #103**
36" 60" 36" CEC (2) Elec. 650 F. **REF #103**
37" 19" 25" Despatch Elec. 500 F. **REF #103**
37" 25" 37" Despatch Elec. 850 F. **REF #103**
37" 25" 50" Despatch Elec. 500 F. **REF #103**
38" 20" 24" Blue-M Elec. 1200 F. **REF #103**
38" 26" 38" Grieve Elec. 1000 F. **REF #103**
48" 24" 48" Blue-M Elec. 600 F. **REF #103**
48" 30" 42" Despatch Gas 850 F. **REF #103**
48" 48" 48" CEC (N2) Elec. 1000 F. **REF #103**
48" 48" 60" Gasmac Burnoff (2) Gas 850 F. **REF #103**
48" 48" 72" Despatch (2) Elec. 500 F. **REF #103**
48" 48" 72" Lydon Elec. 500 F. **REF #103**
54" 68" 66" Despatch Elec. 500 F. **REF #103**
54" 108" 72" Despatch Elec. 500 F. **REF #103**
56" 30" 60" Gruenberg Elec. 450 F. **REF #103**
60" 60" 72" ACE Burnoff Gas 850 F. **REF #103**
72" 72" 72" Michigan Gas 500 F. **REF #103**
120" 168" 120" Wisconsin Oven Gas 500 F. **REF #103**

BOX FURNACES
J.L. Becker Slot Forge Furnace, 1986, Brand New, Never Used **REF #101**
L & L Special Furnace Electrically Heated Box Furnace, 1991 **REF #101**
J.L. Becker Box Temper Furnace, 1989 **REF #101**
Sunbeam Electric Box Furnace, good running condition **REF #101**
Surface 30-48-30 Electric Temper Furnace, good/ very good condition **REF #101**
Atmosphere Furnace Co. 36-48-30 Electric Temper Furnace, good/ very good condition **REF #101**
Atmosphere Furnace Co. 36-48-30 Electric Temper Furnace, good/ very good condition **REF #101**
Atmosphere Furnace Co. 36-48-30 Electric Temper Furnace, good/ very good condition **REF #101**
Surface Combustion 30-48-30 Gas Fired Temper Furnace, good/ very good condition **REF #101**
Surface 30-48-30 Gas Fired Temper Furnace, good/ very good condition **REF #101**
8" 18" 8" Blue-M Elec. 2000 F. **REF #103**
12" 24" 8" Lucifer-Up/Down (Retort) Elec. 2150/1400 F. **REF #103**
12" 24" 8" C.I. Hayes (Atmos) Elec. 1800 F. **REF #103**
12" 24" 12" Hevi-Duty (2) Elec. 1950 F. **REF #103**
12" 24" 12" Lucifer-Up/Down Elec. 2400/1400 F. **REF #103**
3" 24" 12" Electra-Up/Down Elec. 2000/1200 F. **REF #103**
15" 30" 12" Lindberg (Atmos) - Retort Elec. 2000 F. **REF #103**
17" 14.5" 12" L & L (New) Elec. 2350 F. **REF #103**
22" 36" 17.5" Lindberg (Atmos) Elec. 2050 F. **REF #103**
24" 36" 18" Thermlnyne (2) - Unused Elec. 1800 F. **REF #103**
36" 48" 24" Sunbeam (N2) Elec. 1950 F. **REF #103**
36" 72" 42" Eisenmann Kiln (Car) Gas 3100 F. **REF #103**
60" 48" 48" Recco (1998) Gas 2000 F. **REF #103**
60" 96" 60" Park Thermal Elec. 1850/2200 F. **REF #103**
126" 420" 72" Drever "Lift Off"-Atmos (2 Avail) Gas 1450 F. **REF #103**
13" 14" 12" ELECTRIC 1300°F **REF #104**
10" 10" 18" ELECTRIC 2000°F **REF #104**
22" 36" 22" ELECTRIC 1600°F **REF #104**
12" 6" 8" ELECTRIC 2000°F **REF #104**
12" 8" 18" ELECTRIC 2800°F **REF #104**
20" 13" 36" ELECTRIC 1850°F **REF #104**
12" 18" 18" ELECTRIC 1250°F **REF #104**
4" 10" 4" ELECTRIC 2000°F **REF #104**
22" 10" 8" ELECTRIC - C/W STAND 1250-2000°F **REF #104**
15" 8" 30" ELECTRIC - ATMOSPHERE 1950°F **REF #104**
11" 11" 17" ELECTRIC - CABINET 2000°F **REF #104**
33" 40" 48" ELECTRIC 500°F **REF #104**
18" 18" 30" ELECTRIC - GLO BAR 2900°F **REF #104**
30" 30" 54" ELECTRIC - AGING 500°F **REF #104**
30" 30" 54" **R** ELECTRIC - AGING 500°F **EF #104**
30" 30" 54" ELECTRIC 500°F **REF #104**
24" 18" 24" NATURAL GAS - BATCH FURNACE **REF #104**
24" 18" 24" NATURAL GAS - BATCH FURNACE **REF #104**
36" 30" 84" ELECTRIC 1200°F **REF #104**
24" 24" 24" ELECTRIC 2000°F **REF #104**
29" 22" 36" NATURAL GAS 1250°F **REF #104**
12" 11" 24" ELECTRIC - BOX 2000°F**REF #104**
24" 24" 24" ELECTRIC - GAS MAC 850°F **REF #104**
18" 12" 12" ELECTRIC 2100°F **REF #104**
48" 30" 36" ELECTRIC - ATMOSPHERE TEMPERING **REF #104**
50" 24" 29" NATURAL GAS 1250°F **REF #104**
36" 18" 24" ELECTRIC 1250°F **REF #104**
17" 17" 36" NATURAL GAS 1250°F **REF #104**
15" 6" 10" ELECTRIC 1850°F **REF #104**
6" DIA 48" ELECTRIC - TUBE FURNACE 1200°C **REF #104**
7" 4" 14" GAS **REF #104**
10" DIA 18" GAS - FORGE FURNACE **REF #104**
9" 6" 15" GAS - FORGE FURNACE **REF #104**
6" 6" 15" GAS - FORGE FURNACE **REF #104**
12" 10" 20" ELECTRIC - SPEEDY MELT FURNACE 2000°F **REF #104**
12" 9" 18" ELECTRIC **REF #104**
12" 12" 18" NATURAL GAS 1250°F **REF #104**
14" 14" 18" ELECTRIC - GLOBAR 2500°F **REF #104**
17" 17" 17" ELECTRIC - HITEMP KILN 2200°F **REF #104**
35" 24" 60" ELECTRIC 1430°F **REF #104**
10" 9" 14" ELECTRIC - FRONT DOOR LOADING 2000°F **REF #104**
12" 12" 24" ELECTRIC - 13KW 2300°F **REF #104**
12" 12" 24" ELECTRIC - 20KW 2000°F **REF #104**
18" 12" 24" ELECTRIC 2000°F **REF #104**
36" 24" 56" ELECTRIC 800°F **REF #104**
24" 24" 36" ELECTRIC - CYCLONE 1250°F **REF #104**
24" 36" 30" ELECTRIC RE-CIRC. BOX FURNACE 2000°F **REF #104**
18" 20" 45" ELECT. RE-CIRC. W/ FLAME CURTAIN & BASKET 2000°F **REF #104**
12" 12" 18" ELECT. RE-CIRC. BATCH (MATCH PAIR WITH I3958) 1250°F **REF #104**
12" 12" 18" ELECT. RE-CIRC. BATCH (MATCH PAIR WITH I3957.) 1250°F **REF #104**

CAR BOTTOM FURNACES
Holcroft 48-144-48 Car Bottom Furnace **REF #101**
Sauder 48-144-48 Car Bottom Furnace **REF #101**
48" 48" 72" GAS FIRED CAR BOTTOM 2000°F **REF #104**
130" 72" 216" GAS FIRED CAR BOTTOM 2000°F **REF #104**
130" 72" 215" GAS FIRED CAR BOTTOM 2400°F **REF #104**
108" 36" 192" GAS FIRED CAR BOTTOM 2400°F **REF #104**
72" 48" 216" GAS FIRED CAR BOTTOM 2000°F **REF #104**

CHARGE CARS
Surface Combustion 30-48 Charge Car (Double Ended), fairly good condition **REF #101**
Atmosphere Furnace Company 36-48 Charge Car (Double Ended) **REF #101**
Surface Combustion 30-48 Charge Car (Double Ended) **REF #101**

CONTINUOUS ANNEALING FURNACES
Wellman Continuous Mesh Belt Annealing Furnace **REF #101**
Aichelin-Stahl Continuous Roller Hearth Furnace & Conveying System, 1996 **REF #101**
Park Thermal Continuous Mesh Belt Furnace, 2005, Excellent Condition – New – Never been used **REF #101**

CONTINUOUS HQT FURNACES
Tokyo Gasden Ro Continuous Mesh Belt HQWT Furnace Line, 1989 **REF #101**

CONTINUOUS TEMPERING FURNACES

Surface Combustion Mesh Belt Temper Furnace **REF #101**
J.L. Becker Conveyor-Type Temper Furnace with Ambient Air Cool Continuous Belt, 1997 IQ Furnaces **REF #101**
Surface Combustion 30-48-30 Pro-Electric IQ Furnace **REF #101**
AFC 36-48-30 IQ Furnace with Top Cool **REF #101**
AFC 36-48-30 IQ Furnace **REF #101**
Surface Combustion 30-48-30 IQ with Top Cool, Excellent Condition, 2000 **REF #101**
Surface Combustion 30-48-30 IQ Furnace, Excellent Condition **REF #101**

DRAW TEMPER FURNACES

18" 12" 30" ELECTRIC 1250ºF **REF #104**
16" 15" 12" ELECTRIC - BOX DRAW 1250ºF **REF #104**
36" 16" 24" ELECTRIC - BOX DRAW 1250ºF **REF #104**
12" 18" 16" ELECTRIC - BOX DRAW 1400ºF **REF #104**
30" 20" 48" ELECTRIC - BOX DRAW 1250ºF **REF #104**
24" 18" 36" NATURAL GAS ROLLER DRAW 1400ºF **REF #104**
30" 30" 48" NATURAL GAS 1200ºF **REF #104**
60" 40" 60" NATURAL GAS - DRAW FURNACE 800ºF **REF #104**
29" 16" 36" ELECTRIC - DRAW/TEMPER 1400ºF **REF #104**
54" 54" 150" ELECTRIC 900ºF **REF #104**
24" 18" 10 FEET ELECTRIC 500ºF **REF #104**
30" 24" 72" GAS - GRAVITY FEED DRAW 1350ºF **REF #104**
12" 14" 12" ELECTRIC - WATER COOLED FAN 1200ºF **REF #104**

ENDOTHERMIC GAS GENERATORS

Lindberg 1500 CFH Endothermic Gas Generator, 1992, good condition **REF #101**
Lindberg 1500 CFH Endothermic Gas Generator, 1996, excellent condition **REF #101**
Surface Combustion 5600 CFH Endo. Gas Generator **REF #101**
Surface Combustion 5600 CFH Endo. Gas Generator **REF #101**
Surface Combustion 5600 CFH Endo. Gas Generator **REF #101**
Surface Combustion 5600 CFH Endo. Gas Generator **REF #101**

EXOTHERMIC GAS GENERATORS

J.L. Becker 12,000 CFH Exothermic Gas Generator w/ Dryer, w **REF #101**
Thermal Transfer 30,000 CFH Exothermic Gas Generator, 1994, excellent condition **REF #101**

FLUIDIZING BED FURNACE

14" 30 DIA 5" ELECTRIC 1600ºF **REF #104**

FREEZERS

Webber 36-48-36 Chamber Freezer, 1980 **REF #101**
Cincinnati Sub Zero 36-48-36 Chamber Freezer, 1995 **REF #101**

MESH BELT FURNACES

17" 8" 10' ELECTRIC 600ºF **REF #104**
23" 4" 10' NATURAL GAS 1250ºF **REF #104**
24" 12" 96" ELECTRIC 500ºF **REF #104**

MESH BELT BRAZING FURNACES

Lindberg Continuous Mesh Belt Brazing Furnace **REF #101**
J.L. Becker 26" Mesh Belt Brazing Annealing Furnace, 2007 **REF #101**
10" J.L. Becker Mesh Belt Furnace with Muffle, 1988 **REF #101**
24" J.L. Becker Mesh Belt Furnace **REF #101**

MISC. EQUIPMENT

Atmosphere Furnace Co. 36-48 Stationary Holding Stations, 1987, 36"W x 48"L work area **REF #101**
Atmosphere Furnace Co. 36-48 Stationary Holding Stations, 1987, 36"W x 48"L work area **REF #101**
Atmosphere Furnace Co. 36-48 Stationary Holding Stations, 1987, 36"W x 48"L work area **REF #101**
Atmosphere Furnace Co. 36-48 Scissors Lift Holding Stations, 1987, 36"W x 48"L work area **REF #101**
Atmosphere Furnace Co. 36-48 Scissors Lift Holding Stations, 1987, 36"W x 48"L work area **REF #101**
Surface Combustion 30-96 Stationary Load Tables, 96-inch rail length, 15-inch rail centers **REF #101**
Surface Combustion 30-96 Stationary Load Tables, 96-inch rail length, 15-inch rail centers **REF #101**
Surface Combustion 30-96 Stationary Load Tables, 96-inch rail length, 15-inch rail centers **REF #101**
Surface Combustion 30-48 Scissors Lift Table, 48-inch rail length **REF #101**
8xxx 2.400 CFH 12 oz (2) North American 1/3HP **REF #103**
8xxx 3.000 CFH 12 oz (3) North American 1/2HP **REF #103**
8xxx 5.400 CFH 4 oz North American 1/3HP **REF #103**
8236 12.000 CFH 12oz (3) North American 1/2HP **REF #103**
8712 15.600 CFH 37 oz, North American 5HP **REF #103**
8193 19.500 CFH 32 oz, Spencer 5HP **REF #103**
8245 23.400 CFH 8 oz. North American 1,5HP **REF #103**
8185 24.000 CFH 24 oz. Buffalo Forge 7.5HP **REF #103**
8251 45.600 CFH 16 oz. Spencer 5HP **REF #103**
8252 66.000 CFH 24 oz . Snencer(New) 10HP **REF #103**
8253 66.000 CFH 24 oz. Spencer 10HP **REF #103**
8250 150.000 CFH 16 oz. Hauck 15HP **REF #103**

OVER - UNDER FURNACES

12" 11" 48" GLO BAR ELECTRIC 3000ºF **REF #104**
9.5" 9.5" 18" COILED ELEMENTS ELECTRIC 2300ºF **REF #104**
22" 11" 14" COILED ELEMENTS ELECTRIC 2200ºF **REF #104**
12" 7" 30" ELECTRIC - CRESS **REF #104**
18" 12" 24" ELECTRIC 2100/1250ºF **REF #104**
12" 12" 36" ELECTRIC 2300/1250ºF **REF #104**

PARTS WASHERS

J.L.Becker Gas-Fired Tub Washer **REF #101**
48-72-48 Gas Fired Spray Washer **REF #101**
Dow Furnace Co. 30-48-30 Electrically Heated Spray, Dunk & Agitate Washer **REF #101**
Atmosphere Furnace Co. 36-48-30 Spray/Dunk Washer **REF #101**
Atmosphere Furnace Co. 36-48-30 Spray/Dunk Washer **REF #101**
Surface Combustion 30-48-30 Electrically Heated Spray Dunk/ Dunk Washer **REF #101**
Surface Combustion 30-48-30 Electrically Heated Washer **REF #101**

PIT FURNACES

Lindberg 28" x 28" Pit-Type Temper Furnace **REF #101**
14" 60" Procedyne - Fluidised Bed Elec. 1850 F. **REF #103**
16" 20" Lindberg Elec. 1250 F. **REF #103**
22" 26" L & N Elec. 1200 F. **REF #103**
28" 48" Lindberg Elec. 1400 F. **REF #103**
38" 48" Lindberg Elec. 1400 F. **REF #103**
40" 60" L & N -Steam/N2 Elec. 1400 F. **REF #103**
40" 60" Wellman-Steam/N2 Elec. 1400 F. **REF #103**
48" 48" Lindberg (Atmos) - Fan Elec. 1850 F. **REF #103**
20" 48" ELECTRIC 1200ºF **REF #104**
30" 36" NATURAL GAS 1250ºF **REF #104**
24" 30" ELECTRIC 1400ºF **REF #104**
16" 18" GAS - CYCLONE 1300ºF **REF #104**
28" 96" NATURAL GAS 1400ºF **REF #104**
24" 28" ELECTRIC - HOMO CARBURIZING 1400ºF **REF #104**
16" 30" ELECTRIC SALT POT 1650ºF **REF #104**
22" 36" 22" ELECTRIC SQUARE PIT 1600ºF **REF #104**
6" 4" 16" ELECTRIC VACUUM PIT 2400ºF **REF #104**
24" 24" ELECTRIC 1400ºF **REF #104**
12" dia 18" ELECTRIC - HOMO PIT 1200ºF **REF #104**
30" 30" 30" ELECTRIC 800ºF **REF #104**
30" DIA 30" ELECTRIC - PIT CYCLONE 1250ºF **REF #104**
12" 20" ELECTRIC - KEYHOLE 1250ºF **REF #104**
4.5" 24" 4" ELECTRIC - SQUARE PIT **REF #104**
24" 48" 24" ELECTRIC - SQUARE PIT 1200ºF **REF #104**
18" 18" 18" ELECTRIC - TOP LOAD 2000ºF **REF #104**
16" Dia. 20" ELECTRIC - CYCLONE 1250ºF **REF #104**
22" Dia 26" ELECTRIC - CYCLONE 1250ºF **REF #104**
22"Dia 26" ELECTRIC 1250ºF **REF #104**
8"dia 9"deep ELECTRIC - TEMPERING 1250ºF **REF #104**
35" 60" GAS **REF #104**
28"DIA 28" ELECTRIC - CYCLONE PIT 1250ºF **REF #104**

VACUUM FURNACES

Brew/Thermal Technology Vacuum Furnace **REF #101**
Abar Ipsen 2-Bar Vacuum Furnace, 1986, good condition **REF #101**
24"W x 36"D x 18"H Hayes (Oil Quench) Elec. 2400 F. **REF #103**
48" Dia 60" High Ipsen (Bottom Load) Elec. 2400 F. **REF #103**
Lindberg, 24"W x 18"H x 36"L, Vacuum Furnace, 2400°F,

ATOMOSPHERE GENERATORS

750 CFH Endothermic Dow Elec. **REF #103**
750 CFH Endothermic Insen Gas **REF #103**
1000 CFH Exothermic Gas Atmosphere **REF #103**
1000 CFH Ammonia Dissociator Lindberg Elec. **REF #103**
1000 CFH Ammonia Dissociator Drever Elec. **REF #103**
1500 CFH Endothermic (Air Cooled) Ipsen Elec. **REF #103**
1500 CFH Endothermic Ipsen Gas **REF #103**
3000 CFH Endothermic air Cooled) Lindberg Gas **REF #103**
3000 CFH Endothermic (Air Cooled) Lindberg (2) Gas **REF #103**
3000 CFH Endothermic (Air Cooled) Lindhera Gas **REF #103**
3600 CFH Fnclothermic (Air Cooled) Surface (2) Gas **REF #103**
3600 CFH Endothermic Surface Gas **REF #103**
5600 CFH Endothermic Surface (3) Gas **REF #103**
6000 CFH Nitrogen Generator (2000) Gas Atmospheres Gas **REF #103**
10 000 CFH Exothermic Seco-Warwick Gas **REF #103**

INTERNAL QUENCH FURNACES

24"W 36"D 18"H Dow (Slow Cool) Line Elec. 2000 F. **REF #103**
24"W 36"D 1 8"H Ispen T-4 - Air Cooled Gas 1850 F. **REF #103**
24"W 36"D 18"H Ispen T-4 - Air Cooled Gas 1850 F. **REF #103**
24"W 36"D 18"H Isoen T-4 - Air Cooled Gas 1850 F. **REF #103**
24"W 36"D 18"H Ispen T-4 - Air Cooled Gas 1850 F **REF #103**
30"W 48"D 30"H Surface Allcase Elec. 1750 F. **REF #103**
30" 30" 48" NATURAL GAS 1750ºF **REF #104**
12" 10" 24" ELECTRIC - BABY PACEMAKER 1850ºF **REF #104**
45" 40" 72" ELECTRIC - ALUMINUM QUENCH 1250ºF **REF #104**
12" 9" 18" IPSEN 2000ºF **REF #104**
87" 36" 87" SURFACE COMBUSTION W/ 12,500G. QUENCH 1850ºF **REF #104**
62" 36" 62" SURFACE COMBUSTION W/ 9,500G. QUENCH 1850ºF **REF #104**
62" 36" 62" SURFACE COMBUSTION W/ 9,500G. QUENCH 1850ºF **REF #104**
15" 12" 30" Electric c/w load carts 1850ºF **REF #104**

CONTINUOUS/BELT FURNACES + OVENS

5"W 36"D 2"H BTU Systems (Inert Gas) Rec. 1922ºF **REF #103**
12"W 48"D 2"H Lindberg (Inert Gas) Elec. 1022ºF. **REF #103**
12"W 15'D 4"H Sargent&Wilbur'94(Mufflel) Gas 2100ºF. **REF #103**
16"W 24'D 4"H Abbott-Retort (1996) Elec 2400ºF. **REF #103**
24"W 12'D 6"H Heat Industries Elec. 750ºF. **REF #103**
24"W 40'D 18"H Despatch Elec. 500ºF. **REF #103**
24"W 40'D 18"H Despatch Gas 650ºF **REF #103**
60"W 45'D 12"H Roller Hearth Annealer (Atmos) Gas 1700ºF **REF #103**
72"W 30'D 15"H Unitherm Gas 500ºF **REF #103**

MARKET PLACE

Manufacturing excellence through quality, integration, materials, maintenance, education, and speed.

AD INDEX

Deep Case Carburizing
Stop-Off Paint
50%
Less Expensive
Ask for COPPER LABEL Stop-Off Coating
✓ Domestically manufactured
✓ Single-day delivery
✓ Guaranteed 50% savings off published competitor's price
HEAT TREAT 2015 Booth #237
AVION MANUFACTURING
Avion Manufacturing
2950 Westway Drive • Suite 106 • Brunswick, Ohio 44212
Ph: 330-220-2779 • Fax: 330-220-3709 • www.avionmfg.com

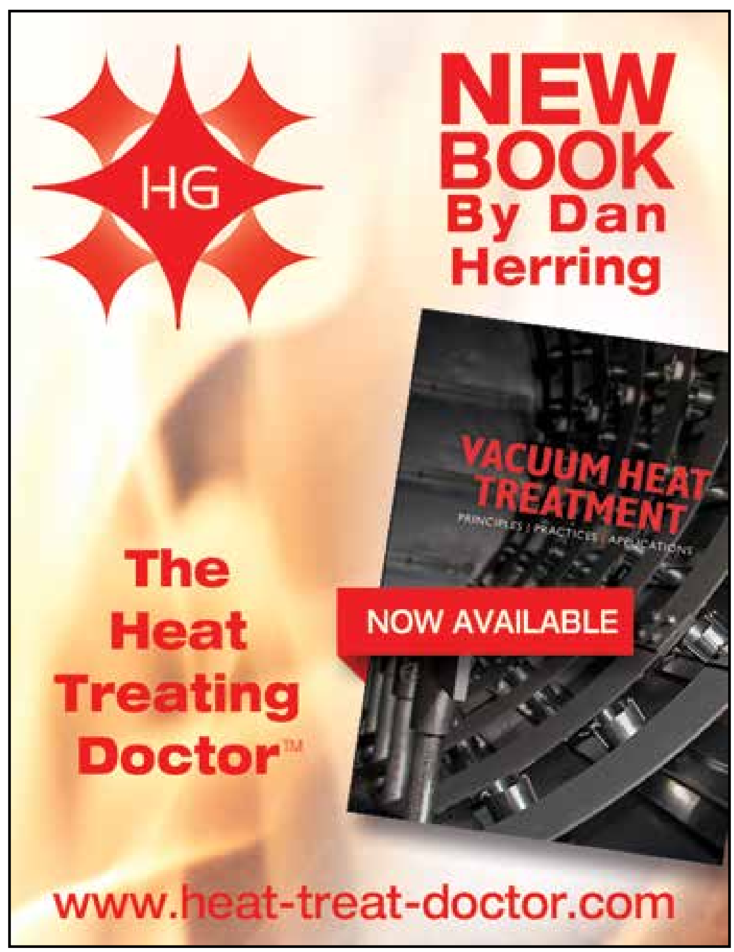

HG
NEW BOOK By Dan Herring
VACUUM HEAT TREATMENT
PRINCIPLES | PRACTICES | APPLICATIONS
NOW AVAILABLE
The Heat Treating Doctor™
www.heat-treat-doctor.com

Q&A

BRIAN RUSSELL
PRESIDENT, DRY COOLERS, INC.

Tell me a little about the history of Dry Coolers, Inc.

We started in 1985 to provide cooling water solutions for heat treating equipment—for vacuum furnaces, induction systems, and convection fans on atmosphere furnaces. We have diligently applied that trade for many years and, since then, we've broken out into other operations related to high-temperature metals.

What exactly is a dry cooler?

They are similar, in theory, to a large radiator in a car — copper tubes, aluminum fins, and fans that blow over them. When you close the loop with a pressure relief valve, like you seal the system in your car with a radiator cap, you can keep all the oxygen out of the water, preventing corrosion and biological problems that scale up the inside of the furnace with minerals. It protects the equipment, cools it more cheaply, and conserves resources.

That was only the beginning, though...

That was our starting base, right. Then, we expanded into doing evaporative cooling systems, with cooling towers and tanks and pumps, still keeping the closed loop concept for the furnaces.

Our customers then led us, by request, into making mechanical chillers—refrigeration machines to cool water even colder. With a dry cooler, you can only get down to close to whatever the outdoor air temperature is—whatever the thermometer says. With an evaporative cooling tower, you can go a little below that down to the evaporating temperature, a little below what the thermometer says. But if you need some 60°F water, you still have to refrigerate it.

Now we make all those things, including some gas coolers. We also do heat recovery and hybrid systems with chillers and air-cooled heat exchangers—what we call a "free cooler" in the winter. We combined different designs to get the best, most efficient reliable experience for a customer.

Tell me about your employees. What kinds of engineers do you have working there?

We have four mechanical engineers and several designers. Our chief engineer, Matt Reid, has been with us 15 years. Gary Burwick is another, an engineer experienced in air-cooled heat exchangers, especially for heat treating equipment. Phil Siemen has a great deal of experience in institutional cooling—almost high end commercial grade systems. We build all of our own control patterns. They're all UL-508A certified. The company is ISO 9001:2008, recertified every year.

Dry coolers has an overseas presence as well, don't you?

Market forces led us to participate in a joint venture with M&C Pumps in China called DCMC Thermal Technologies. A lot of businesses have moved to Asia—in the 80's and 90's we were exporting a lot of equipment to China through our furnace OEMs in America and in Europe. Many of our customers would build a green field facility in Europe and wouldn't want to take a chance with the local cooling system, so they'd package our equipment with their whole furnace line and ship it over there.

As that business started to go away, many of the furnace companies have opened factories in China, notably Ipsen, Seco Warwick, and AFC. They've requested that we help them over there. So we teamed up with a pump manufacturer there, who is our joint venture partner. Now we're actively selling quench oil coolers and vacuum furnace cooling systems in China.

How do you see your industry continuing to spread?

I think the expertise in metallurgy in general, whether it's for forging or gears or just heat treating, is a pretty small group of people, really. It's a global industry, so that expertise is spreading around the world.

There's always a strong market in North America and Europe, but there are also other areas of the world. We found that we were welcomed in open arms in China, either by domestic Chinese companies or wholly owned foreign enterprise furnace manufacturers. We've been well received because we have a good reputation from being in this business for so long. Many of our first customers that we started with—AFC, Surface Combustion, Ipsen—they were our original OEMs and we still sell to them today. To have a good long track record and be a good partner with the customer, they'll want to take that overseas.

Tell our readers about the software you use to design the dry coolers:

For heat exchanger selection and thermal calculations, we've written almost all that software internally. For design we use 3D CAD modeling for all our products, mostly solid works. We use AutoCad electrical for designing the electrical pads and circuits. And we have an ERP (Enterprise Resource Planning) system that runs a database that we've created. We've been computerized since the beginning, so we have all of our records, all the machines we've ever built from the beginning. It makes for a pretty efficient process. We've always tried to stay at the cutting edge of electronic technology. Now we're finally at the point where we're putting some of our software on the web for our customers, so they can go create their own proposals. We're starting out with the air-cooled quench oil coolers, and we'll branch out from there.

FOR MORE INFORMATION: For more information on Dry Coolers products and services, visit them online at www.drycoolers.com or call (800) 525 8173.

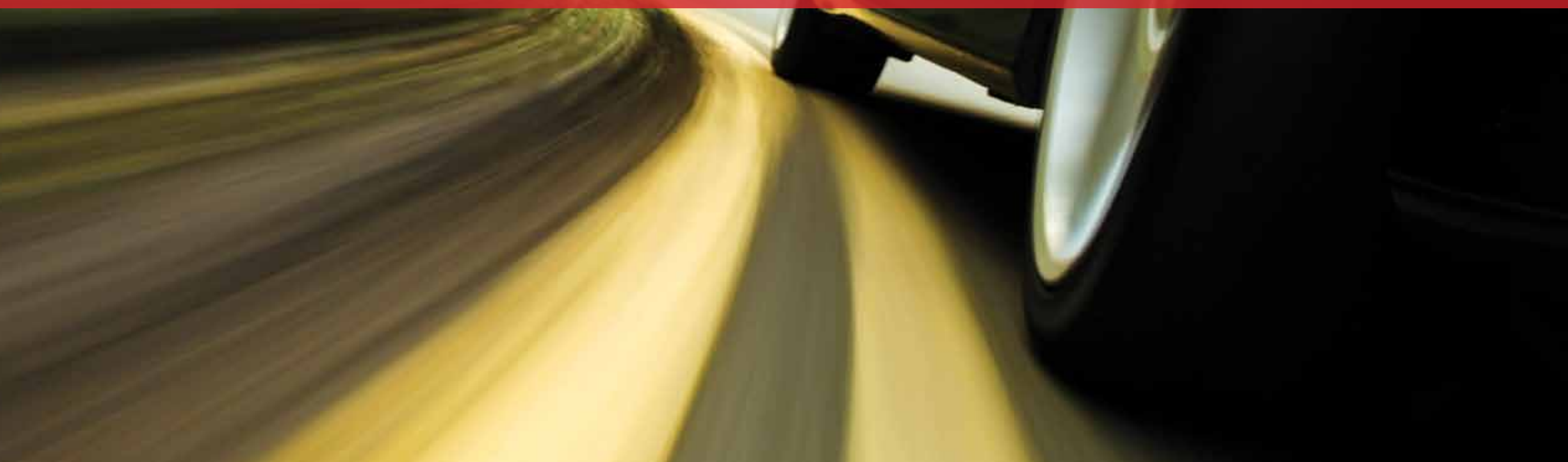

HOW LONG DO YOUR RADIANT TUBES LAST?

WE GUARANTEE 5 YEARS OF LIFE

With Steeltech Ltd.'s AES Radiant Tube Assemblies, we guarantee 5 years of life.* You may also realize up to 20% FUEL SAVINGS. Contact your Steeltech representative today for more information or call Steeltech directly for a quote!

LIGHTWEIGHT FIXTURES

BOOST YOUR EFFICIENCY AND INCREASE THROUGHPUT

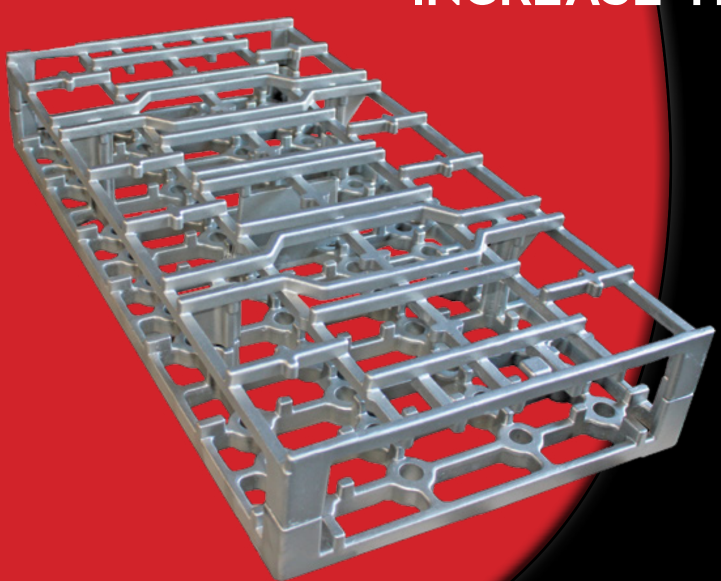

- Variety of designs, including hanging and stackable fixtures
- Custom designs and reverse engineering available
- Increased load capacity and service life
- Light weight designs resulting in reduced energy consumption

PH: 800.897.7833 WWW.STEELTECHLTD.COM
ALLOYS@STEELTECHLTD.COM

STEELTECH
Improve your bottom line.™

*Some Restrictions Apply